THE MOTION AND ASSOCIATED MASS TRANSFER CHARACTERISTICS OF GAS BUBBLES IN VISCOELASTIC LIQUIDS

By

Erdinc Zana

In Partial Fulfillment of the Requirements
For the Degree of Doctor of Philosophy

California Institute of Technology
Pasadena, California
1975

(Submitted February 12, 1975)

Dedicated to Terry and Jason

ACKNOWLEDGEMENTS

I would like to express my sincere thanks to my research advisor, Professor L. G. Leal, who suggested and directed this research project and who provided advice and an alternate point of view on many issues.

Special thanks are due to Messrs. George Griffith and John Yehle who assisted in design and automation of the experimental apparatus.

During my stay at Caltech I enjoyed the friendship of many present and past graduate students including B. P. Ho, G. E. Robertson, T. J. McMillen, L. B. Schreiber, P. E. Wood, D. E. Cormack, W. Lennard, R. H. Goldberg and T. D. Tarbell.

Finally, I would like to express my sincere appreciation to my wife, Terry, for her friendship and understanding, my son, Jason, who gives me immeasurable happiness by his presence, and my parents for their encouragement.

ABSTRACT

The motion and associated mass transfer characteristics of gas bubbles in viscoelastic liquids is investigated in the limits of $Pe \ll 1$ and $Pe \gg 1$. Full numerical and approximate analytical solutions are obtained for $Pe \ll 1$ case in order to investigate the roles of shear viscosity, relaxation and retardation times, surface tension and the Henry's law constant on the dissolution rate. It is shown that the collapse characteristics and the behavior of internal pressure in the viscoelastic liquid differ considerably from the case of a purely Newtonian liquid, particularly during the early and late stages of the dissolution process.

The $Pe \gg 1$ case is studied experimentally. The mass transfer rates from gas bubbles rising in viscoelastic liquids are measured and the data are shown to correlate very well with Weissenberg number. It is also shown that mass transfer rate from a gas bubble is greatly enhanced by viscoelasticity over its value for a Newtonian liquid with the same shear viscosity. The terminal rise velocities of bubbles in viscoelastic liquids are also measured. The well known discontinuity in the bubble rise velocity is fully investigated. It is shown that the magnitude of the velocity discontinuity may be accounted for by considering shear dependent viscosity and viscoelasticity. A tentative explanation for the abruptness of the velocity transition is presented.

Finally, the streamline flow visualization experiments for viscoelastic liquids past a solid sphere are presented. The results show that the streamlines are shifted in the upstream direction and the amount of shift increases with viscoelasticity.

TABLE OF CONTENTS

CHAPTER I

INTRODUCTION

INTRODUCTION

The motion and associated mass transfer characteristics of gas bubbles in liquids have been of considerable interest to scientists and engineers from a variety of disciplines. The mathematicians and physicists have been interested in bubble motion in liquids from a fundamental point of view, since these problems pose as difficult and interesting test cases for many analytical and/or numerical tools of mathematics. Chemical metallurgical and, to a certain extent, civil engineers are interested in the problems associated with bubble motion and mass transfer due to its practical importance in design and development of gas/liquid contact operations, such as distillation, extraction, fermentation, brewery, etc.

The problem of bubble motion and mass transfer is very difficult to study either theoretically or experimentally. First of all, the equations governing the motion of and mass transfer from gas bubbles in a liquid medium are highly non-linear, and hence the bulk theoretical treatment of it is almost impossible. Experimental difficulty is mainly due to the existence of a large number of physical parameters that effect the system. As a result, the problem of bubble motion and mass transfer in Newtonian liquids has been the subject of a large number of investigations. The extension of these studies to non-Newtonian liquids has accorded very little attention despite the technological importance of non-Newtonian liquids in modern chemical process and design engineering. All of the theoretical and experimental difficulties associated with Newtonian systems are also encountered in non-Newtonian, viscoelastic systems. But the main difficulty with

viscoelastic systems at the present state of art is the lack of an equation of state that is both realistic and mathematically tractable. Simple linear models of viscoelasticity are known to fail to predict the behavior of viscoelastic liquids even for relatively simple flow configurations. Non-linear models not only introduce a large number of physical parameters (time constants), many of which cannot be even measured by any presently known techniques, but also adds to the mathematical complexity by adding non-linearity to already highly non-linear flow systems.

The modified versions of Oldroyd's 8-constant model are used for the problems considered in this thesis. A justification for choosing Oldroyd's model is given in chapter II section A.3 (also see Bird et al., 1966). The modifications to Oldroyd's 8-constant model are done based on the physical nature of the specific problem considered.

It is convenient, from the theoretical point of view, to consider the influence of "viscoelasticity" on mass transfer as being a result of two distinct effects: first is the alteration of mass transfer rates due to changes in the streaming flow past the bubble, which is present even if the bubble volume is held constant (as in the constant-volume mass transfer experiments of Calderbank et al., 1970); second is the alteration due to the strong viscoelastic effect on the pure-straining "extensional" flow which is induced when the bubble volume is changing. In general, both effects occur simultaneously, each influencing the other in a non-trivial way. Nevertheless, it is clear that the latter will dominate for a highly soluble gas bubble in a strongly "viscous" fluid, while the former should be of greatest significance in the

opposite case of a slightly soluble bubble in a fluid of low viscosity. Indeed, it is shown in Chapter II by careful derivation of the governing equations and boundary conditions that the case of a stationary, dissolving bubble and the case of a translating, "constant" volume bubble are the leading approximations in the two asymptotic limits, $Pe \equiv (Ua/D) << 1$ and $Pe >> 1$, respectively.

A. Pe << 1; The Dissolution of a Slowly Translating Bubble in a Viscoelastic Liquid

All of the early studies on dissolution of a stationary gas bubble in Newtonian liquids (cf. Scriven, 1959; Epstein and Plesset, 1950; Ready and Cooper, 1966; Cable and Evans, 1967; Duda and Vrentas, 1971)* were confined to limiting cases in which it was assumed that the viscosity of the liquid medium played no role in determining the rate of bubble collapse. Barlow and Langlois (1962) were the first to consider the effects of viscosity, using a so-called "thin shell" approximation to simplify the governing diffusion and momentum equations. The "thin shell" approach assumes, in essence, that the diffusion and hydrodynamic effects are confined to a narrow region near the bubble interface.

The problem of a collapsing spherical cavity in a viscoelastic fluid was recently studied by Street (1968), and by Goddard and Fogler (1970). In the cavity problem, there is no mass transfer; rather, the collapse occurs as a result of the internal cavity pressure being smaller than the equilibrium value. The resultant problem is, of course, greatly simplified relative to the collapse of a spherical bubble since

---

* See Chapter II for references

the diffusion balance becomes totally irrelevant and the driving pressure differential is (assumed) constant throughout the collapse process.

In the mass-transfer induced collapse of a bubble, on the other hand, the internal pressure is unknown and the mass and momentum balances are intimately coupled; for example, a highly soluble gas bubble in a highly viscous liquid will tend to produce a low internal pressure as the bubble collapse is impeded by the strong dissipative effects in the fluid. Thus, in this case, the full nonlinear diffusion, stress-motion and stress constitutive model must be considered simultaneously. Neither the Newtonian nor viscoelastic cases has been done previously.

In Chapter II both exact numerical and approximate analytic solutions are given for the mass-transfer induced collapse of a stationary gas bubble in the Oldroyd (1958) three-constant fluid B as modified by Barnes, Townsend and Walters (1971). A complete description of this model is presented in Section A.3 of Chapter II. The flow induced by collapse of bubble boundary is a pure uniaxial extensional motion, and the modified fluid B admits uniaxial strain-increasing (elongational) viscosities, as observed experimentally for most viscoelastic fluids (cf. Denson and Gallo, 1971). The degree of strain dependence is controlled by the model parameters and these were varied over a wide range (including the Newtonian fluid limit) for the numerical solutions.

B. Pe >> 1; The Dissolution of a Bubble with Slowly Varying Volume in a Viscoelastic Liquid

This problem is considered in Chapter IV. Almost all the previous

work on convective mass transport for constant volume bubbles has been on Newtonian liquids. As mentioned before, the theoretical or experimental extension of this problem to non-Newtonian, viscoelastic liquids is difficult. The major problem in working with viscoelastic systems is the characterization of viscoelasticity. This problem is considered in Section B of Chapter IV. It is shown, based on dimensional analysis of the rheological equation of state that a single dimensionless parameter, Weissenberg number ($We \equiv \lambda U_\infty / R_{eq}$) may be used as a measure of viscoelasticity when Reynolds number ($Re \equiv U_\infty R_{eq}/\nu$) is small, and the parameter We/Re when Re number is large.

There has been very little prior experimental work reported which is relevant to the rate of mass transfer from bubbles when they are translating through a fully non-Newtonian fluid. The first reasonably systematic investigations are due to Barnett, Humphrey and Litt (1966),* and Calderbank (1967) who studied the rate of dissolution of carbon dioxide bubbles in various pseudoplastic liquids. The mass transfer data on viscoelastic liquids are even more limited. All the known data in literature are due to Calderbank (1970) (one fluid), and Hirose and Moo-Young (1971) (three fluids). Both studies are limited in scope and are not done with viscoelasticity as being the prime motive.

The mass transfer data on one Newtonian and four viscoelastic liquids for bubble sizes $0.20 \leq R_{eq} \leq 0.42$ are presented in Section G, Chapter IV. Viscoelastic liquids are chosen to cover a wide range of fluid elasticity (see Section D). In addition to mass transfer considerations, the effect of elasticity on bubble shapes and velocities is studied and the results are given in Sections E and F of Chapter IV,

---

* See Chapter IV for references

respectively.

Of all the experimentally observed differences on the motion of a constant volume gas bubble in a Newtonian and a viscoelastic liquid, none is more intriguing than the existence of a large and discontinuous transition in the bubble rise velocity at some critical radius when the bubble is moving in a viscoelastic liquid. No such transition exists in Newtonian systems. This phenomena is first observed by Astarita and Apuzzo (1965) and similar observations are reported by Calderbank et al. (1970) and Leal et al. (1971) since then. The generally accepted reason for this transition is a change in the bubble surface boundary conditions from no-slip to a freely circulating behavior. There remain two more questions associated with this phenomena. The first one is related to the large increase in bubble rise velocity in viscoelastic liquids during the transition (5- to 10-fold increase) as compared to the increase in a Newtonian system (1.5-fold). This question is discussed in details in the introduction of Chapter IV, and a qualitative explanation is presented based on a "slow flow" asymptotic analysis of the problem in Appendix A. The remaining question is about the abruptness of the velocity transition. Two possible explanations to this phenomenon are given in Section F of Chapter IV.

Finally, in Chapter III the streamline flow visualization experiments for a viscoelastic liquid past a solid sphere is presented. The motivation for these experiments is two-fold. First, a detailed picture of the flow field around a solid sphere moving in a viscoelastic liquid may be useful in explaining the above-mentioned phenomena associated with the bubble motion in viscoelastic liquids. The second motivation

is to resolve an apparent controversy between the theoretical and experimental work of Ultman and Denn (1970)*, and the work of Leslie (1961), Caswell and Schwarz (1962), Giesekus (1963) and Broadbent and Mena (1974). This controversy centers around the magnitude and the direction of viscoelastic effects on the streamline configuration. Ultman and Denn (1970) claim that the streamlines for a viscoelastic flow past a solid sphere or cylinder are shifted considerably in the upstream direction as a result of fluid elasticity. On the other hand, the results of Leslie's analysis indicate an extremely small downstream shift in the streamlines. Several experiments are conducted with solid spheres moving in viscoelastic liquids with varying viscoelasticity. The results indicate that there indeed is an upstream shift in the streamlines with fluid elasticity, but this shift is quite small, contrary to Ultman and Denn's claim.

* See Chapter III for references

CHAPTER II

DISSOLUTION OF A STATIONARY GAS BUBBLE IN A QUIESCENT, VISCOELASTIC LIQUID

Dissolution of a Stationary Gas Bubble in a Quiescent, Viscoelastic Liquid

E. Zana and L. G. Leal

Chemical Engineering

California Institute of Technology

Pasadena, California 91109

ABSTRACT

The problem of diffusion-induced collapse of a spherical bubble is studied theoretically for both a Newtonian liquid and a viscoelastic liquid of the modified Oldroyd fluid B type. Full numerical and approximate analytical solutions are obtained in order to investigate the roles of shear viscosity, relaxation and retardation times, surface tension and the Henry's law constant on the bubble collapse process. It is shown that the collapse characteristics and the behavior of the internal bubble pressure in the viscoelastic liquid differ considerably from the case of a purely Newtonian liquid, particularly during the early and late stages of the dissolution process.

INTRODUCTION

Dissolution of stationary, spherical bubbles in an ambient suspending liquid has been the subject of a rather large number of investigations, due primarily to its importance in chemical process and design technology. However, the majority of the studies to date have been confined to the collapse of bubbles (or cavities) by mass transfer in the absence of any hydrodynamic resistance, i.e. it was implicitly assumed that the viscosity of the liquid medium was sufficiently small that it did not effect the rate of bubble collapse (cf. Epstein and Plesset, 1950; Scriven, 1959; and Cable and Evans, 1967). The first attempt to include viscous effects was due to Barlow and Langlois (1962) who considered the growth of a stationary gas bubble in a Newtonian fluid due to the influx of dissolved gas from the liquid to the gas phase. Because of the complexity and non-linearity of the coupled diffusion and momentum equations, they did not obtain exact analytical or numerical solutions, but instead considered a simpler, ad hoc, approximation in which diffusion and hydrodynamic effects were assumed to be confined to a very narrow shell-like region immediately adjacent to the bubble surface. The resulting equations were solved numerically for a single value of viscosity and several values of initial bubble radius, but no systematic study of the effect of liquid viscosity on the bubble growth rate was reported.

The most noteworthy recent investigations are the study by Street (1968) who considered the growth of a spherical stationary cavity in a viscoelastic 3-constant Oldroyd fluid, and the related work of Fogler and Goddard (1970) who considered the collapse of a spherical cavity in a viscoelastic, linear-integral model of the generalized Maxwell type. In both cases, the driving mechanism for change of the cavity volume was assumed to be a simple

difference between the actual and equilibrium internal pressures. Since no mass transfer was considered, the cavity pressure was assumed to remain constant, hence greatly simplifying the analysis.

In the present work, we consider the diffusion-induced collapse of a spherical bubble in both a Newtonian and a viscoelastic ambient fluid. The study differs qualitatively from the prior investigations of Street (1968) and Fogler and Goddard (1970) in that the mass transfer process and the collapse-induced fluid flow are intimately coupled through the internal concentration of dissolving gas, and thus the internal pressure, which does not, in general, remain constant. Since the flow induced by a collapsing bubble is essentially a pure uniaxial extension, it may be anticipated that major changes should occur in mass transfer (bubble collapse) rates as the fluid becomes more viscoelastic. This conjecture is strongly supported by the present analysis. Surprisingly, however, in spite of the known enhancement of the steady elongational viscosity with increasing viscoelasticity, the elastic contributions can, in some circumstances, actually enhance the bubble collapse rate. In addition, even the Newtonian viscosity can play a strong role in governing the overall bubble collapse rate. Considering the fact that all real liquids exhibit viscous or viscoelastic behavior, we believe that these results are of considerable practical importance, as well as being of fundamental interest.

We begin by deriving the governing equations in a very general form, including variable pressure, liquid density, viscosity, elasticity and surface tension. After a brief discussion of viscoelastic constitutive equations leading to the choice of a modified 3-constant Oldroyd model, the governing equations are systematically non-dimensionalized in order to gain

further insight into the relative importance of the various phenomena which enter into the diffusion-induced collapse problem. Next, exact numerical solutions are obtained for the limiting case of a stationary spherical bubble in the absence of fluid inertia, this representing the first term in a full asymptotic solution valid for $Pe \ll 1$, $Sc \gg 1$. The dimensionless parameters governing the rate of diffusion, the viscosity, the elasticity and the surface tension are all varied over a wide range. Finally, an approximate analytical analysis is developed as a vehicle for understanding the results obtained from the numerical solutions.

THE GOVERNING EQUATIONS

We begin by considering the general problem of the dissolution of a spherical gas bubble which is rising by buoyancy through a viscoelastic ambient fluid. We assume that the bubble rises with a velocity $U_\infty g(t)$, where $g(t)$ is a monotonically decreasing function of time which is required to account for the decreasing buoyancy force as the bubble volume decreases, and possibly also time-dependent effects in the suspending fluid caused by the unsteady nature of the bubble motion. We shall utilize a spherical coordinate system $(r, \bar{\theta}, \bar{\phi})$ which is fixed with respect to the center of the bubble. In this system the bubble surface at any time t is simply denoted as $R = af(t)$. For convenience, U_∞ and a may be taken as the velocity of rise and the bubble radius at $t = 0$.

With these conventions, the governing momentum, continuity and convective-diffusion equations are simply

$$\rho\left\{\frac{\partial \vec{u}}{\partial t} + \vec{u} \cdot \nabla\vec{u}\right\} = -\nabla p + \nabla \cdot \underline{\underline{\tau}} \tag{1}$$

$$\frac{\partial \rho}{\partial t} + \vec{u} \cdot \nabla\rho + \rho\nabla \cdot \vec{u} = 0 \tag{2}$$

$$\frac{\partial c}{\partial t} + \vec{u} \cdot \nabla c + c(\nabla \cdot \vec{u}) = D\left[\nabla \cdot \left(\rho\dot{\nabla}\left(\frac{c}{\rho}\right)\right)\right] \tag{3}$$

which must be solved subject to the boundary conditions

$$\left.\begin{aligned} c &\to 0 \\ u_r &\to U_\infty g(t)\cos\theta \\ u_\theta &\to -U_\infty g(t)\sin\theta \end{aligned}\right\} \quad r \to \infty \tag{4a}$$

and

$$\left.\begin{aligned} c &= c_a(t) \\ u_r &= u_a(t) \\ \tau_{r\theta} &= 0 \end{aligned}\right\} \quad \text{at} \quad r = af(t) \tag{4b}$$

Here, $u_a(t)$ and $c_a(t)$ are the velocity of the liquid phase and the concentration of dissolved gas in the liquid, both evaluated at the bubble-liquid interface. In writing the boundary conditions (4a) and (4b), we have anticipated that $u_\phi \equiv 0$ and that the velocity and concentration fields will be independent of the azimuthal angle ϕ. Furthermore, we have neglected the possibility of buoyancy-induced convection as a result of gradients of c in the liquid phase. In order to make further progress, it is necessary to specify the constitutive relation for $\underline{\underline{\tau}}$, as well as additional relationships which may be used to determine g(t), f(t), c_a and u_a.

a. The Constitutive Model

In the analysis of transport problems involving viscoelastic liquids, it is clearly essential to employ a constitutive equation of state that is capable of reproducing the experimentally observed characteristics of the fluid at least in those viscometric flows which are related to the problem in question. Relevant to the dissolution of a rising spherical gas bubble are realistic behavior for the shear viscosity, the primary and secondary normal stress differences (particularly N_1), the relaxation and growth of shear and normal stresses, and both transient and steady characteristics of the elongational viscosity for uniaxial extension as a function of the rate of elongation. Other than realistic transient characteristics in unsteady extensional flows, all of these features have been considered in recent attempts to evaluate and classify various proposed constitutive models (cf. Huppler, MacDonald, Ashare, Spriggs, Bird and Holmes, 1967; Huppler, Ashare and Holmes, 1967; and Spriggs, Huppler and Bird, 1966). A model which represents all of the observed characteristics at least qualitatively (Spriggs, Huppler and Bird, 1966) is the Oldroyd (1958) eight-constant

differential model

$$\tau_{ik} + \lambda_1 \frac{\mathcal{D}\tau_{ik}}{\mathcal{D}t} + \mu_o \tau_{jj} e_{ik} - \mu_1 (\tau_{ij} e_{jk} + \tau_{jk} e_{ij}) + \nu_1 \tau_{j\ell} e_{j\ell} \delta_{ik}$$
$$= 2\eta_o \left\{ e_{ik} + \lambda_2 \frac{\mathcal{D}e_{ik}}{\mathcal{D}t} - 2\mu_2 e_{ij} e_{jk} + \nu_2 e_{j\ell} e_{j\ell} \delta_{ik} \right\} \tag{5}$$

Here, $\underline{\underline{e}}$ is the rate of strain tensor, and $\mathcal{D}/\mathcal{D}t$ is the Jaumann derivative, defined as

$$\frac{\mathcal{D}a_{ik}}{\mathcal{D}t} = \frac{\partial a_{ik}}{\partial t} + u_j \frac{\partial a_{ik}}{\partial x_j} + \omega_{ij} a_{jk} + \omega_{kj} a_{ij}$$

where $\underline{\underline{\omega}}$ is the vorticity tensor. Unfortunately, in its most general form the model is of limited value in solving actual fluid flow problems. It is highly non-linear and has a relatively large number of material constants, some of which cannot be measured in any of the common rheometers. Oldroyd himself suggested two simplified versions, the so-called fluids A and B, which were "designed" to predict negative and positive Weissenberg climbing effect, respectively. Other simplified versions of (5) have been suggested by more recent investigators, notably Williams and Bird (1962). Of these various models, perhaps the most successful is the modified fluid B, suggested by Walters (1970) and Barnes, Townsend and Walters (1969), in which

$$\lambda_1 = \mu_1 > \lambda_2 = \mu_2 \; ; \quad \mu_o \neq 0 \; , \quad \nu_1 = \nu_2 = 0 \quad . \tag{6}$$

It is this model which we adopt for the present study. In addition to the positive Weissenberg climbing effect, it gives $N_1 > 0$ and increasing with shear rate, $N_2 = 0$, a shear-rate dependent shear viscosity

$$\eta(\gamma) = \eta_o \left[\frac{1 + \lambda_2 \mu_o \gamma^2}{1 + \lambda_1 \mu_o \gamma^2} \right] \tag{7}$$

and an elongational viscosity which increases with elongation rate, $\dot{e}$, in a steady uniaxial extensional flow,

$$\frac{\bar{\eta}}{\eta_\infty} = 3\,\frac{1 - 2\lambda_2\dot{e}(1 + 4\lambda_1\dot{e})}{\left[1 - 4\dot{e}\left(\lambda_1 - \frac{\mu_o}{2}\right)\right]\left[1 + 2\dot{e}\left(\lambda_1 - \mu_o\right)\right]} \tag{8}$$

for $\dot{e} < 1/4\left(\lambda_1 - \frac{\mu_o}{2}\right)$. In addition, Townsend (1973) has demonstrated realistic stress relaxation and retardation behavior in numerical calculations of a simple channel flow. Finally, the model has the added advantage for numerical studies of complex flow problems that the effect of elasticity can be studied with or without the presence of a shear-dependent viscosity since the latter can be suppressed simply by setting μ_o equal to zero, without significantly altering other viscoelastic features of the model. For all of these reasons, we adopt the modified Oldroyd fluid B for the present work.

Although it is our intention (forthcoming publication) to extend the analysis of the present paper to include the influence of free-stream convective effects, it will be shown in the next section that the first approximation for small Pe which we consider here is dominated by the purely radial flow which is induced by the collapsing bubble. In this case, the fluid motion is equivalent to a simple, unsteady uniaxial extension (cf. Fogler and Goddard, 1970). Consequently, the most important features of the model for our present purposes are its behavior in transient and steady elongational motion. These features are discussed in more detail in the appendix.

b. Mass, Volume and Force Balances

In addition to the governing equations (1) - (4) and the constitutive equation of state (5) (subject to (6)), five additional macroscopic relationships are necessary to close the system. These are:

i) A mass balance at the bubble-liquid interface

ii) A volume balance on the entire bubble-liquid system

iii) A force balance on the bubble (drag - buoyancy)

iv) A force balance at the bubble-liquid interface

v) Henry's Law

The balance (ii) leads to an expression for the radial source velocity including its magnitude at the bubble surface, $u_a(t)$, while the mass balance (i) is used to obtain a relationship between the radius function $f(t)$ and the concentration $c_a(t)$. Although the derivations basically parallel the work of Ready and Cooper (1966), we do not assume that the bubble gas concentration is constant. In fact, we shall show later that it can vary widely as a function of time. The analysis of Ready and Cooper (1966) was based upon the assumption of no viscous or elastic resistance to the bubble collapse, and hence constant gas concentrations.

We begin by considering the balance (i) between the instantaneous rate of loss of gas bubble mass and the flux density of gas at the interface,

$$\frac{dm_b}{dt} + \int_S j_a^* dS = 0 \tag{9}$$

where m_b is the bubble mass $\left(\frac{4}{3}\pi a^3 f^3 c_b\right)$, and j_a^* represents the flux density of gas at $r = af(t)$ measured relative to the moving interface. Here, S is the spherical surface area at $r = af(t)$ and c_b is the concentration of gas inside the bubble. The flux density of the dissolved gas molecules in the solution, j_a, is related to j_a^*;

$$j_a^* = j_a + c_a\left(u_a - a\frac{df}{dt}\right) \tag{10}$$

where j_a is given by the Fick's law

$$j_a = -\frac{D}{1 - \gamma c_a}\left(\frac{\partial c}{\partial r}\right)_{r=af} \tag{11}$$

and $\gamma = \bar{v}_A - \bar{v}_B$, where $\bar{v}_A$ and $\bar{v}_B$ are the partial specific volumes of gas (solute) and liquid (solvent) in solution, respectively. Substituting (10) and (11) into (9), and using Henry's law, $c_a = kc_b$, to relate c_a and c_b, we finally obtain

$$c_a\dot{f} + \frac{1}{3} f\dot{c}_a = -\frac{k}{2a}\int_0^{\pi}\left\{c_a[u_a - a\dot{f}] - \frac{D}{1-\gamma c_a}\left(\frac{\partial c}{\partial r}\right)_{af}\right\}\sin\theta d\theta \qquad (12)$$

The radial source velocity (including u_a) is obtained from a volume balance on the entire gas-liquid system (ii)

$$\int_{S_r} u_r dS = 4\pi a^3 f^2\left[\dot{f} - \frac{\bar{v}_A}{k}\left(c_a\dot{f} + \frac{1}{3} f\dot{c}_a\right)\right] + \int_{S_r}\frac{\gamma D}{1-\gamma c}\left(\frac{\partial c}{\partial r}\right)_r dS \qquad (13)$$

Here, S_r represents an arbitrary spherical surface centered about the bubble and having a radius r. The term on the left hand side is simply the net volume influx by bulk motion at a radius r, while the terms on the right are, respectively, the rate of change of bubble volume, the rate of change of the liquid volume due to the dissolved gas and the rate of change of liquid volume due to the efflux of dissolved gas by diffusion at r. Further progress requires detailed information regarding the functional forms of u_r and c on this surface, and we shall return to both (12) and (13) at a later stage when this information is available.

Finally, internal bubble pressure may be simply related to the pressure and stress fields in the liquid phase, as

$$p_B = \left(p - \tau_{rr}\right)_{r=af} - \frac{2\sigma}{af} \quad . \qquad (14)$$

Relating bubble pressure to bubble gas concentration through the ideal gas law and combining the result with Henry's law, equation (14) also leads to a relationship between the surface concentration c_a in the liquid and the

pressure and stress fields. It is perhaps worth noting here that the bulk rheology enters the relationship (14) directly and thus plays an important and often controlling role in the dependence of internal bubble conditions on the external dynamics.

In general, an additional relationship between the hydrodynamic drag and the buoyancy force would also be necessary to relate g(t) and f(t). However, in the present investigation we will limit our detailed analysis to the asymptotic limit $Pe \to 0$ in which g(t) only appears at higher orders in Pe, making this last relationship redundant.

Although the equations (12) - (14) will later be simplified somewhat for the particular limiting case considered here, they are sufficient as they stand when combined with equations (1) - (5) to provide a complete description of the dissolution of gas bubbles in a modified Oldroyd visco-elastic fluid B.

c. Dimensional Analysis

At this stage, it is useful to consider the dimensionless form of the governing equations in order to gain further insight into the relative importance of the various phenomena which enter into the problem. For brevity we shall temporarily confine our attention to the original equations (1) - (4).

We begin by introducing the most obvious non-dimensional variables

$$\bar{r} = \frac{r}{a} \qquad \vec{\bar{u}} = \frac{\vec{u}}{U_\infty} \qquad \bar{p} = \bar{p}\left(\frac{\eta_o U_\infty}{a}\right)$$
$$\theta = \frac{c}{c_a(t)} \qquad \bar{t} = \frac{D}{a^2} t \quad . \tag{15}$$

The proper choice for the characteristic pressure depends, of course, on whether or not the flow is dynamically slow and thus we have anticipated our subsequent analysis by using the viscous pressure $(\eta_o U_\infty/a)$. The

characteristic time, a^2/D, is chosen since the time-dependence of the bubble motion is completely due to the diffusion-induced collapse. Substituting (15) into (1)-(4), we obtain

$$\frac{1}{Pe}\frac{\partial \vec{\bar{u}}}{\partial \bar{t}} + \vec{\bar{u}} \cdot \nabla \vec{\bar{u}} = \frac{1}{Re}\left[-\nabla \bar{p} + \nabla \cdot \underline{\underline{\tau}}\right] \tag{16}$$

$$\frac{1}{Pe}\left\{\frac{\partial \theta}{\partial \bar{t}} + \left(\frac{\dot{\theta}_a}{\theta_a}\right)\theta\right\} + \vec{\bar{u}} \cdot \nabla\theta + \theta\nabla \cdot \vec{\bar{u}} = \frac{1}{Pe}\nabla^2\theta \tag{17}$$

with boundary conditions

$$\left.\begin{aligned} &\bar{u}_r \to g(\bar{t})\cos\theta \\ &\bar{u}_\theta \to -g(\bar{t})\sin\theta \end{aligned}\right\} \text{ as } \bar{r} \to \infty \tag{18a,b}$$

$$\theta \to 0 \tag{18c}$$

$$\left.\begin{aligned} &\bar{u}_r = \bar{u}_a(\bar{t}) \\ &\bar{\tau}_{r\theta} = 0 \end{aligned}\right\} \quad r = f(t) \tag{18d,e}$$

$$\theta = 1 \tag{18f}$$

In the next section, it will be shown, using equation (13), that

$$u_a(t) \sim a\frac{\partial f}{\partial t}$$

provided the specific volume of the solute (dissolving gas) is much smaller in the liquid phase than in the gas phase, and that γ (equation 11) is negligibly small (both tolerable assumptions for gas bubbles). Hence, nondimensionalizing according to (15), it follows

$$\bar{u}_a(\bar{t}) = \frac{1}{Pe}\frac{\partial f}{\partial \bar{t}} \tag{19}$$

Depending on the magnitude of Pe, two distinct asymptotic cases may now be identified.

i) Pe >> 1; forced convection mass-transfer in which the velocity field is dominated by the free streaming motion which is due to the buoyancy-driven bubble rise. The induced velocity due to bubble collapse is, in this case, asymptotically small according to (20), while the significant variations in the concentration θ are confined to a thin diffusion boundary layer adjacent to the bubble surface. For a Newtonian fluid at high or low Re, the solution for θ is well-known. The difficult extension to a non-Newtonian suspending fluid will not be pursued here.

ii) Pe << 1; forced convection mass-transfer in which the velocity field is dominated by the motion induced by the bubble collapse. Although the characteristic scales inherent in (15) do provide a perfectly general formulation for arbitrary values of the Peclet number, they are clearly inconvenient for the limiting case $Pe \to 0$, since according to equation (19), $\bar{u}_a \to \infty$ at the bubble surface. The difficulty is that, as $Pe \to 0$, the collapse-induced velocity at the bubble surface becomes asymptotically large relative to the characteristic velocity of rise, U_∞, which is therefore inappropriate as the characteristic velocity scale. For convenience, we therefore rescale the velocity using the magnitude of the induced radial velocity component as the characteristic velocity scale, i.e.

$$u_c = \frac{D}{a}$$

With this rescaling, the equations (17) - (19) become (after dropping the overbars)

$$\frac{\partial \vec{u}}{\partial t} + \vec{u} \cdot \nabla \vec{u} = Sc(-\nabla p + \nabla \cdot \underline{\underline{\tau}}) \qquad (20)$$

$$\frac{\partial\theta}{\partial t} + \left(\frac{\dot{\theta}_a}{\theta_a}\right)\theta + \vec{u} \cdot \nabla\theta + \theta\, \nabla\cdot \vec{u} = \nabla \cdot [\rho\nabla(\theta/\rho)] \qquad (21)$$

with the boundary conditions at infinity

$$u_r \to Pe\ g(t)\cos\theta \qquad (22a)$$

$$u_\theta \to -Pe\ g(t)\sin\theta \qquad (22b)$$

$$\theta \to 0 \qquad (22c)$$

and at the bubble-liquid interface, $r = f(t)$

$$u = u_a(t) \qquad (22d)$$

$$\tau_{r\theta} = 0 \qquad (22e)$$

$$\theta = 1 \qquad (22f)$$

Hence, as we have noted earlier, the problem for small Pe reduces to convective-diffusion induced collapse of a stationary gas bubble in a viscoelastic liquid. Physically, this limit may be thought of as arising in the case of rapid mass transfer in a highly "viscous" fluid. Furthermore, for most liquids the Schmidt number, Sc, is $O(10^3)$ or higher, so that of the two possible limits $Sc \gg 1$ or $Sc \ll 1$, it is the former problem, $Sc \gg 1$ and $Pe \ll 1$, which we shall discuss in detail in the present communication.

ASYMPTOTIC ANALYSIS FOR SMALL Pe

We consider the case Pe << 1, Sc >> 1 with 1/Sc << Pe. Thus, we assume that the nonlinearities due to inertia effects in (16) are of less importance than those inherent in $\underline{\underline{\tau}}$ at higher orders in Pe. The solution is most conveniently obtained as an asymptotic expansion in Pe of the form

$$A = A_o + PeA_1 + \ldots \tag{23}$$

where A stands for any of the variables $\vec{u}$, p, θ, f(t), $\theta_a(t)$, ρ or $\underline{\underline{\tau}}$, which is relevant to the problem. It may be noted, as indicated in the preceding section, that the velocity field $\vec{u}_o$ is simply the "source" solution corresponding to a mass sink at the origin, so that $\vec{u}_o = \vec{i}_r U_r^{(0)}$ and θ_o are both functions of radial position r and time t, but are independent of the polar angles θ, ϕ. Hence, substituting the expansions (23) with $u_r^{(0)} = u_o(r,t)$ and $\theta^{(0)} = \theta_o(r,t)$, into the governing equations (20) - (22), and the modified Oldroyd fluid B constitutive equations (5) and (6), we obtain at first order in Pe

$$\frac{\partial p^{(0)}}{\partial r} = \frac{\partial \tau_{rr}^{(0)}}{\partial r} + \frac{2}{r}\left(\tau_{rr}^{(0)} - \tau_{\theta\theta}^{(0)}\right) \tag{24}$$

$$\underline{\underline{\tau}}^{(0)} + N_{\lambda_1}\left\{\frac{\partial \underline{\underline{\tau}}^{(0)}}{\partial t} + u_r^{(0)}\frac{\partial \underline{\underline{\tau}}^{(0)}}{\partial r} - 2\underline{\underline{e}}^{(0)} \cdot \underline{\underline{\tau}}^{(0)}\right\} + N_{\mu_o} tr\left(\underline{\underline{\tau}}^{(0)}\right)\underline{\underline{e}}^{(0)}$$

$$= 2N_{\mu}\left\{\underline{\underline{e}}^{(0)} + N_{\lambda_2}\left\{\frac{\partial \underline{\underline{e}}^{(0)}}{\partial t} + u_r^{(0)}\frac{\partial \underline{\underline{e}}^{(0)}}{\partial r} - 2\underline{\underline{e}}^{(0)} \cdot \underline{\underline{e}}^{(0)}\right\}\right\} \tag{25}$$

$$\frac{\partial \theta^{(0)}}{\partial t} + u_r^{(0)}\frac{\partial \theta^{(0)}}{\partial r} + \frac{\dot{\theta}_a^{(0)}}{\theta_a^{(0)}}\theta^{(0)} = \frac{\partial^2 \theta^{(0)}}{\partial r^2} + \frac{2}{r}\frac{\partial \theta^{(0)}}{\partial r} \tag{26}$$

with boundary conditions on $\vec{u}_o$ and θ_o

$$\left.\begin{array}{l} \vec{u}_o \to 0 \\ \theta_o \to 0 \end{array}\right\} \quad \text{as } r \to \infty \tag{27}$$

and

$$\left.\begin{array}{l} (u_o)_r = u_a(t) \\ \tau_{r\theta}^{(0)} = 0 \\ \theta_o = 1 \end{array}\right\} \quad \text{at } r = f(t) \tag{28}$$

Here,

$$N_{\lambda_1} \equiv \lambda_1/(a^2/D)$$

$$N_{\lambda_2} = \lambda_2/(a^2/D)$$

$$N_{\mu} = \eta_o/(p_\infty a^2/D)$$

$$N_{\mu_o} = \mu_o/(a^2/D)$$

It should be noted for later reference that N_{λ_1} and N_{λ_2} are simply the intrinsic relaxation and retardation time scales for the fluid, non-dimensionalized with respect to the diffusional time scale (a^2/D).

Using the simplified forms (24)-(26) , the expansion (23), and the dependence of $u_r^{(0)}$ and $\theta^{(0)}$ on only r and t, the macroscopic balances (12) - (14) may now also be written in a simpler form. First, the equation (14) may be combined with (24), in dimensionless form, to obtain

$$\theta_a^{(0)}(t) = 1 + N_\sigma \frac{2}{f^{(0)}(t)} - 2\int_{r=f}^{\infty} \frac{1}{r}\left[\tau_{rr}^{(0)} - \tau_{\theta\theta}^{(0)}\right]dr \tag{29}$$

with $N_\sigma \equiv \sigma/(ap_\infty)$. Second, the O(1) radial velocity component $u_r^{(0)}$ may now be obtained from the volume balance, equation (13). In particular, introducing expansions of the form (23) into equation (13) and integrating, we obtain (in dimensional form),

$$u_r^{(0)} = \frac{a^3 f^{(0)^2}}{r^2}\left|\dot{f}^{(0)} - \frac{\bar{v}_A}{k}\left[c_a^{(0)}\dot{f}^{(0)} + \frac{1}{3} f^{(0)}\dot{c}_a^{(0)}\right]\right| + \frac{\gamma D}{1 - \gamma c^{(0)}}\left[\frac{\partial c^{(0)}}{\partial r}\right]_r \tag{30}$$

Furthermore, combining (22d), (12) and (30), we obtain

$$c_a^{(0)}\dot{f}^{(0)} + \frac{1}{3} f^{(0)}\dot{c}_a^{(0)} = k\frac{D}{a}\left[\frac{\partial c^{(0)}}{\partial r}\right]_{af} - c_a\bar{v}_a\left[c_a^{(0)}\dot{f}^{(0)} + \frac{1}{3} f\dot{c}_b^{(0)}\right] \tag{31}$$

Nondimensionalizing and rearranging, the equations (30) and (31) may be rewritten in the form

$$u_r^{(0)} = \frac{f^{(0)^2}}{r^2}\dot{f}^{(0)} - \beta\frac{f^{(0)^2}}{r^2}\left[\theta_a^{(0)}\dot{f}^{(0)} + \frac{1}{3} f^{(0)}\dot{\theta}_a^{(0)}\right] + \frac{\gamma c_a^{(0)}}{1 - \gamma c_a^{(0)}\theta^{(0)}}\left[\frac{\partial\theta^{(0)}}{\partial r}\right]_r \tag{32a}$$

and

$$\dot{f}^{(0)} = k\left[\frac{\partial\theta}{\partial r}\right]_f - \frac{1}{3} f^{(0)}\frac{\dot{\theta}_a^{(0)}}{\theta_a^{(0)}} + \beta k\left[\theta_a{}^{(0)}\dot{f}^{(0)} + \frac{1}{3} f^{(0)}\dot{\theta}_a{}^{(0)}\right] \tag{33a}$$

where $\beta\left(\equiv \bar{v}_A/\bar{v}_s\right)$ is the ratio of the volume attributed to a mass of solute (gas) in the solution to the volume occupied by the same mass in the gaseous phase. Clearly, β can be of order one or larger for liquid drops or solid pellets dissolving in an ambient liquid, but it is very small for gas bubbles. Furthermore, if the solute and solvent have nearly the same partial specific volumes in the solution phase, γ is also negligibly small. Therefore, for gas bubbles satisfying these conditions, the equations (32a) and (33a) further simplify to

$$u^{(0)} = \frac{f^{(0)^2}}{r^2}\dot{f}^{(0)} \tag{32b}$$

$$\dot{f}^{(0)} = k\left[\frac{\partial\theta^{(0)}}{\partial r}\right]_f - \frac{1}{3} f^{(0)}\frac{\dot{\theta}_a^{(0)}}{\theta_a^{(0)}} \tag{33b}$$

Although these simplified equations are, at best, an approximation which

neglects the effects of specific volume change, we shall nevertheless utilize them for our subsequent analysis on the ground that the errors introduced will not fundamentally alter the relationship between bulk rheological properties and bubble dissolution, which is our prime interest.

The equations (25), (26), (32b), (33b) and (27) provide a complete description of the first asymptotic approximation for the dissolution of a gas bubble in a viscoelastic liquid for $Pe \ll 1$ and $Sc \gg 1$, and we shall discuss both exact numerical and approximate analytical solutions of these equations in the remainder of the present paper. Subsequent communications will consider the limit $Pe \gg 1$, as well as the second, $O(Pe)$, contribution to the present problem.

NUMERICAL SOLUTION SCHEME

It is now evident why no exact analytical or numerical solution has been found for the diffusion-induced collapse of a gas bubble in a viscoelastic liquid. Not only are the differential equations describing the system non-linear, but they are coupled with each other through f(t) and $r_a(t)$. Furthermore, the equations for f(t) and $r_a(t)$ are also coupled first order integro-differential equations.

Two potentially serious difficulties which enter into a numerical solution of the governing system of equations and boundary conditions are the movement of the bubble boundary, and the infinite extent of the bulk liquid phase. Associated with the second of these problems is the fact that very large gradients in concentration can exist near the bubble-liquid interface, particularly at short times, so that very small numerical mesh sizes are required in this region. Duda and Vrentas (1971) have, in fact, suggested that many of the inaccuracies of previous numerical solutions were due to inadequate resolution of concentration gradients near the bubble surface, while simultaneously attempting to fill the whole physical space domain with a uniform finite-difference mesh. For these reasons, we introduce a two-step change of variables, first from r to x, with

$$x = \frac{1}{3}\left[r^3 - f^3(t)\right] \tag{34}$$

and second, from x to y,

$$y = 1 - e^{-x} \quad . \tag{35}$$

The initial transformation (34) immobilizes the moving bubble boundary, and in addition, simplifies the modified Oldroyd constitutive model from a partial differential equation in r and t, to an

ordinary differential equation in t. The second transformation (35), maps the infinite fluid region in x into a finite region in y ($0 \leq y \leq 1$).

Introduction of (34) and (35) into (32b), (33b), (25), (26) and (27) yields the following transformed set of equations:

$$\frac{\partial\theta}{\partial\tau} - \left[f^3(t) - 3\ell n(1-y)\right]^{4/3} \frac{\partial^2\theta}{\partial y^2} - 4\left[f^3(t) - 3\ell n(1-y)\right]^{1/3} \frac{\partial\theta}{\partial y} + \left(\frac{\dot{\theta}_a(t)}{\theta_a(t)}\right)\theta = 0 \tag{36}$$

$$N_{\lambda_1} \frac{\partial\tau_{rr}}{\partial\tau} + \left[1 + 4\gamma\left(N_{\lambda_1} - \frac{N_{\mu_o}}{2}\right)\right]\tau_{rr} + 4N_\mu\gamma\left\{1 + N_{\lambda_2}\left(\frac{\dot{\gamma}}{\gamma} + \gamma\right)\right\} - 4N_{\mu_o}\gamma\tau_{\theta\theta} = 0 \tag{37}$$

$$N_{\lambda_1} \frac{\partial\tau_{\theta\theta}}{\partial\tau} + \left[1 - 2\gamma\left(N_{\lambda_1} - N_{\mu_o}\right)\right]\tau_{\theta\theta} - 2N_\mu\gamma\left\{1 - N_{\lambda_2}\left(\frac{\dot{\gamma}}{\gamma} - 5\gamma\right)\right\} + N_{\mu_o}\gamma\tau_{rr} = 0 \tag{38}$$

$$\theta_a(t) = 1 + \frac{2N\sigma}{f(t)} - 2\int_0^1 \frac{\tau_{rr} - \tau_{\theta\theta}}{\left[f^3(t) - 3\ell n(1-y)\right]}\, dy \tag{39}$$

$$\dot{f}(t) = kf^2\left(\frac{\partial\theta}{\partial y}\right)_{y=0} - \frac{1}{3}\left(\frac{\dot{\theta}_a(t)}{\theta_a(t)}\right) f(t) \tag{40}$$

where

$$\gamma = f^2\dot{f}/\left[f^3 - 3\ell n(1-y)\right]$$

$$\dot{\gamma} = \left(2f\dot{f}^2 + f^2\ddot{f}\right)/\left[f^3(t) - 3\ell n(1-y)\right].$$

These equations are to be solved subject to the initial and boundary conditions

$\theta(0,t) = 1$ for all t

$\theta(1,t) = 0$ for all t

$\theta(y,0) = 0$ for all y, except $y = 0$

$\tau_{rr}(y,0) = 0$

$\tau_{\theta\theta}(y,0) = 0$

$f(0) = 1$

The initial conditions on τ_{rr}, $\tau_{\theta\theta}$ and θ arise from the assumptions of no motion and no mass transfer for $t \leq 0$.

a. Newtonian Fluid

The equations (36) - (40) can be further simplified for a Newtonian ambient fluid. In this case, the constitutive equations of state (37) and (38) reduce to the simple algebraic relationships

$$\tau_{rr} = -4N_{\mu}\gamma \tag{41}$$

$$\tau_{\theta\theta} = 2N_{\mu}\gamma \tag{42}$$

Using (41) and (42), the integral term in equation (39) can be readily evaluated to give

$$\theta_a(t) = 1 + \frac{2N\sigma}{f(t)} + 4N_{\mu}\frac{\dot{f}(t)}{f(t)} \tag{43}$$

During the developmental stage of the present work, this Newtonian problem was the first to be considered using (36), (40) and (43) with appropriate boundary conditions on θ. The equation (36) was approximated by the DuFort-Frankel explicit finite difference formulae, with the exception of the first time step, where a forward difference scheme had to be used for the time derivative. Given $(\partial\theta/\partial y)_{y=0}$, the coupled ordinary differential equations (40) and (43) were stepped forward in time using the Runge-Kutta method.

b. Viscoelastic Fluid

In the case of a viscoelastic fluid, the solution is more difficult. Here, the constitutive equations of state are no longer algebraic relationships, but ordinary differential equations; and the equation (39) is coupled to these equations through the integral, I,

$$I = \int_0^1 \frac{\tau_{rr} - \tau_{\theta\theta}}{[f^3(t) - 3\ell n(1 - y)]}\, dy \quad . \tag{44}$$

The diffusion equation was, once again, represented by a finite difference equation which is explicit in time, i.e. in solving for the concentration, θ, at the j^{th} step in time, the space derivatives are evaluated using the concentration values from the previous time step, $(j - 1)$. The constitutive equations of state, which may be expressed in the form

$$\frac{\partial \tau_{ii}}{\partial \tau} = F(\tau_{ii}, f, \dot{f}, \ddot{f}) \text{ where } i = r \text{ or } \theta \tag{45}$$

were approximated in finite difference form using an implicit scheme in order to insure reasonable numerical stability characteristics for the overall computation. Thus,

$$\frac{\tau_{ii}^{j} - \tau_{ii}^{j-1}}{\Delta t} = F\left(\tau_{ij}^{j}, f^{j}, \dot{f}^{j}, \ddot{f}^{j}\right) \tag{46}$$

where superscript j denotes the value at the j^{th} step in time. Hence, to calculate τ_{ii} at the j^{th} step, one must know f, $\dot{f}$ and $\ddot{f}$ at the same time step. The first derivative $\dot{f}^{j-1}$ is obtained from (40), and then used along with $(f)^{j-1}$ to calculate $(f)^{j}$, i.e.

$$f^{j} = f^{j-1} + \Delta t(\dot{f})^{j-1} \tag{47}$$

At this stage, the problem is reduced to solving the equations (46) and (39) for τ_{rr}, $\tau_{\theta\theta}$, and $\ddot{f}$ at the j^{th} time step. Since these equations cannot be reduced to a form where all the unknowns, τ_{rr}, $\tau_{\theta\theta}$ and $\ddot{f}$ are given explicitly in terms of known variables, a Newton-Raphson type iteration was used to obtain the solution. At the j^{th} step in time, the basic iteration is thus

i) Calculate the integral $(I)^{j}$ from equation (39), since $(f)^{j}$ and $(\theta_a)^{j}$ are already known at j^{th} time step, i.e.,

$$(I)^{j} = \frac{1}{2}\left\{1 + \frac{2N\sigma}{(f)^{j}} - (\theta_a)^{j}\right\} \tag{48}$$

ii) Guess $(\ddot{f})^{j}_{n=1}$ and calculate τ_{rr} and $\tau_{\theta\theta}$ from (46) using the guessed value of $(\ddot{f})^{j}_{n=1}$. Calculate the integral $(I)^{j}_{n=1}$ from its definition, equation (44). Here, the subscript "n" indicates the n^{th} approximation to the variable at j^{th} time step.

iii) Define a function

$$G^{j}_{n} = G\left\{(\ddot{f})^{j}_{n}\right\} = (I)^{j} - (I)^{j}_{n} \tag{49}$$

When $(I)^{j}_{n} = (I)^{j}$, $G^{j}_{n} = 0$. Therefore, the root of the function G at the j^{th} time step is $(\ddot{f})^{j}$. If $|G^{j}_{n}(\ddot{f}^{j}_{n})| > \varepsilon$, where $\varepsilon << 1$ is a specified tolerance, then a better approximation to $(\ddot{f})^{j}$ is given by

$$(\ddot{f})^{j}_{n+1} = (\ddot{f})^{j}_{n} - G\left\{(\ddot{f})^{j}_{n}\right\}/G'\left\{(\ddot{f})^{j}_{n}\right\}$$

where the derivative of G, $G'\left\{(\ddot{f})^{j}_{n}\right\}$, is calculated numerically from

$$(G')^{j}_{n} = \left[G'\left\{(\ddot{f})^{j}_{n} + \alpha\right\} - G'\left\{(f)^{j}_{n}\right\}\right]/\alpha \ , \ \alpha << 1 \tag{50}$$

iv) Repeat steps (ii)-(iii) using the updated value of $(\ddot{f})^{j}_{n+1}$ until $|(G)^{j}_{n+1}| < \varepsilon$. A standard Simpson integration rule was used to calculate the integral, I.

The radial mesh and the time step sizes were varied to insure that the results obtained did not depend on them. It was found out that much smaller time steps were needed at the beginning of the dissolution process due to the rapid initial collapse of the bubble which was caused by the extremely large initial concentration gradients at the bubble-solution interface. Therefore, the integration was started with very small time steps and the size of these steps was increased as the bubble dissolution process continued.

In addition, the finite difference approximation to the concentration gradient at the bubble surface was improved by using a four-point Lagrange's interpolation technique instead of a simple forward difference formula.

There was a further difficulty in initiating the integration as it was necessary to specify not only f at t = 0, but also $\dot{f}(0)$. The sensitivity of the solution to the initial value of $\dot{f}$ was checked for the Newtonian case, and it was found out that the solutions for concentration field, bubble radius and pressure converged to the same value after five to ten time steps for different start-up values of $\dot{f}$. In the viscoelastic problem, the solution is affected for longer times, of order λ_1. However, it will be shown in the approximate analysis of the viscoelastic problem that the contribution of $\dot{f}(0)$ to the solution of f(t) is of a form which has no qualitative effect on the results but only a non-essential quantitative effect for times $t = 0(\lambda_1)$. Therefore, a value of zero was used for $\dot{f}(0)$.

The numerical scheme of this study was checked against the previous work of Cable and Evans (1967), and Duda and Vrentas (1971) on the bubble dissolution in an inviscid liquid by setting the viscous, elastic and surface tension parameters equal to zero. Unfortunately, there was no work in the literature on the bubble dissolution in Newtonian or viscoelastic fluids to compare our results against. The agreement with Duda and Vrentas' work, which is the more accurate of the two shown in table 1 and figure 1, is excellent.

NUMERICAL RESULTS

There are basically six independent dimensionless parameters controlling the rate of bubble dissolution; N_{μ}, N_{σ}, N_{μ_o}, N_{λ_1}, N_{λ_2} and k.

As we have previously suggested, the chief role of N_{μ_o} is to confer a deformation rate-dependent shear viscosity to the behavior of the modified fluid B. For uniaxial extension at steady state, N_{μ_o} also has the non-essential effect (for our purposes) of increasing the so-called critical rate of elongation which we discuss in detail in the appendix. In unsteady uniaxial extension, the chief additional effect associated with nonzero values of N_{μ_o} is the possibility for $\mu_o > \frac{3}{4}\lambda_1$ of sinusoidal oscillations, superposed on the main exponential transient terms. Again, this effect is of secondary interest for our present purposes. For simplicity, in the present study, we have thus set $N_{\mu_o} = 0$.

The Henry's law constant, k, enters the theory as the constant of proportionality between the rate of change of the bubble radius, $\dot{f}$, and the concentration gradient for mass transfer. Thus, for relatively large values of k, it may be anticipated that the rate of bubble collapse will tend to be limited chiefly by the fluid rheology rather than by the rate of mass transfer. On the other hand, for small k, or for very weak viscous or elastic effects, the rate of collapse may be completely controlled by the mass transfer process. In order to illustrate the role of the Henry's law constant more clearly, we have made a limited number of calculations which are presented as figures 2 and 3. The former shows bubble radius as a function of time and the second, the time-dependence of the internal bubble pressure. There are four curves in each figure, two each for k = 0.1 and 1.0 with fixed N_{λ_1}, N_{σ} and N_{μ}, but with N_{λ_2} = 0.1 and 0.01 in each case (hence, there are

two values of $N_{\lambda_2}/N_{\lambda_1}$ for each k). For k = 1, the two cases N_{λ_2} = 0.1 and 0.01 differ significantly. For the smaller value of k, however, the bubble collapse is totally controlled by the mass-transfer process, and the two curves for N_{λ_2} = 0.1 and 0.01 are completely indistinguishable. In the present investigation, we are primarily interested in determining the role of the rheological properties of the fluid, and of the surface tension, on the rate of bubble collapse. Hence, the remainder of the numerical solutions which we shall discuss here were obtained for k = 1.

It may also be noted from figure 3 that the bubble pressure remains nearly constant at its initial value for k = 0.1. This is very interesting since all the previous investigators, studying the bubble collapse in the absence of viscous and elastic effects, have simply assumed that in diffusion induced bubble collapse, the boundary moves at the precise rate required to keep the bubble pressure constant. The numerical results of our work, where the bubble pressure was allowed to vary, do indeed provide a limited verification for the validity of that assumption provided k is small. However, it is also clear from the curves for k = 1 that in the presence of significant viscous and/or elastic effects, the bubble pressure can no longer be assumed to remain constant.

Given the complexity of the numerical calculation and the large number (4) of remaining parameters, it is still not feasible to exhaustively blanket the whole parameter space. Instead, we present only a reasonably small number of selected parameter variations, which we believe to illustrate the main effects of bulk rheology and surface tension on the bubble collapse rate.

a. The role of viscosity in a Newtonian fluid

We begin by briefly considering the dependence of bubble collapse rates on the viscosity of the bulk phase for the simple case of a Newtonian fluid

($N_{\lambda_1} = N_{\lambda_2} = 0$) with N_σ held constant. A plot of bubble radius versus time is shown in figure 4 for several values of N_μ. The rate of collapse may be seen to decrease rather sharply with increasing bulk viscosity. This is not surprising, of course, since the increased viscosity increases the "resistance" of the liquid phase to the bubble boundary motion. The significant feature is the magnitude of the viscous effect. For example, an order of magnitude increase in N_μ more than triples the bubble lifetime.

b. The role of elasticity

The effect of elasticity on the bubble collapse process is more interesting. A plot of bubble radius as a function of time for $N_\mu = 0.1$, $N_\sigma = 0.001$ and $N_{\lambda_1} = 0.1$ is shown in figure 5 for three different values of $N_{\lambda_2} = 0.1$, 0.05 and 0.01. It may be noted, first of all, that the curves cross each other at a dimensionless time of approximately 0.1. Thus, a decrease in N_{λ_2} with constant N_{λ_1} actually contributes to an increased rate of bubble collapse during the initial stages of the collapse process, but then acts to retard the bubble motion for the remainder of the bubble's lifetime. It was pointed out earlier that the fluid flow induced by collapse of a spherical stationary bubble is an unsteady uniaxial extension. Therefore, one would expect the elastic influence on the collapse process to be a direct consequence of its influence on the elongational viscosity $\bar{\eta}$. We have shown in the appendix that $\bar{\eta}$ is an increasing function of the rate of elongation for fixed N_{λ_1}, N_{λ_2} and steady flow, and is also increasing for either increasing N_{λ_1} or decreasing N_{λ_2} provided $N_{\lambda_2} \leq N_{\lambda_1}$. As a result of the enhancement of $\bar{\eta}$ with decrease of N_{λ_2} for steady flow, one would expect the bubble to collapse more slowly as N_{λ_2} is decreased, provided changes in the induced flow occur sufficiently slowly. This is precisely what is observed for times $t \geq 0.1$. Clearly, the enhanced collapse rate with decreased N_{λ_2} for

$t < 0.1$ cannot be explained in terms of the increase in steady-state elongational viscosity. However, it can be simply understood in a qualitative sense by considering the transients associated with stress growth which are discussed in the appendix. Recall that this is a start-up problem, i.e. initially the bubble is stationary and there is no fluid motion. Therefore, when the bubble boundary is set to motion at $t = 0$ by mass-transfer, there is a transient period of stress growth with an approximate time scale of the order of the intrinsic (stress) relaxation time N_{λ_1}. During this period, the instantaneous resistance to motion is less than it would be at steady-state in the same fluid with the same elongation rate $\dot{e}$ and consequently the collapse rate overshoots its corresponding steady-state value. Ultimately, as the stresses build up, they too overshoot causing the elongation rate to decrease until it finally approaches a slowly varying state in which the steady elongational viscosity is effective in governing the collapse rate. In figure 6 we have plotted $\dot{f}/f$ as a function of time for the same cases that were shown in figure 5. It is clear that, (a) the magnitude of the overshoot in deformation rate increases with decrease of N_{λ_2}, holding N_{λ_1} fixed; (b) the time of maximum overshoot decreases in the same circumstances. Furthermore, as indicated in figure 7, the elastic overshoot is damped to a great extent by viscosity. Finally, in figure 8 we have plotted the total axial stress for two different cases, showing the more rapid stress build-up in the fluid with largest N_{λ_2} which leads to larger stresses at short times in spite of considerably reduced values at long times. We shall consider some of these phenomena in more detail in the next section. We note that a similar overshoot of the rate of change of cavity volume was also reported by Street for cavity growth in a viscoelastic liquid in spite of the fact that the

fluid dynamics of Street's problem is fundamentally different from the present collapse problem--the bubble growth induces a biaxial extensional flow, whereas the collapse produces a uniaxial extension. An overshoot of the stress has also been observed experimentally by many authors (cf. Bird et. al., 1967) after the onset of steady simple shear. Finally, it should perhaps be remarked that the critically damped nature of the stress-overshoot (cf. figure 6) is a result of putting N_{μ_o} equal to zero. As we have indicated previously, for $N_{\mu_o} > \frac{3}{4} N_{\lambda_1}$, a superposed damped oscillation in time would be expected.

A similar, though more dramatic, transient effect may be obtained by increasing the stress relaxation time N_{λ_1} holding the retardation time N_{λ_2} fixed. This is actually suggested by the physical description above, and by figure 5, which shows that the time scale associated with overshoot is essentially fixed, proportional to N_{λ_1}, independent of the retardation time. Hence, for relaxation times N_{λ_1} which are more nearly comparable with the time for total bubble collapse, a larger overshoot would be expected. This is confirmed by the results of figure 9 in which N_{μ}, N_{σ}, N_{λ_2} are held fixed and N_{λ_1} increased from 0.1 to 1.0 (i.e., $\lambda_1 \sim$ the characteristic diffusion time a^2/D). It should be noted that the "crossing" time of intersection with the curve for $N_{\lambda_1} = N_{\lambda_2}$ is increased to 0.35 for $N_{\lambda_1} = 0.5$ and approximately 0.4 for $N_{\lambda_1} = 1$. As we shall discuss in the next section, the relatively small increase from $N_{\lambda_1} = 0.5$ to $N_{\lambda_1} = 1$ is probably an indirect result of the "critical" steady elongation rate, $\dot{e} = 1/4N_{\lambda_1}$, which is associated with the singularity in equation (8).

c. The role of surface tension

Finally, we turn to the effects of surface tension. The surface tension is known to increase the bubble collapse rate by providing an

additional driving force, particularly for very small bubbles. Epstein and Plesset (1950) reported an increased rate of dissolution as the bubble volume decreased for bubbles with constant internal pressure in an inviscid fluid. A similar effect was also found in the present study for the case of a viscous Newtonian fluid, as we have shown in figure 10. In each of the four cases which we have plotted, the viscosity is held constant, but the surface tension is increased from a low value of $N_\sigma = 0.001$ to a maximum of 0.5. It may be seen that increasing the surface tension causes an increased rate of bubble collapse, with the effect becoming more pronounced as the bubble volume is decreased at "large" times. Most frequently, for k = 1, the collapse process is driven jointly by gas dissolution (mass transfer) and the squeezing influence of the tensile surface tension forces at the interface, with the viscous and viscoelastic effects tending to resist the process. However, when the surface tension is large enough, or the bubble small enough, the surface tension driving force may dominate leading to increasingly rapid collapse. In this case, if the collapse rate increases sufficiently far, the mass transfer process may actually change from a driving force for collapse, to an additional resistance as the internal bubble pressure is rapidly increased. The latter effect may actually be observed in figure 11 where we have plotted the internal bubble pressure as a function of time. For N_σ = 0.001, 0.01 and 0.1, the pressure remains reasonably uniform, in spite of the enhanced collapse rates, indicating that the mass transfer process occurs sufficiently rapidly to avoid any large pressure build-up in these cases. For $N_\sigma = 0.5$, however, the surface-tension dominated collapse becomes so rapid that the mass-transfer process simply cannot keep up, and there is a rapid increase in internal bubble pressure. One of the most interesting

and potentially important modifications of the collapse process in the viscoelastic fluid may now be noted from figure 12 in which internal bubble pressure is plotted as a function of time for the same values of N_μ and N_σ as in figure 11, but with $N_{\lambda_1} = 0.1$ and $N_{\lambda_2} = 0.05$. In this case, as N_σ is increased, there is a clear tendency toward increased internal pressures, as expected, but no tendency toward the rapidly increasing, unbounded pressures found in the Newtonian case. In the presence of fluid elasticity, as we shall show in the next section, the bubble collapse rate simply cannot exceed a value corresponding to the critical extension rate $1/4N_{\lambda_1}$, at which equation (8) is singular, except for short times. For short times, however, there is no singularity (see appendix) and the bubble can attain large collapse rates which, combined with a large surface-tension value, could cause the bubble's internal pressure to increase. In fact, it will be shown by the asymptotic analysis in the following section that the bubble pressure for $t \ll 1$ is given by

$$\theta_a = 1 + \frac{2N_\sigma}{f} - 4N_\mu\alpha - \left\{10N_\mu\left(1 - \frac{N_{\lambda_2}}{N_{\lambda_1}}\right)\alpha^2\right\} t \ .$$

Hence, for large values of surface-tension parameter, N_σ, the contribution of surface tension to bubble pressure can exceed those of viscosity and elasticity resulting in an increasing pressure for short times. This is precisely what is observed from figure 12 for surface-tension parameter, $N_\sigma = 0.5$. With increasing time and strain rates $\geq 1/4N_{\lambda_1}$, however, there will be a rapid (exponential) increase in the elongational viscosity, and a corresponding tendency toward decreasing rates of bubble collapse. It is this latter effect which inhibits the rapid growth of internal pressure in the bubble.

ASYMPTOTIC BEHAVIOR AND DISCUSSION

In the previous section, we have used numerical solutions of the governing equations to consider the influence of the various rheological parameters and of surface tension on the diffusion-induced collapse of a stationary, spherical gas bubble in an Oldroyd model fluid B. Here, we pursue an approximate analytical solution which allows a somewhat more detailed explanation for the various phenomena which were discovered. We begin with the nondimensional governing equations in the form

i) Equation of motion

$$\theta_a = 1 + \frac{2N_\sigma}{f(t)} - 2\int_0^\infty \frac{\tau_{rr} - \tau_{\theta\theta}}{[3x + f^3]}\, dx \tag{51}$$

ii) Equations of state

$$\frac{\partial \tau_{rr}}{\partial \tau} + \left(\frac{1}{N_{\lambda_1}} + 4\gamma\right)\tau_{rr} = -4\,\frac{N_\mu}{N_{\lambda_1}}\,\gamma\left\{1 + N_{\lambda_2}\left(\frac{\dot{\gamma}}{\gamma} + \gamma\right)\right\} \tag{52}$$

$$\frac{\partial \tau_{\theta\theta}}{\partial \tau} + \left(\frac{1}{N_{\lambda_1}} - 2\gamma\right)\tau_{\theta\theta} = \frac{2N_\mu}{N_{\lambda_1}}\,\gamma\left\{1 - N_{\lambda_2}\left(\frac{\dot{\gamma}}{\gamma} - 5\gamma\right)\right\} \tag{53}$$

iii) Mass balance

$$\frac{\dot{f}(t)}{f(t)} = kf(t)\left(\frac{\partial \theta}{\partial x}\right)_{x=0} - \frac{1}{3}\,\frac{\dot{\theta}_a(t)}{\theta_a(t)} \tag{54}$$

iv) Diffusion equation

$$\frac{\partial \theta}{\partial \tau} + \frac{\dot{\theta}_a}{\theta_a}\,\theta - (3x + f^3)^{4/3}\,\frac{\partial^2 \theta}{\partial x^2} - 4(3x + f^3)^{1/3}\,\frac{\partial \theta}{\partial x} = 0 \tag{55}$$

The equations (52) and (53) can easily be solved using the integration factors

$$\exp\int\left(\frac{1}{N_{\lambda_1}} + 4\gamma\right)dt \quad \text{and} \quad \exp\int\left(\frac{1}{N_{\lambda_1}} - 2\gamma\right)dt\,, \quad \text{respectively.}$$

This yields

$$\tau_{rr} = -\frac{4N_\mu}{N_{\lambda_1}} \int_0^\tau e^{(\xi-\tau)/N_{\lambda_1}} \left[\frac{[3x + f^3(\xi)]^{1/3}}{[3x + f^3(\tau)]^{4/3}}\right] \left(1 + N_{\lambda_2} a_r(\xi,x)\right) f^2(\xi)\dot{f}(\xi)d\xi \qquad (56)$$

$$\tau_{\theta\theta} = \frac{2N_\mu}{N_{\lambda_1}} \int_0^\tau e^{(\xi-\tau)/N_{\lambda_1}} \left[\frac{[3x + f^3(\tau)]^{2/3}}{[3x + f^3(\xi)]^{5/3}}\right] \left[1 + N_{\lambda_2} a_\theta(\xi,x)\right] f^2(\xi)\dot{f}(\xi)d\xi \qquad (57)$$

where,

$$a_r(x,\xi) = \frac{\ddot{f}(\xi)}{\dot{f}(\xi)} + 2\frac{\dot{f}(\xi)}{f(\xi)} + \frac{f^2(\xi)\dot{f}(\xi)}{[3x + f^3(\xi)]}$$

$$a_\theta(x,\xi) = \frac{\ddot{f}(\xi)}{\dot{f}(\xi)} + 2\frac{\dot{f}(\xi)}{f(\xi)} - 5\frac{f^2(\xi)\dot{f}(\xi)}{[3x + f^3(\xi)]}$$

Substituting (56) and (57) into the equation of motion (1), we obtain

$$\theta_a = 1 + \frac{2N_\sigma}{f} + \frac{2N_\mu}{N_{\lambda_1}} \int_0^\tau e^{(\xi-\tau)/N_{\lambda_1}} f^2(\xi)\dot{f}(\xi) \int_0^\infty \left\{4\left(1 + N_{\lambda_2} a_r\right)\left[\frac{[3x + f^3(\xi)]^{1/3}}{[3x + f^3(\tau)]^{4/3}}\right]\right.$$
$$\left. + 2\left(1 + N_{\lambda_2} a_\theta\right)\left[\frac{[3x + f^3(\tau)]^{2/3}}{[3x + f^3(\xi)]^{5/3}}\right]\right\} \frac{dx}{[3x + f^3(\tau)]}\, d\xi \qquad (58)$$

Street has shown that integrals of the general form

$$I(a,b) = \int_0^\infty \frac{dx}{[3x + f^3(\tau)]^{a/3} [3x + f^3(\xi)]^{b/3}}$$

have a value

$$I(a,b) = \frac{1}{(3 - a)[f^3(\xi) - f^3(\tau)]^2} \left\{1 - \frac{f^3(\tau)}{f^3(\xi)}^{1-a/3}\right\} \text{ if } (a + b)/3 = 2 \qquad (59)$$

and

$$I(a,b) = \frac{1}{[f^3(\xi) - f^3(\tau)]^2} \left\{\frac{1}{3 - a}\left[1 - \left(\frac{f^3(t)}{f^3(\xi)}\right)^{1-a/3}\right] - \frac{1}{6 - a}\left[1 - \left(\frac{f^3(t)}{f^3(\xi)}\right)^{2-a/3}\right]\right\} \qquad (60)$$

if $(a + b)/3 = 3$.

Making use of (59) and (60), equation (58) can be simplified to

$$\theta_a = 1 + \frac{2N_\sigma}{f(t)} + 4N_\mu \frac{\dot{f}}{f} - 2N_\mu \left(1 - \frac{N_{\lambda_2}}{N_{\lambda_1}}\right) \int_0^t e^{(\xi - t)/N_{\lambda_1}} \left\{ \left(1 + \frac{f^3(\xi)}{f^3(\tau)}\right) \frac{\ddot{f}(\xi)}{f(\tau)} + 3 \frac{f^2(\xi)}{f^2(\tau)} \frac{\dot{f}^2(\xi)}{f^2(\tau)} \right\} d\xi \tag{61}$$

Elimination of τ_{rr} and $\tau_{\theta\theta}$ from the equation of motion thus reduces the system to three equations, (54), (55) and (61), and three unknowns, f, θ_a, θ. Exact solution of this system is very difficult. However, if one assumes that the elongation rate at the bubble surface is independent of time, which is equivalent to assuming an exponential decay of bubble size with time, i.e., $\dot{f}/f \equiv -\alpha \equiv$ const., then the equation (61) can easily be evaluated to obtain a relationship between the bubble pressure and the elongation rate, α.

$$\theta_a = 1 + \frac{2N_\sigma}{f} - 4N_\mu \alpha - 2N_\mu \left(1 - \frac{N_{\lambda_2}}{N_{\lambda_1}}\right) \alpha^2 \left\{ \frac{N_{\lambda_1}}{1 - N_{\lambda_1}\alpha} + \frac{4N_{\lambda_1}}{1 - 4N_{\lambda_1}\alpha} \right\}$$

$$+ 2N_\mu \left\{ \left[\left[1 - \frac{N_{\lambda_2}}{N_{\lambda_1}} \right] \left[\frac{N_{\lambda_1}}{1 - N_{\lambda_1}\alpha} \right] \alpha^2 - \dot{f}(0) \right] \exp\left\{ - \frac{1 - N_{\lambda_1}\alpha}{N_{\lambda_1}} t \right\} \right.$$

$$\left. + \left[\left[1 - \frac{N_{\lambda_2}}{N_{\lambda_2}} \right] \left[\frac{4N_{\lambda_1}}{1 - 4N_{\lambda_1}\alpha} \right] \alpha^2 - \dot{f}(0) \right] \exp\left[- \frac{1 - 4N_{\lambda_1}\alpha}{N_{\lambda_1}} t \right] \right\} \tag{62}$$

Although clearly an "ad hoc" assumption, the numerical results of figure (6) and (7) indicate that it will be quite good for long times (relative to N_{λ_1}) or for highly viscous materials. At short times, α varies quite rapidly in some cases so that the resulting equation (62) can at most provide a "local" or instantaneous view of the bubble dynamics. Using the equations (62), and

(54) with $\dot{f}/f = -\alpha$, a number of the qualitative features of the numerical solutions may be investigated.

We first consider the effect of the initial f value on the problem. In particular, it may be seen from equation (62) that $\dot{f}(0)$ appears only in the coefficients of the transient, exponential terms. Thus, the main influence of $\dot{f}(0)$ is a quantitative one for short times, $t < 0(\lambda_1)$. Neither the long-time results nor the qualitative nature of the results for $t < 0(\lambda_1)$ are changed by variations in $\dot{f}(0)$. Because of this, the value $\dot{f}(0) = 0$ was used for convenience in the present calculations. To be consistent, we shall also drop the $\dot{f}(0)$ terms from (62) for the remainder of this section.

Using $\dot{f}/f = -\alpha$, the equation (54) can be expressed as

$$\alpha = - kf\left(\frac{\partial\theta}{\partial x}\right)_{x=0} + \frac{1}{3}\frac{\dot{\theta}_a}{\theta_a} \quad . \tag{63}$$

It may be seen from this equation that the bubble collapse rate is determined by two factors; (i) the rate at which mass is transferred out of the bubble into the bulk medium; (ii) the rate of change of the bubble pressure. It is through the second factor that the surface tension and hydrodynamic parameters enter the determination of bubble collapse rate. The extreme case in which surface tension, viscosity and elasticity are all negligible may be simply considered by noting that equation (62) reduces to

$$\theta_a = \text{constant} = 1 \tag{64}$$

which is the same condition that has been previously assumed by all investigators who studied bubble dissolution in inviscid liquids. Using (64), the equation (63) reduces to

$$\alpha = - kf\left(\frac{\partial\theta}{\partial x}\right)_{x=0} \tag{65}$$

which is the collapse rate in the limit of complete diffusion control.

When surface tension, viscosity or elasticity must be considered, one must re-examine equation (62) in conjunction with the detailed dependence of the uniaxial extensional viscosity on elongation rate which is derived in the appendix.

We begin with the contribution of viscosity. It may be seen from the equation (62) that increasing N_μ will always reduce bubble pressure, all else being equal, and thus reduce the bubble collapse rate. In addition, since the viscous term in (62) is independent of time, any increase of N_μ may be expected to decrease the bubble collapse rate *at all stages* of the collapse process. These features confirm the results of figure 4.

In contrast to the viscosity, the presence of surface tension tends to increase the bubble pressure and thus increases the rate of bubble collapse, particularly as the bubble volume becomes small. Indeed, as shown in figure 11, the surface tension causes the bubble pressure to increase rapidly near the end of the collapse process in Newtonian fluids. Examination of equation (62) for the limiting case $t \to \infty$ (or $f \to 0$) with $\alpha < 1/4N_{\lambda_1}$ yields the equation

$$\theta_a = 1 + \frac{2N_\sigma}{f} - 4N_\mu\alpha - 2N_\mu\left\{1 - \frac{N_{\lambda_2}}{N_{\lambda_1}}\right\}\alpha^2\left\{\frac{N_{\lambda_1}}{1 - N_{\lambda_1}\alpha} + \frac{4N_{\lambda_1}}{1 - 4N_{\lambda_1}\alpha}\right\} \qquad (66)$$

thus confirming similar behavior for the viscoelastic fluid provided only that the collapse rate does not grow too large. However, for $\alpha \to 1/4N_{\lambda_1}$, or for $\alpha > 1/4N_{\lambda_1}$, and $t \to \infty$, equation (62) becomes

$$\theta_a = 1 + \frac{2N_\sigma}{f} - 4N_\mu\alpha - 2N_\mu\left\{1 - \frac{N_{\lambda_2}}{N_{\lambda_1}}\right\}\alpha^2\left\{\frac{N_{\lambda_1}}{1 - N_{\lambda_1}\alpha} + \frac{4N_{\lambda_1}}{4N_{\lambda_1}\alpha - 1}\exp\left[\frac{4N_{\lambda_1}\alpha - 1}{N_{\lambda_1}}t\right]\right\} \qquad (67)$$

According to (67), if the collapse rate exceeds $\alpha = 1/4N_{\lambda_1}$ and $\left\{1 - \frac{N_{\lambda_2}}{N_{\lambda_1}}\right\} \neq 0$, the magnitude of the elastic contribution to the bubble pressure

quickly grows to very large values and the rate of collapse is rapidly decreased. The net result of the equations (66) and (67) is thus that the bubble pressure does increase, at first, but always remains finite, corresponding to the numerical results shown in figure 12. Noting that the critical collapse rate, α, appearing in the bubble pressure expression, equation (66), is the same rate as the critical elongation rate $1/4N_{\lambda_1}$ for the extensional viscosity, it is now clear that the dynamics of the bubble collapse process is controlled by the viscoelastic properties of the suspending fluid. In particular, the choice of a constitutive model which exhibits a critical elongation rate has played an essential role in the nature of the final results. Unfortunately, even though it is generally agreed that the elongational viscosity for uniaxial extension increases rapidly with the rate of extension, there is not enough meaningful experimental data to come to a completely conclusive decision on the existence of a critical stretching rate (see appendix). Indeed, in light of the extreme difficulty in measuring the uniaxial viscosity directly, it may be suggested that the bubble dissolution problem could provide one way to determine the existence of such a critical stretching rate if an experiment could be designed to measure the collapse rate and the pressure of a stationary bubble in a viscoelastic medium where the collapse process is controlled by the rheology of the fluid.

Finally, the importance of retaining the transient terms in the uniaxial viscosity expression cannot be overemphasized in explaining the viscoelastic phenomena resulting from uniaxial stretching, particularly during the early stages of elongation. For example, the overshoot in bubble collapse rate and increase in the bubble internal pressure with surface tension just after the collapse process started can only be predicted if the transient terms

are considered. For $t \ll 1$, the uniaxial viscosity is of the form (see appendix)

$$\frac{\bar{\eta}}{\eta_o} = 3\left[1 - 2N_{\lambda_2}\dot{e}\right]\frac{t}{N_{\lambda_1}} \qquad t \ll 1 \tag{68}$$

and the bubble pressure is

$$\theta_a = 1 + \frac{2N_\sigma}{f(t)} - 4N_\mu\alpha - 10N_\mu\left[1 - \frac{N_{\lambda_2}}{N_{\lambda_1}}\right]\alpha^2 t \qquad t \ll 1 \tag{69}$$

It is clear from equation (68) that the uniaxial viscosity is actually smaller than its Newtonian value and that it remains smaller until after some time greater than the relaxation time, N_{λ_1}. Therefore, during this time, viscoelastic liquid would show less resistance to bubble collapse resulting in an overshoot of collapse rates over its critical value at large times, $\alpha = 1/4N_{\lambda_1}$. The equation (68) supports the conjecture made in conjunction with figures 5 and 9 that the time scale associated with the overshoot is essentially fixed, proportional to the relaxation time N_{λ_1}. The significance of equation (69) was discussed earlier in conjunction with the surface tension induced build-up of internal bubble pressure for short times and hence will not be repeated here.

APPENDIX

UNIAXIAL EXTENSIONAL FLOW OF NON-NEWTONIAN FLUIDS

It was pointed out in the section on constitutive models that the fluid motion induced by the collapse of a stationary gas bubble is an unsteady simple uniaxial extension. Therefore, it is necessary to employ a model which can predict uniaxial viscosity as a realistic function of elongation rate and time. In this appendix, we will demonstrate the behavior of the elongational viscosity for the model employed in this study. Of particular importance is the prediction of an exponentially increasing viscosity with time for elongation rates above some critical value. This will be followed by a brief summary of experimental results reported in the literature and arguments for (and against) the existence of such a critical elongation rate in real fluids.

We consider simple start-up of a uniaxial extensional flow from an initial state of rest and of zero stress, i.e.

$$\left.\begin{aligned} &\underline{u} = 0,\ \underline{\underline{\tau}} = 0;\ t < 0 \\ &u_3 = 2\dot{e}x_3 \\ &u_i = \dot{e}x_i \quad i = 1, 2 \end{aligned}\right\} \quad t \geq 0 \tag{A1}$$

The stress field for $t \geq 0$ is then easily obtained by solving the constitutive equation explicitly using the initial condition $\underline{\underline{\tau}} = 0$ at $t = 0$ and then simply expressing the solution in terms of the elongational viscosity, which is defined

$$\bar{\eta} \equiv \frac{\tau_{33} - \tau_{11}}{2\dot{e}} \tag{A2}$$

The result, for $\mu_o = 0$, is

$$\frac{\bar{\eta}}{\eta_o} = 3\left[\frac{1 - 2\lambda_2\dot{e}(1 + 4\lambda_1\dot{e})}{(1 + 2\lambda_1\dot{e})(1 - 4\lambda_1\dot{e})}\right] - 2\,\frac{1 - 4\lambda_2\dot{e}}{1 - 4\lambda_1\dot{e}}\exp\left[-\frac{1 - 4\lambda_1\dot{e}}{\lambda_1}t\right] \tag{A3}$$

$$- \frac{1 + 2\lambda_2\dot{e}}{1 + 2\lambda_1\dot{e}}\exp\left[-\frac{1 + 2\lambda_1\dot{e}}{\lambda_1}t\right]$$

In the Newtonian limit, $\lambda_1, \lambda_2 \to 0$, this reduces to the well-known Trouton (1906) formula

$$\frac{\bar{\eta}}{\eta_o} = 3$$

The limiting behavior as $t \to \infty$ for $4\lambda_1\dot{e} < 1$ is simply

$$\frac{\bar{\eta}}{\eta_o} = 3\left[\frac{1 - 2\lambda_2\dot{e}(1 + 4\lambda_1\dot{e})}{(1 + 2\lambda_1\dot{e})(1 - 4\lambda_1\dot{e})}\right] \tag{A4}$$

which clearly depends individually on λ_1, λ_2 and $\dot{e}$, but has the following general properties

1. $\bar{\eta}/\eta_o \geq 3$ and is an increasing function of the elongation rate $\dot{e}$ for $0 \leq \lambda_2/\lambda_1 \leq 1$.
2. $\bar{\eta}/\eta_o$ increases as λ_2 decreases for λ_1 fixed and $\lambda_2 \leq \lambda_1$.
3. $\bar{\eta}/\eta_o$ increases as λ_1 increases for λ_2 fixed and $\lambda_2 \leq \lambda_1$.
4. $\bar{\eta}/\eta_o \equiv 3$ for all $\lambda_1 = \lambda_2$.

This limiting behavior (A4) has been obtained without regard to the transients in most previous work and has been interpreted to suggest:

1. that $\lambda_1 = \lambda_2$ corresponds to the Newtonian limit for all λ_1 (cf. Street, 1968);
2. that there exists a maximum possible elongation rate

$$\dot{e} = \frac{1}{4\lambda_1}$$

for viscoelastic fluids, with extremely large tensile stresses always occurring for values of $\dot{e}$ approaching this critical value (cf. Metzner, 1967 and Metzner and Astarita, 1967)

The first of these statements is clearly only true for $\lambda_1 = \lambda_2 = 0$, as may be seen on examining (A3) including the transients

$$\frac{\bar{\eta}}{\eta_o} = 3 - 2\exp\left[-\frac{1 - 4\lambda_1\dot{e}}{\lambda_1}t\right] - \exp\left[-\frac{1 + 2\lambda_1\dot{e}}{\lambda_1}t\right] \qquad \text{(A5)}$$

Only for large times, and $\dot{e} < 1/4\lambda_1$, does (A5) approach the Newtonian fluid value for nonzero λ_1.

The inference (No. 2 above) of a maximum elongation rate and corresponding unbounded tensile stresses has been the subject of considerable controversy, and a number of authors have advanced theoretical and philosophical arguments tending either to support or oppose these concepts (cf. Tanner, 1968; Tanner and Simmons, 1967; Meister, 1971; Astarita, 1967). However, the little experimental data that do exist appears to be consistent with the concept of greatly enhanced elongational viscosity in steady (or nearly steady) flows. For example, Ballman (1965) and Cogswell (1968) have reported values of $\bar{\eta}$, obtained by stretching rods of very viscous molten polymers. This technique necessitates restriction of the measurements to low deformation rates. In spite of these deformation rate restrictions, the ratio of elongational viscosity to that of shear viscosity, which is three for Newtonian liquids, was as high as 12. Astarita (1968) has reported elongational viscosities at high deformation rates and for very short times of deformation; these were higher than the shear viscosity by a factor of at least 10^4. Metzner and Metzner (1970) made some measurements of $\bar{\eta}/\eta_o$ from the stress field developed in viscoelastic media issuing from a small

orifice at high velocities. They reported $\bar{\eta}/\eta_o$ values ranging from 270 to 1730 when estimates of deformation rates which lead to the most conservative values of this ratio were employed. Alternate and more probable estimates of the actual deformation rate yielded ratios as high as 29,000.

It is clear, in comparing the behavior of (A4) with (A3) that caution must be employed in attempting to utilize only the constant terms in the expression for $\bar{\eta}/\eta_o$ to explain the dynamics of general uniaxial extensional flows as most previous investigators have done. Indeed, as Denn and Marrucci (1971) have noted, uniaxial elongation is generally a transient phenomena and $\bar{\eta}/\eta_o$ must be considered as a function not only of the elastic parameters, but also of time. In fact, at the limiting value of $4\lambda_1\dot{e} \to 1$, the $\bar{\eta}/\eta_o$ equation (A3) for the Oldroyd model used here can be evaluated for small times and gives

$$\frac{\bar{\eta}}{\eta_o} = \frac{2}{3}\left\{\left(1 + 2\lambda_2\dot{e}\right) + 3\left(1 - 4\lambda_2\dot{e}\right)\frac{t}{\lambda_1} - \left(1 + 2\lambda_2\dot{e}\right)\exp\left(-3t/2\lambda_1\right)\right\} \quad \text{(A6)}$$

This expression reduces to equation (14) of Denn and Marrucci (1971) when $\lambda_2 = 0$. It should be noted that the extensional viscosity does not even reach the Newtonian value until after a time of the order of the relaxation time, $t = O(\lambda_1)$. Denn and Marucci have argued (correctly, we believe) that $\bar{\eta}/\eta_o$ does not go to infinity at the elongation rate $\dot{e} = 1/4\lambda_1$ as would be wrongly concluded if one considered only the constant term, equation (A4), but rather that $\dot{e} = 1/4\lambda_1$ does represent a critical condition in the sense that for elongation rates below that value, $\bar{\eta}/\eta_o$ remains bounded and reaches a finite asymptote. For the limiting case, $\dot{e} >> 1/4\lambda_1$, the expression (A3) can be approximated by

$$\frac{\bar{\eta}}{\eta_o} = \frac{1 - 4\lambda_2\dot{e}}{2\lambda_1\dot{e}} \exp(4\dot{e}t) \tag{A7}$$

This is nothing more than the intuitively agreeable result that deformations which occur more rapidly than the intrinsic relaxation time scales of the material (i.e., which exceed the capability of material response) will lead to a build-up of stress, in this case exponentially in time. Meister gave essentially the same explanation in slightly modified terms, namely that under very large elongation rates, the viscoelastic material acts like a solid, eventually leading to a structural break if the strain is continued.

Finally, it should be pointed out that the qualitative behavior of uniaxial viscosity with elongation rate, relaxation time, λ_1, and retardation time, λ_2, remains unchanged when $\mu_o \neq 0$. The generalization of (A3) to this case takes the form

$$\begin{aligned}\frac{\bar{\eta}}{\eta_o} = {} & A(\lambda_1, \lambda_2, \mu_o)\exp\left\{-\left[(1 - \lambda_1\dot{e}) + 3\lambda_1\dot{e}\left(1 - \frac{4}{3}\frac{\mu_o}{\lambda_1}\right)^{1/2}\right]\frac{t}{\lambda_1}\right\} \\ & + B(\lambda_1, \lambda_2, \mu_o)\exp\left\{-\left[(1 - \lambda_1\dot{e}) - 3\lambda_1\dot{e}\left(1 - \frac{4}{3}\frac{\mu_o}{\lambda_1}\right)^{1/2}\right]\frac{t}{\lambda_1}\right\} \\ & + 3\,\frac{1 - 2\lambda_2\dot{e}(1 + 4\lambda_1\dot{e})}{(1 - \lambda_1\dot{e})^2 - 9\lambda_1^2\dot{e}^2\left(1 - \frac{4}{3}\frac{\mu_o}{\lambda_1}\right)}\end{aligned} \tag{A8}$$

where A and B are to be determined from the initial conditions on the tensil stresses. Because of the square-root term in the exponential decay coefficient there are two possible types of transient behavior

i) for $\mu_o > \frac{3}{4}\lambda_1$, the transient behavior is one of sinusoidal oscillations superposed on the main exponential term.

ii) for $\mu_o < \frac{3}{4}\lambda_1$ the transients decay exponentially in time. μ_o also has the non-essential effect of increasing the critical rate of elongation at steady state. In fact, for $\frac{\mu_o}{\lambda_1} << 1$

$$\frac{\bar{\eta}}{\eta_o} = A\exp\left\{-\left[1 - 4\lambda_1\dot{e}\left(1 - \frac{1}{2}\frac{\mu_o}{\lambda_1}\right)\right]\frac{t}{\lambda_1}\right\} + B\exp\left\{-\left[1 + 2\lambda_1\dot{e}\left(1 - \frac{\mu_o}{\lambda_1}\right)\right]\frac{t}{\lambda_1}\right\}$$

$$+ 3\frac{1 - 2\lambda_2\dot{e}(1 + 4\lambda_1\dot{e})}{\left[1 - 4\lambda_1\dot{e}\left(1 - \frac{1}{2}\frac{\mu_o}{\lambda_1}\right)\right]\left[1 + 2\lambda_1\dot{e}\left(1 - \frac{\mu_o}{\lambda_1}\right)\right]} \qquad \text{(A9)}$$

which yields a critical elongation rate of

$$\dot{e} \equiv \frac{1}{4\lambda_1} - \frac{1}{8}\frac{\mu_o}{\lambda_1^2} \qquad \text{(A10)}$$

which is less than the value of $1/4\lambda_1$ when $\mu_o = 0$.

In summary, the modified Oldroyd fluid B is shown to predict a critical elongation rate, in qualitative agreement with most existing experimental studies. It is also shown that, due to the transient effects, the uniaxial viscosity in a viscoelastic liquid is smaller than that of a Newtonian fluid of equivalent shear viscosity for a short period of time, even though the uniaxial viscosity of viscoelastic liquid becomes extremely large for large times at elongation rates above the critical value. Therefore, in explaining dynamic phenomena involving extensional flows of viscoelastic fluids, it is of extreme importance to consider the transient terms as well as the time independent terms, particularly if the phenomena is of unsteady type. For example, in the last section, where an asymptotic analysis of the diffusion-induced bubble collapse problem is presented, the transient terms have been shown to be of utmost importance in explaining the overshoot of bubble collapse

rate and the increase in internal bubble pressure for short times following the beginning of the collapse process.

REFERENCES

(1) Astarita, G., Ind. Eng. Chem. Fund., 6, 257 (1967)

(2) Astarita, G., Ind. Eng. Chem. Fund., 7, 171 (1968)

(3) Ballman, R. L., Rheol. Acta, 4, 137 (1965)

(4) Barlow, E. J., Langlois, W. E., IBM J. Res. Develop., 6, 329 (1962)

(5) Barnes, H. A., Townsend, P., Walters, K., Nature (London), 224, 585 (1969)

(6) Barnes, H. A., Townsend, P., Walters, K., Rheol. Acta, 10, 517 (1971)

(7) Cable, M., Evans, D. J., J. Appl. Phys., 38, 2899 (1967)

(8) Cogswell, F. N., Plastics Polymers, 109 (1968)

(9) Dealy, J. M., Poly. Eng. Sci., 11, 433 (1971)

(10) Denn, M. M., Marrucci, G., A.I.Ch.E. J., 17, 101 (1971)

(11) Denson, C. D., Gallo, R. J., Poly. Eng. Sci., 11, 174 (1971)

(12) Duda, J. L., Vrentas, J. S., J. Heat Mass Trans., 14, 395 (1971)

(13) Epstein, P. S., Plesset, M. S., J. Chem. Phys., 18, 1505 (1950)

(14) Fogler, H. S., Goddard, J. D., Phys. Fluids, 13, 1135 (1970)

(15) Huppler, J. D., MacDonald, I. F., Ashare, E., Spriggs, T. W., Bird, R. B., Holmes, L. A., Trans. Soc. Rheol., 11, 181 (1967)

(16) Huppler, J. D., Ashare, E., Holmes, L. A., Trans. Soc. Rheol., 11, 159 (1967)

(17) Lodge, A. S., "Elastic Liquids", Academic Press, New York (1964)

(18) Meister, B. J., Trans. Soc. Rheol., 15, 63 (1971)

(19) Metzner, A. B., Astarita, G., A.I.Ch.E. J., 13, 550 (1967)

(20) Metzner, A. B., A.I.Ch.E. J., 13, 316 (1967)

(21) Metzner, A. B., Metzner, A. P., Rheol. Acta, 9, 174 (1970)

(22) Oldroyd, J. G., Proc. Roy. Soc., A245, 278 (1958)

(23) Ready, D. W., Cooper, A. R., Chem. Eng. Sci., 21, 917 (1966)

(24) Roscoe, R., Brit. J. Appl. Phys., 15, 1095 (1964)

(25) Scriven, L. E., Chem. Eng. Sci., 10, 1 (1959)

(26) Spriggs, T. W., Huppler, J. D., Bird, R. B., Trans. Soc. Rheol., 10, 191 (1966)

(27) Street, J. R., Trans. Soc. Rheol., 12, 103 (1968)

(28) Tanner, R. I., Simmons, J. M., Chem. Eng. Sci., 22, 1803 (1967)

(29) Tanner, R. I., Trans. Soc. Rheol., 12, 155 (1968)

(30) Trouton, F. T., Proc. Roy. Soc. (London) A77, 426 (1906)

(31) Walters, K. Z., Angew. Math. Phys., 21, 592 (1970)

(32) Williams, M. C., Bird, R. B., Phys. Fluids, 5, 1867 (1963)

ACKNOWLEDGEMENT

This work was supported by a grant from the National Science Foundation, GK-35468.

LEGEND

Figures:
1. Comparison of present work with Duda and Vrentas' results
2. Effect of Henry's law constant on bubble collapse in a viscoelastic liquid
3. Effect of Henry's law constant on internal bubble pressure in a viscoelastic liquid
4. Effect of viscosity on bubble collapse in a Newtonian liquid
5. Effect of elasticity on bubble collapse in a viscoelastic liquid
6. Effect of elasticity on exponential decay coefficient
7. Damping effect of viscosity on overshoot of exponential decay coefficient in a viscoelastic liquid
8. Effect of elasticity on total axial stress at bubble-liquid interface
9. Effect of relaxation time on bubble collapse rate
10. Effect of surface tension on bubble collapse in a Newtonian liquid
11. Effect of surface tension on internal bubble pressure in a Newtonian liquid
12. Effect of surface tension on internal bubble pressure in a viscoelastic liquid

Table:
1. Comparison of Lifetimes, Newtonian case

Table 1: Comparison of Lifetimes

	Cable & Evans (1967)	Duda & Vrentas (1971)	Present Work
$\alpha = 0.0$, $\beta = 1.0$	0.441	0.284	0.290
$\alpha = 1.0$, $\beta = 0.1$	5.83	4.22	4.30

(α and β in Cable & Evans' notation corresponds to N_b/N_a and N_a in Duda and Vrentas' work, respectively.)

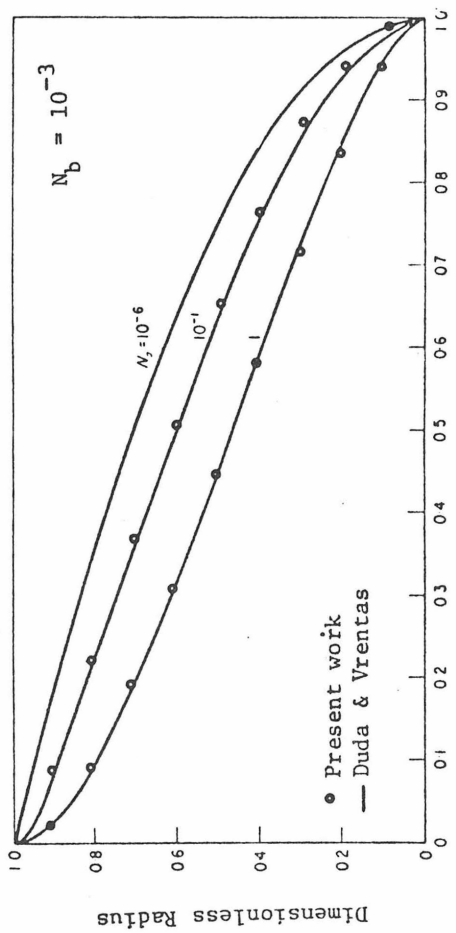

Figure 1. Comparison of present work with Duda & Vrentas' results

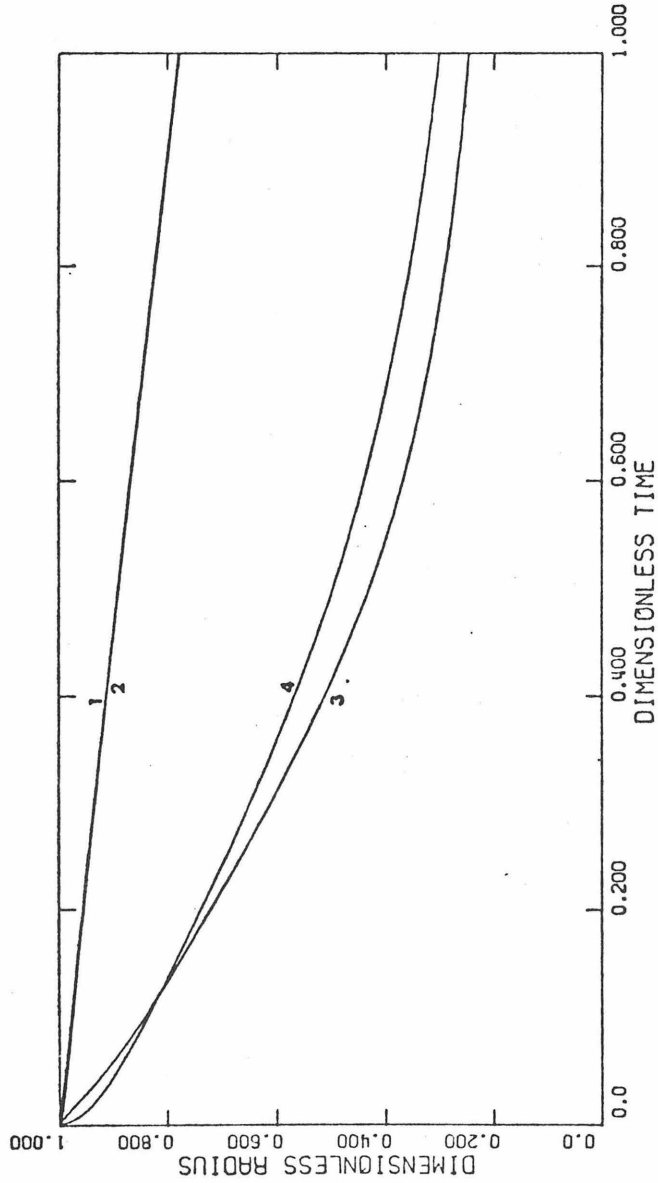

Figure 2. Effect of Henry's law constant on bubble collapse in a viscoelastic medium

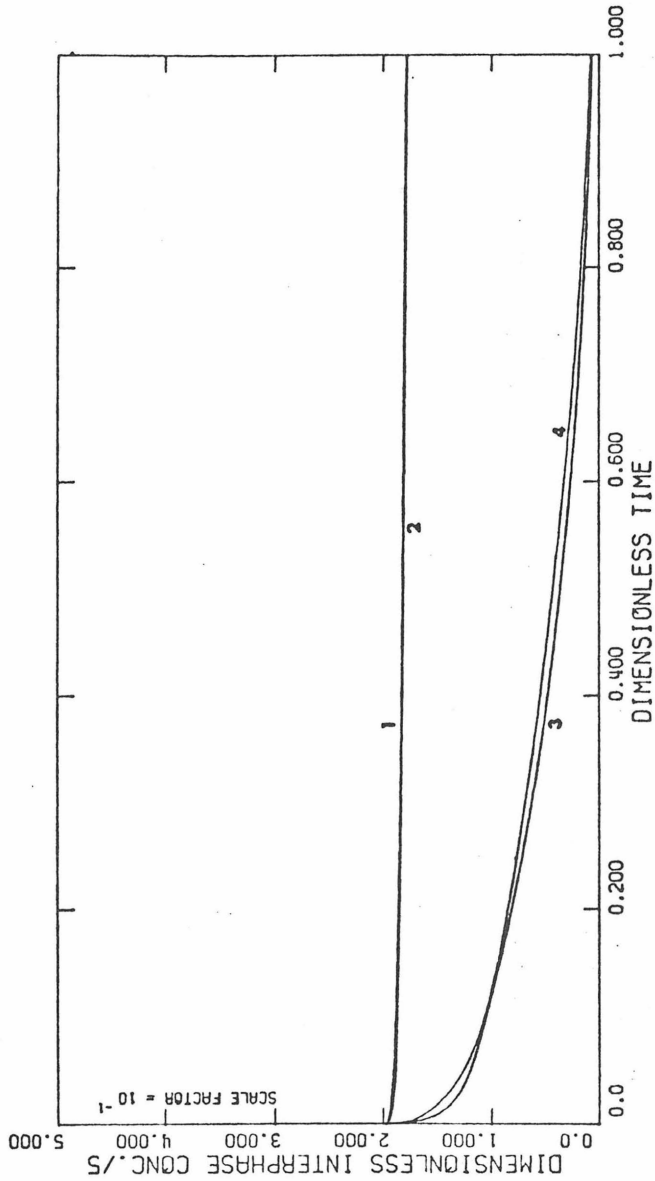

Figure 3. Effect of Henry's law constant on internal bubble pressure in a visco-elastic medium

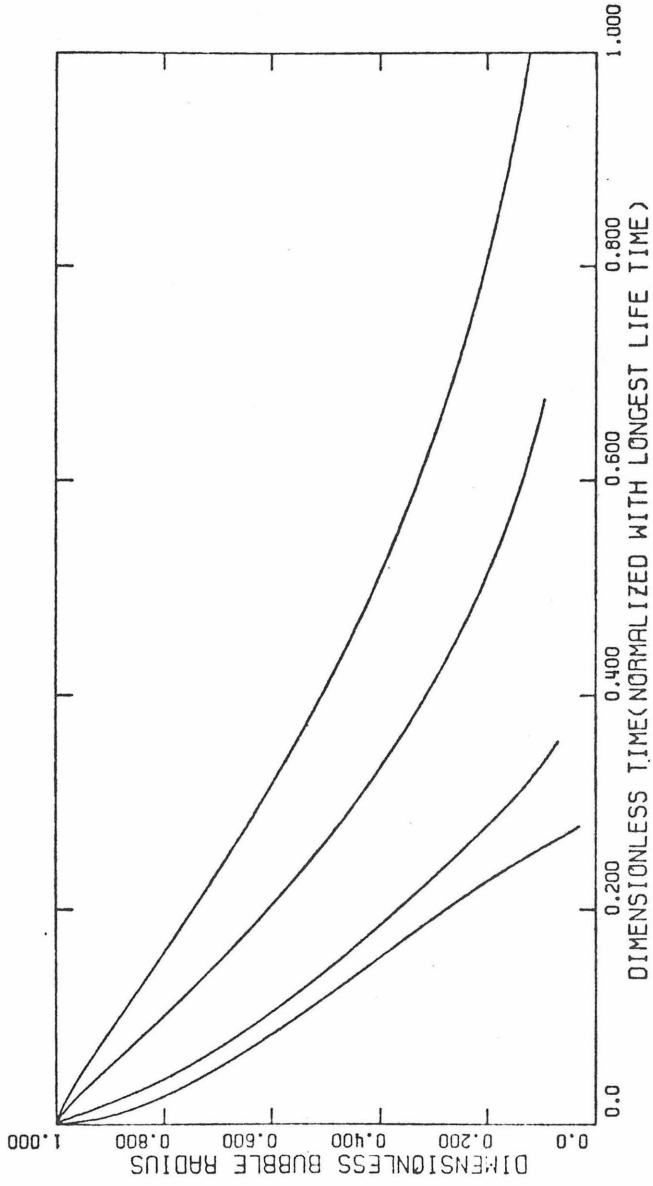

Figure 4. Effect of viscosity on bubble collapse in a Newtonian liquid

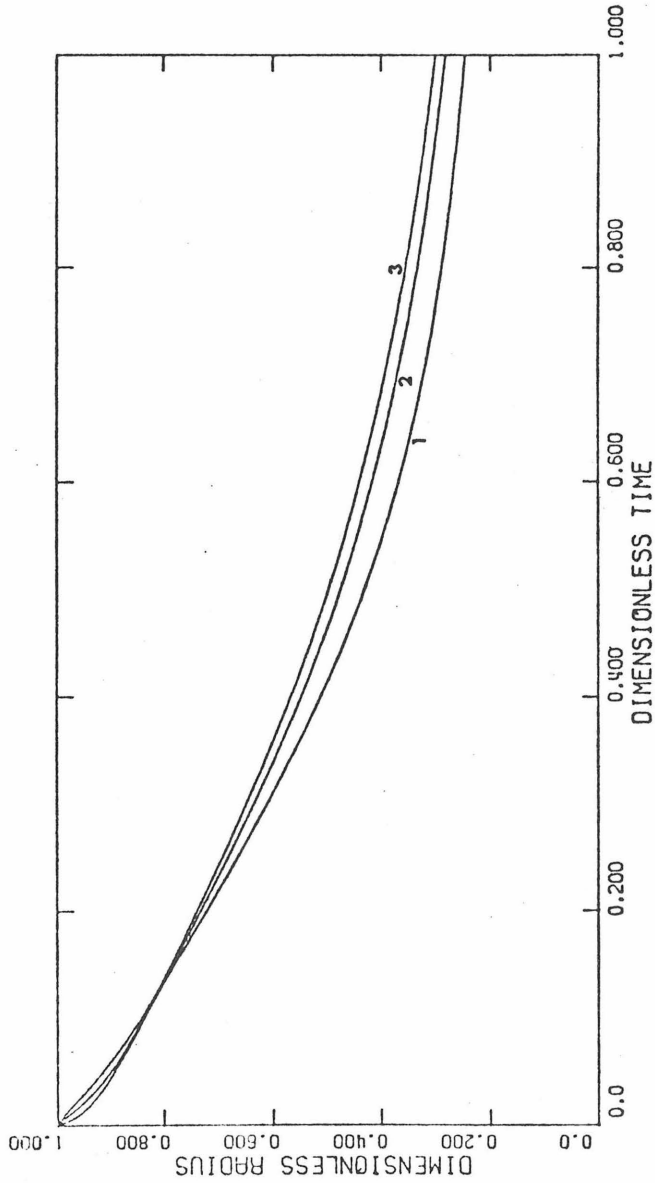

Figure 5. Effect of elasticity on bubble collapse in a viscoelastic liquid

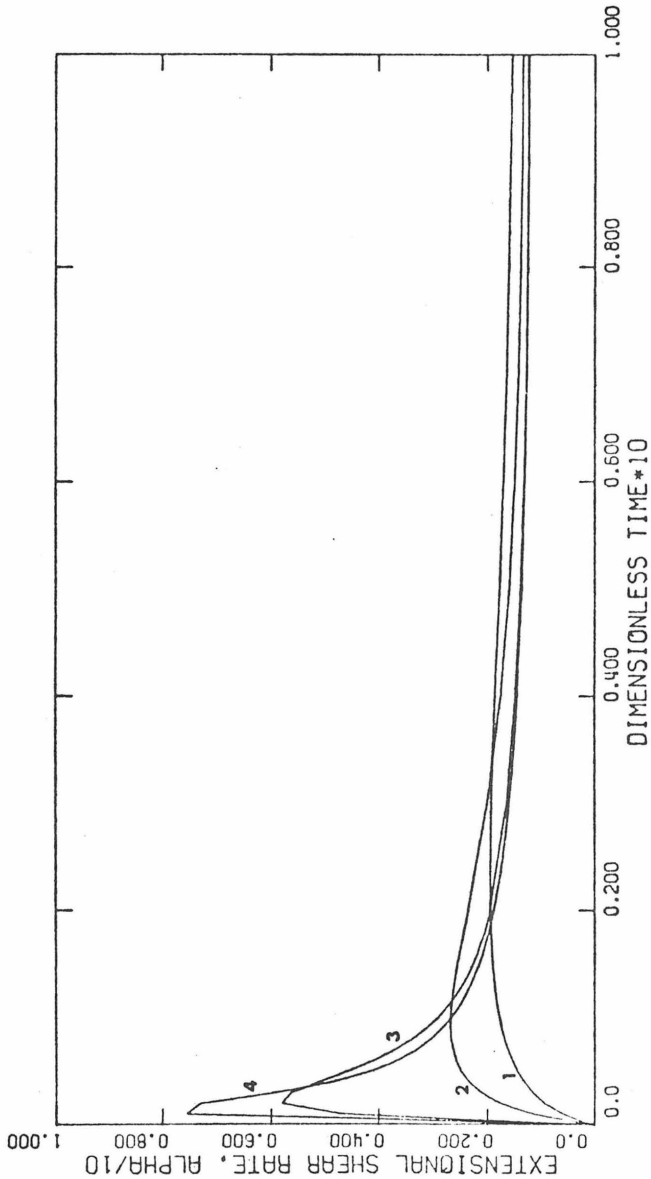

Figure 6. Effect of elasticity on the exponential decay coefficient of bubble size, α

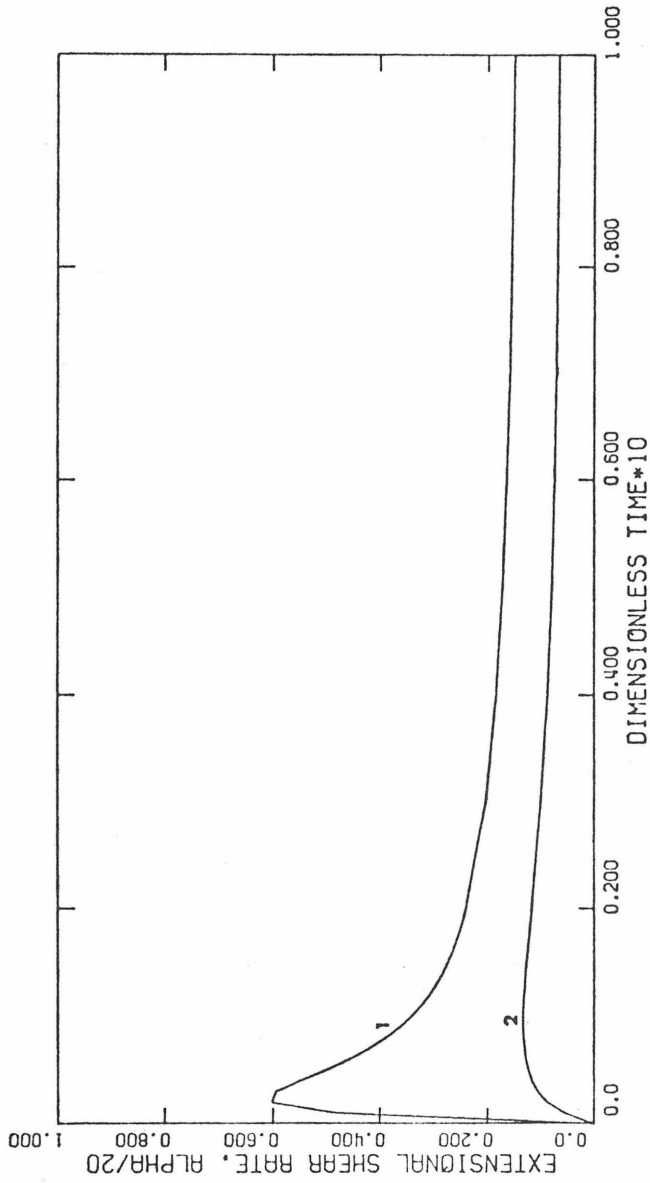

Figure 7. Damping effect of viscosity on the overshoot of exponential decay coefficient in a viscoelastic liquid

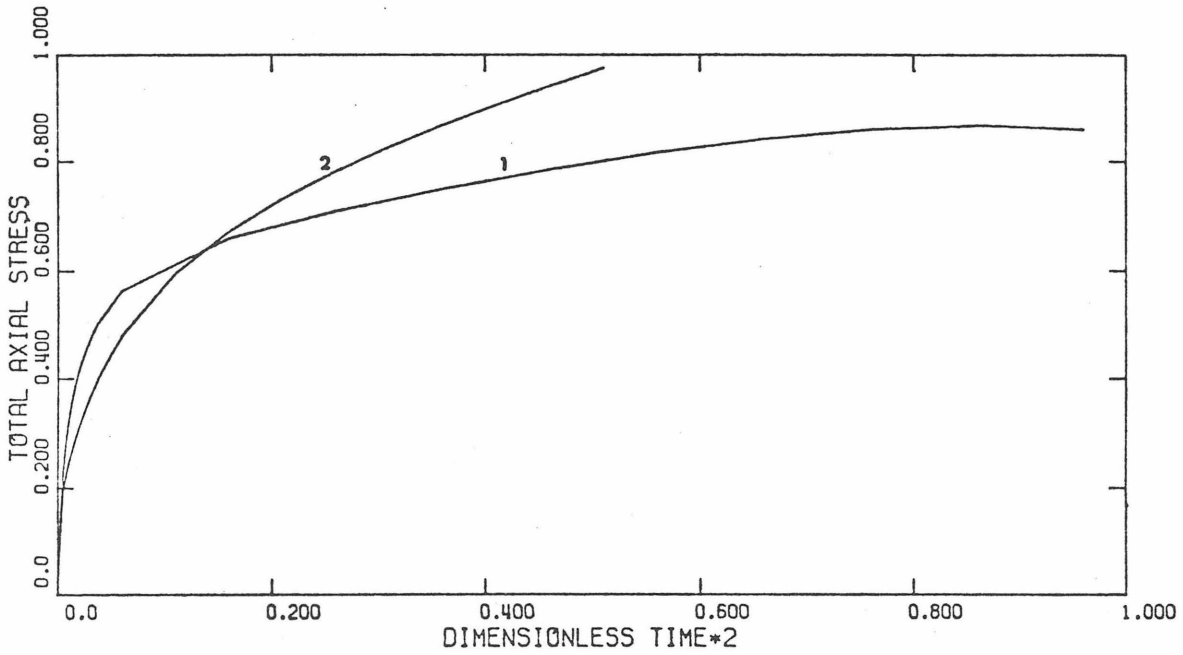

	VISC	SURF	ELAS1	ELAS2
1	0.1000000	0.0010000	0.1000000	0.1000000
2	0.1000000	0.0010000	0.1000000	0.0100000

Figure 8. Effect of elasticity on total axial stress at bubble-liquid interface

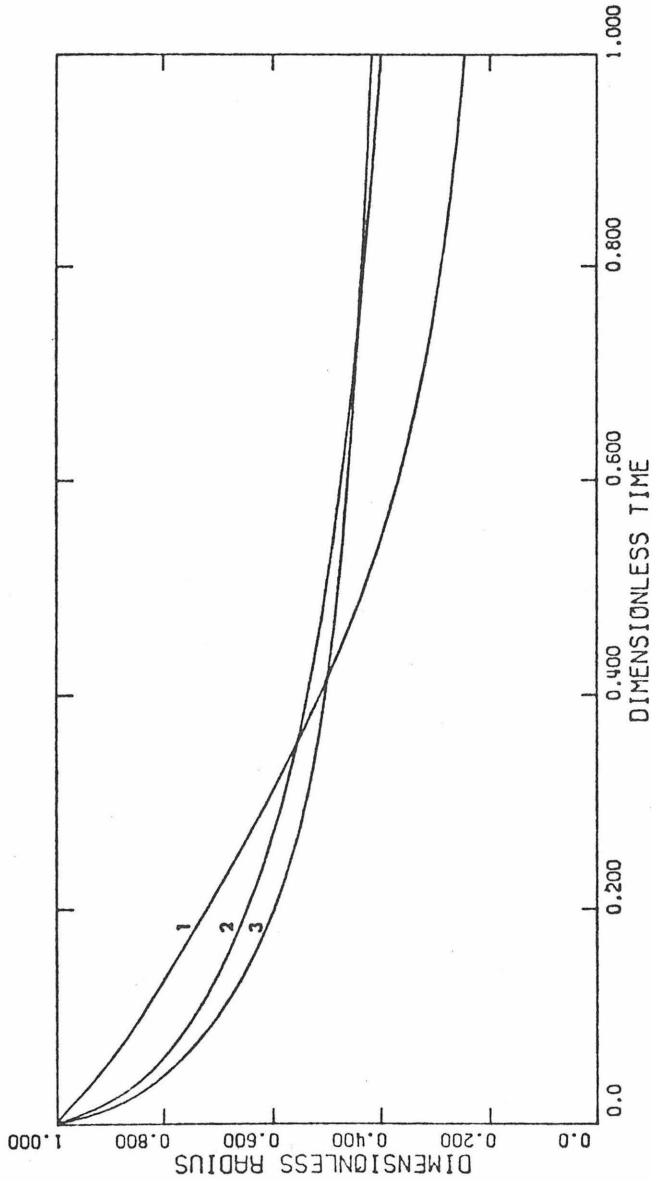

Figure 9. Effect of relaxation time, λ_1, on bubble collapse rate

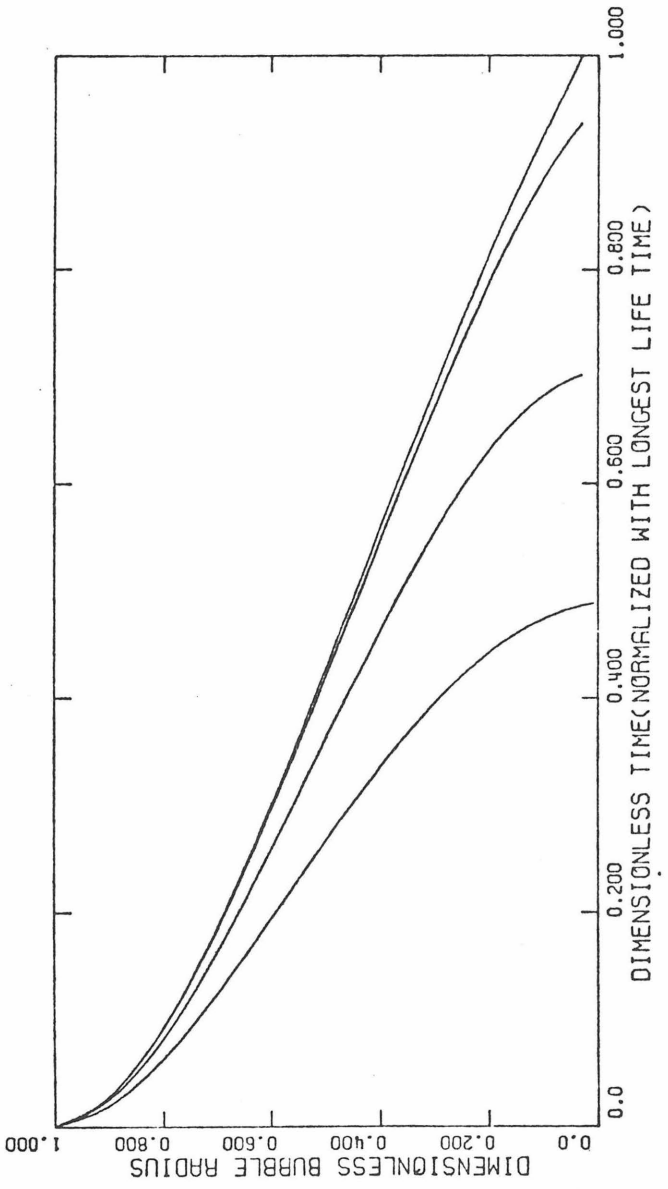

Figure 10. Effect of surface tension on bubble collapse in a Newtonian liquid

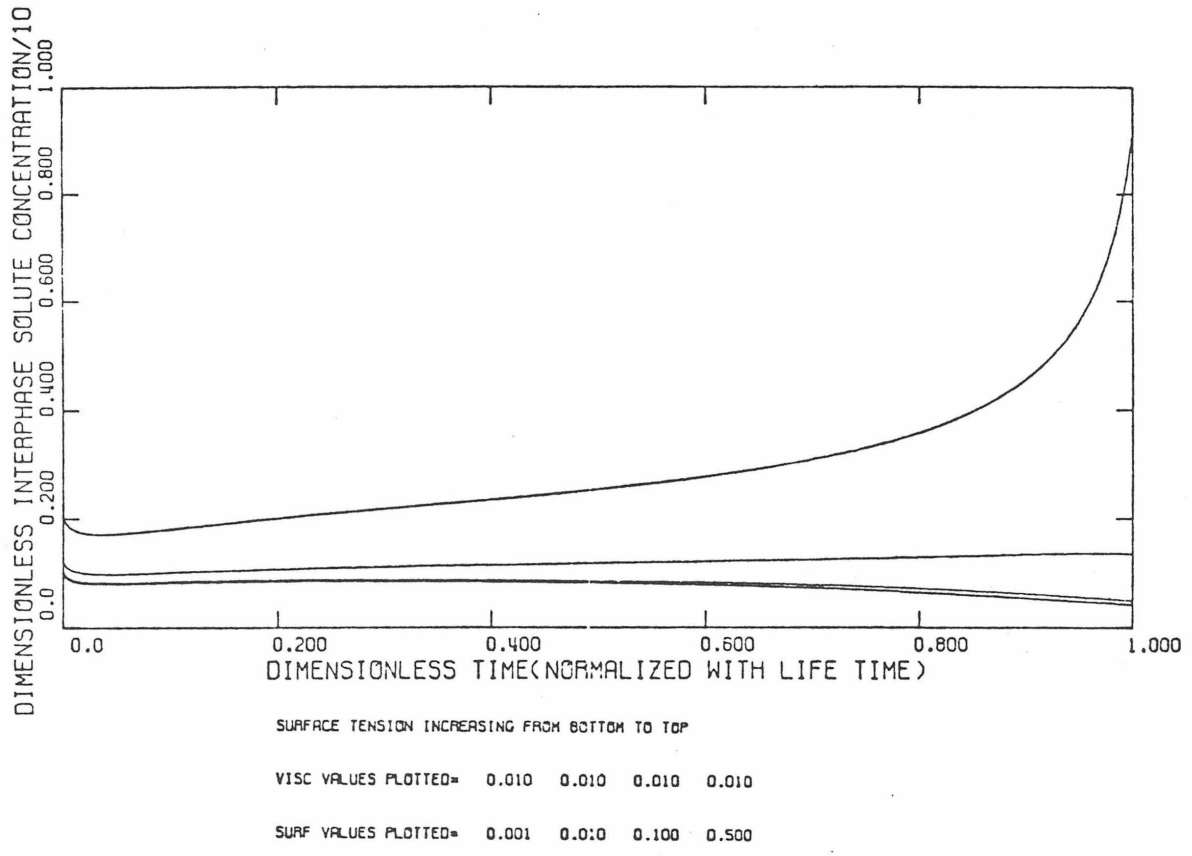

Figure 11. Effect of surface tension on internal bubble pressure in a Newtonian liquid

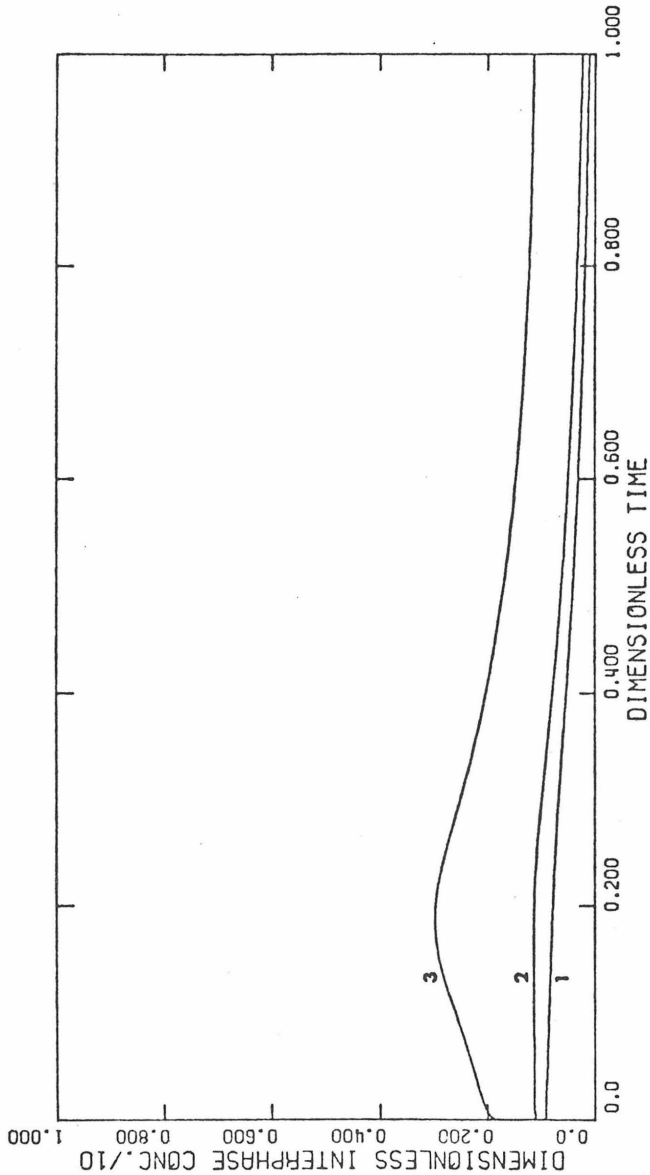

Figure 12. Effect of surface tension on internal bubble pressure in a viscoelastic liquid

CHAPTER III

A NOTE ON THE CREEPING MOTION OF A VISCOELASTIC FLUID PAST A SPHERE

A NOTE ON THE CREEPING MOTION OF A VISCOELASTIC FLUID PAST A SPHERE

E. Zana, G. Tiefenbruck and L. G. Leal

Chemical Engineering
California Institute of Technology
Pasadena, California 91125

INTRODUCTION

Among the general class of nonviscometric flows of a viscoelastic liquid, one of the most important is the uniform translation past a submerged object, such as a cylinder or sphere. In spite of this, relatively little progress has been made in the theoretical description of such flows since the governing equations are nonlinear not only in the convective acceleration (or inertia) terms, but also in the constitutive model for the fluid. Indeed, with one exception which we shall discuss below, all theoretical studies to date have been restricted to the limit of "slow" flow in which the nonlinear contributions are either neglected altogether, or at least are embedded within the framework of a small parameter perturbation expansion about the linear, Newtonian creeping flow state. The conditions required for validity of such an analysis are $Re << 1$, $We << 1$, where $Re(\equiv ud/\nu)$ is the Reynolds number and $We(\equiv \lambda u/d)$ is the Weissenberg number which is a ratio of the largest characteristic relaxation or retardation time for the fluid, λ, and the convective time scale d/u of the fluid motion. The Weissenberg number thus provides a measure of the relative importance of the fluid's elasticity. The best known example of an analysis of this type is the creeping ($Re \equiv 0$) flow solution for the rheologically slow ($We << 1$) flow of a viscoelastic fluid past a sphere, which was obtained (independently) by Leslie (1961), Caswell and Schwarz (1962) and Giesekus (1963). The solution shows a small downstream shift in the streamlines at $O(We)$, and a decrease in the drag at $O(We^2)$. More recently, Mena and Caswell (1974) have carried the small We analysis one step further for both a cylinder and a sphere by including inertia terms in formal matched asymptotic expansions for small, but nonzero Reynolds number.

The only investigation which purports to provide an approximate representation of the flow for strong elasticity (i.e. moderate to large We) is the analysis of Ultman and Denn (1971), which is based upon an Oseen-like linearization of the dynamic inertia terms, as in the usual Newtonian case, and also of the nonlinearities in the generalized Maxwell constitutive model which was adopted for the work. An approximate numerical method was used to "satisfy" the appropriate boundary conditions at the body surface. Both in the original analysis and in subsequent discussions of the work (cf. Astarita and Marrucci, 1974) it has been implicitly assumed that the Oseen linearization provides a uniformly valid first approximation to both the convective and constitutive nonlinearities provided only that $Re << 1$, without any fundamental restriction on We. Indeed, realistic solutions were claimed by Ultman and Denn (1970) for $Re \lesssim 1$, provided only that We satisfied the additional condition $ReWe \lesssim .05$, which was obtained by requiring the mean square error in satisfying boundary conditions at the body surface to be no greater than that obtained in the Newtonian case for $Re = 1$. It is important to emphasize that the condition on We was intended as a restriction on the accuracy of the approximation involved in solving the governing linearized equations of motion, rather than an inherent restriction on the validity of the linearization itself. One feature of the governing equations, which seems to support their validity for $Re << 1$, but Weissenberg number essentially unrestricted is the fact that they change type from elliptic to hyperbolic at $ReWe = 1$. As Ultman and Denn (1970) and a number of subsequent investigators have pointed out, this change in type seems to correlate reasonably well with (and even explain in a qualitative sense) a

variety of experimental observations which are otherwise difficult to comprehend (cf. James and Acosta 1970, Ultman and Denn, 1970). In spite of such apparent successes of the theory, however, certain of its other features are difficult to accept. For example, Ultman and Denn's (1971) calculations for ReWe as small as .05 (where the small We solutions might be expected to be relevant) show an enormous upstream shift of the streamlines--assumed by Ultman and Denn to be a physically realistic consequence of nonzero, if weak fluid elasticity. In addition, the calculated flow structure near the body surface in some cases shows streamlines actually crossing the body boundary. Finally, the calculated results show an apparent separation phenomena which occurs for very small values of Re provided that We is larger than 5/12. While clearly not impossible, such fundamental changes in flow structure with very small changes in ReWe or We from the Newtonian value (zero) must be viewed with some skepticism and we believe subjected to further study.

Unfortunately, there have been very few attempts to actually observe the streamlines experimentally for the motion of a viscoelastic fluid past either a solid sphere or cylinder. The only studies of which we are aware are those of Ultman (1970)--reported in Ultman and Denn (1971)--and of Broadbent and Mena (1974). The values of Re and We for these two experiments are given in Table 1.[†] In both cases, Re << 1 and We << 1. However, the results obtained were very different. Ultman and Denn (1971) published a single die-streak photograph for the motion of 1.7% aqueous solution of

[†]In the case of Broadbent and Mena (1974), We was calculated from the coefficient of the quadratic term in the expression for the drag in flow past a solid sphere which was measured in the same work. The value of We for Ultman and Denn (1971) was apparently mis-printed as 3.2. However, simple calculation using Ultman and Denn's stated values for λ of :04 sec, velocity u = .077 cm/sec, and cylinder diameter, 2R = 3/8 inch leads to the value quoted here of 3.2×10^{-3}.

CMC-7H past a cylinder which showed the apparent existence of a large upstream shift in streamlines, as predicted by their theory. On the other hand, similar photographs for a cylinder and a sphere obtained by Broadbent and Mena showed essentially no shift in the streamlines either upstream or downstream. The latter result would appear to be in accord with the small Re, small We theories listed at the beginning of this section which predict only a very slight and likely imperceptible downstream shift but is clearly contradictory both to the experiment and theory of Ultman and Denn (1971). However, both Broadbent and Mena and Ultman and Denn's flow visualization experiments were restricted to a single value of Re and We, and the data consist of one (U. - D.) or two (B. - M.) die-streaks at a moderate distance from the body.

Motivated by the restricted amount of available data, and by the apparent contradictions between the existing experimental and theoretical studies, the present work was undertaken to obtain detailed visualization of the motion of a viscoelastic fluid past a solid sphere for $Re \ll 1$ but with We varied over a wide range. This work has led us to a re-examination of the theoretical analysis of Ultman and Denn (1971), which we describe briefly in the last section of the present communication.

EXPERIMENTAL RESULTS

The experiments were conducted in a vertical tank with dimensions 6" x 6" x 7'. The sphere was supported in the liquid by a thin but stiff horizontal wire which was attached several diameters from the sphere to lightweight vertical strings as shown in Figure 1. Preliminary experiments showed that this configuration for the sphere produced little, if any,

disturbance of the flow in the meridional symmetry plane, where observations were made. The relative motion between the sphere and surrounding fluid was produced by simply pulling the sphere vertically upward at a known rate through the otherwise quiescent fluid. Flow visualization was accomplished using micron size polyethylene particles as tracer material. These particles were found to be nearly neutrally buoyant and, in fact, would neither float to the surface nor sink to the bottom of the tank on a time scale of several weeks. The field of view was illuminated through two very narrow slits (4" in length and .15 mm in width) which were placed on either side of the column at a position which bisected the sphere as it moved through the field of view. Photographs were obtained using a Graflex single lens reflex camera, which was mounted on a movable platform. The film used was type 57, high speed (ASA 3000) Polaroid, and exposure times of several seconds were typical. A more detailed description of the apparatus and experimental methods may be found in Zana (1975).

The experiments were designed to yield small values of the Re (maximum 0.1), but a wide range of We. This was accomplished by using two different solutions of the commercial polymer Separan AP30, several different size spheres, and a relatively wide range of translational velocities. The basic conditions of the experiments are summarized in Table 2.

The key data from the present experimental study are the streakline flow visualization photographs. Several representative examples covering the range $Re < 0.12$ and $10^{-2} \leqslant We \leqslant 22$ are reproduced in Figure 2. Included is the case $Re = 10^{-4}$, $We = 10^{-2}$ (Figure 2a) which corresponds approximately to the prior experiments cited in Table 1, and a case $Re = .08$, $We = .62$ (Figure 2c) corresponding to the value $ReWe = .05$ for which the Ultman and

Denn calculations show strong upstream shifting of the streamlines.

At the smallest values of We, the streamlines at all radial positions are perfectly symmetric fore and aft, with no discernable shift in either the upstream or downstream directions. This behavior is clearly at odds with the experimental observation of Ultman and Denn (1971), but consistent with the more recent photograph of Broadbent and Mena (1974). For larger values of We, however, there is a definite upstream shift in the streamlines, which increases in degree with increase of We, but at a decreasing rate for the larger values of We. Two streamlines, which terminate at the same downstream points (0.1 and 0.6 sphere diameters from the axis of symmetry) were traced from Figures 2a and 2e in order to illustrate more clearly the magnitude of the upstream shift. These are reproduced in Figure 3a. Clearly, even for We = 10 where elastic effects would be expected to be large, the magnitude of the upstream shift is relatively small and primarily limited to the region nearest to the sphere. Nowhere in the flow is the shift anywhere near the magnitude suggested by Ultman and Denn's study. A more direct comparison is provided in Figure 3b where we have traced two streamlines from Figure 2c, for ReWe = .05, together with several of Ultman and Denn's calculated streamlines for the same value of ReWe (Figure 5 of their paper). Again it is evident that the magnitude of the experimentally observed shift is extremely small compared to that predicted by their theory.

In order to provide at least a qualitative measure of the dependence of the upstream shift on We, three streamlines starting downstream at 0.1, 0.2 and 0.4 sphere radii from the symmetry axis were traced out from the experimental pictures for several different values of We, and the difference

in the area bounded by these streamlines between the upstream and downstream half of the flow field was measured. This difference, normalized with respect to the total area under the same streamline, is listed in Table 3 for eight different values of We, with Re < 0.12. In a Newtonian fluid in this Reynolds number range, no inertia-induced shifting can be detected. Although the actual numbers $\Delta A/A_{total}$ are somewhat arbitrary, we believe that they nevertheless provide a useful relative measure of skewness for different values of We and different distances from the body. For the smallest values of We, no shift could be detected, as we have suggested above. However, with increase of We (and also of ReWe), the magnitude of the streamline shift increases up to approximately We $\simeq$ 10 (ReWe $\sim$ 1) where the rate of increase with We appears to decline fairly rapidly. This later result is similar to James and Acosta's (1970) heat transfer measurements from a cylinder in which Nu number was found to become independent of the uniform stream velocity at velocities greater than the shear wave velocity (i.e. ReWe $\gtrsim$ 1). One final point is to note that the region of flow influenced by the presence of sphere increases with increasing elasticity. This can be seen by comparing the streamlines 0.6 diameters away from the symmetry line in Figures 3a, and 3b. For We = 0.6, no shift can be detected at this distance from the sphere. For We = 10, however, there is a definite upstream shift, though it is greatly reduced in magnitude compared to that for the streamlines which are closer to the body (cf. Table 3).

DISCUSSION

The experimental results of the preceding section have shown conclusively that the theory of Ultman and Denn greatly exaggerates the degree of upstream skewing of the streamlines. In view of this, plus the physical significance which has been associated with the change in type of Ultman and Denn's model at ReWe = 1, we have undertaken to re-examine the validity of its basic assumptions. Among these, the most fundamental is the linearization of the constitutive model and equations of motion using an Oseen-type approximation. As we have noted previously, both Ultman and Denn (1971) and subsequent investigators have assumed that this linearization is valid for $Re \ll 1$ only, with any restriction on We being a result of subsequent approximations which are required to solve the linearized equations and boundary conditions.

We contend, however, that the linearized equations themselves do not provide a uniformly valid approximation to the elastic flow contributions for the type of problem considered, even if Re and We are both vanishingly small. In order to clearly illustrate this point, it is useful to briefly consider the equations of motion, and an Oldroyd rate-type constitutive equation of the same general form as that adopted by Ultman and Denn. In dimensional form, these are

$$\rho\left(\frac{\partial u_i}{\partial t} + u_k \frac{\partial u_i}{\partial x_k}\right) = -\frac{\partial p}{\partial x_i} + \frac{\partial}{\partial x_k}\tau_{ik} \tag{1}$$

and

$$\tau_{ik} + \lambda_1 \frac{D\tau_{ik}}{Dt} + \mu_o \tau_{jj} e_{ik} - \mu_1(\tau_{ij}e_{jk} + \tau_{jk}e_{ij}) \tag{2}$$

$$+ \nu_1 \tau_{j\ell} e_{j\ell} \delta_{ik} = 2\mu\left[e_{ik} + \lambda_2 \frac{De_{ik}}{Dt} - 2\mu_2 e_{ij}e_{jk} + \nu_2 e_j\, e_{j\ell}\delta_{ik}\right]$$

where D/Dt is the generalized Oldroyd time derivative, and λ_i, μ_i and ν_i are all material coefficients. For slow flows, these equations may be non-dimensionalized with respect to the free stream velocity U, the body diameter ℓ, and the characteristic viscous stress, $\mu U/\ell$. Denoting the non-dimensionalized quantities with overbars, we thus substitute

$$u_i = U\bar{u}_i \ , \quad x_i = \ell\bar{x}_i \ , \quad p = \left(\frac{\mu U}{\ell}\right)\bar{p} \ , \quad \tau_{ik} = \left(\frac{\mu U}{\ell}\right)\bar{\tau}_{ik}$$

and

$$t = \left(\frac{\ell}{u}\right)\bar{t}$$

into the equations (1) and (2) to obtain

$$\frac{\partial \bar{u}_i}{\partial \bar{t}} + \bar{u}_k \frac{\partial \bar{u}_i}{\partial \bar{x}_k} = \frac{1}{Re}\left(- \frac{\partial \bar{p}}{\partial \bar{x}_i} + \frac{\partial}{\partial \bar{x}_k}\bar{\tau}_{ik}\right) \tag{3}$$

with

$$\bar{\tau}_{ik} + We\left[\frac{D\bar{\tau}_{ik}}{D\bar{t}} + \frac{\mu_o}{\lambda_1}\bar{\tau}_{jj}\bar{e}_{ik} - \frac{\mu_1}{\lambda_1}(\bar{\tau}_{ij}\bar{e}_{jk} + \bar{\tau}_{jk}\bar{e}_{ij}) + \frac{\nu_1}{\lambda_1}(\bar{\tau}_{j\ell}\bar{e}_{j\ell}\delta_{ik})\right] = 2\bar{e}_{ik} + 2We\left[\frac{\lambda_2}{\lambda_1}\frac{D\bar{e}_{ik}}{D\bar{t}} - 2\frac{\mu_2}{\lambda_1}\bar{e}_{ij}\bar{e}_{jk} + \frac{\nu_2}{\lambda_1}\bar{e}_{j\ell}\bar{e}_{j\ell}\delta_{ik}\right] \tag{4}$$

The quantities (μ_o/λ_1), (μ_1/λ_1), (ν_1/λ_1), λ_2/λ_1, μ_2/λ_1, and ν_2/λ_1 are all dimensionless ratios of intrinsic time constants for the constitutive model and are generally of order unity.

The Oseen-type linearization may now be formally invoked to simplify the exact equations (3) and (4), i.e. we assume

$$\bar{u}_i = \delta_{i1} + u_i' \ ; \quad \bar{e}_{ik} = e_{ik}' \ ; \quad \bar{\tau}_{ik} = \tau_{ik}' \ ; \quad p = p'$$

and neglect all terms which are quadratic in any of the primed variables.

With $\lambda_2 \equiv 0$, the resulting equations are those which were obtained by Ultman and Denn (1971). The key question is whether the linearized equations provide a uniformly valid approximation to the exact equations (3) and (4) in some appropriate limit. In the special case We $\equiv$ 0, corresponding to a Newtonian fluid, it is by now well-known that the Oseen linearization does provide such an approximation for the nonlinear inertia terms provided only that Re << 1. Far from the body (i.e. $\bar{r} = O(Re^{-1})$), where the convective term is the same order of magnitude as the pressure and viscous terms, the Oseen linearization is a good first approximation since $|u_i'| << 1$. Near to the body where the linearization is poor, the convective terms are asymptotically small compared to the pressure and viscous terms (provided Re << 1), and the linearized equation of motion still provides a valid first approximation to the exact equation (3).

When the Oseen linearization is applied to (4), the only terms surviving (for a steady flow) are

$$\tau_{ik}' + We \frac{\partial \tau_{ik}'}{\partial \bar{x}} = 2e_{ik}' + 2We \frac{\lambda_2}{\lambda_1} \frac{\partial e_{ik}'}{\partial \bar{x}} \qquad (5)$$

Clearly, the equation (5) will provide a good approximation to (4) at large distances from the body. However, near to the body for arbitrary We, it will not. At first, it may seem that a similar argument could be applied to the neglected nonlinear terms in the constitutive model for We << 1, as was just used in discussing the nonlinear term in (3) for Re << 1. Indeed, near to the body where the linearization is inaccurate, all of the nonlinear terms are dominated by the Newtonian terms provided We << 1, as before. The difference is that far out, where the linearization is accurate, the correctly modelled term which is left is still small compared to the dominant Newtonian terms if We << 1, as required in the region near to the

body. Thus, unlike the linear approximation of the inertia terms which is of greatest relative significance in the region where it is also most accurately modelled, the elastic contribution is restricted by the requirement We << 1 to be of second order significance compared to the dominant Newtonian terms everywhere in the flow domain. Furthermore, in view of inaccuracy of the Oseen linearization near to the body, it is clear that the linearized equation (5) does not even provide a uniformly valid first approximation to the small elastic corrections. One consequence is that the asymptotic solution for small but nonzero We using (5) does not agree even qualitatively with the corresponding limiting solutions of Leslie (1961) and others which are based on the full constitutive model (4). Most evident is the difference in streamline displacement which is downstream in the solutions of Leslie (1961) and others, but completely unchanged through $O(We^2)$ using (5). Furthermore, the drag coefficient is predicted to decrease at $O(We^2)$ according to Leslie, but again to remain unchanged when the linearized model is used.

Our conclusion, then, is that the Oseen-linearized theory of Ultman and Denn (1971) for the motion of a viscoelastic fluid past a submerged body is not a uniformly valid approximation of the elastic contributions to the fluid behavior for <u>any</u> value of We.[†] Thus, though the calculations of Ultman and Denn did show an upstream shift of the streamlines, as also observed experimentally (but with much smaller magnitude), the theoretical result must be considered as completely without substance since it was based on a model which is incapable of correctly modelling the physics. A

[†] A similar conclusion is also inherent in the independent work of Mena and Caswell (1974). These authors show that the Oseen equations may be utilized in the outer region of a matched asymptotic expansion for small Re (and We), but do not consider the apparent alternative which one is led to from the Newtonian case (We ≡ 0) of using the Oseen equations to provide a uniformly valid first approximation.

similar remark must also be made with regard to the apparent correlation between the change in type of Ultman and Denn's equations at ReWe = 1, and the occurrence of experimentally observed discontinuities in certain features of the flow at a similar value of ReWe (cf. Ultman and Denn (1970)). A clear understanding of the physics responsible for these and other equally important features of the motion of a viscoelastic fluid past a submerged body must await further investigation.

ACKNOWLEDGEMENTS

This work was supported, in part, by the National Science Foundation through grants GK35468 and ENG74-17590.

REFERENCES

1. Lamb, H., Hydrodynamics, Cambridge University Press, Cambridge (1932)
2. Oseen, C. W., Hydrodynamik, Akademische Verlagsgesellschaft Leipzig (1927)
3. Proudman, I., and Pearson, J. R. A., J. Fluid Mech., 2, 237 (1957)
4. Mena, B., and Caswell, B., submitted to Z.A.M.P. (1974)
5. Broadbent, J. M., and Mena, B., submitted to Z.A.M.P. (1974)
6. Ultman, J. S., and Denn, M. M., Chem. Eng. J., 2, 81 (1971)
7. Zana, E., Ph.D. Thesis, California Institute of Technology, Pasadena, California (1975)
8. Leslie, F. M., Quart. J. Appl. Math., 14, 36 (1961)
9. Giesekus, H., Rheol. Acta, 3, 59 (1963)
10. Caswell, B., and Schwarz, W. H., J. Fluid Mech., 13, 417 (1962)
11. Astarita, G., and Marucci, G., Principles of Non-Newtonian Fluid Mechanics, McGraw-Hill Co. (UK) Limited, Berkshire, England (1974)
12. Ultman, J. S., and Denn, M. M., 14, 307 (1970)
13. James, D. F., and Acosta, A. J., J. Fluid Mech., 42, 269 (1970)

TABLE CAPTIONS

Table 1: Re and We Numbers for the Experiments of Ultman and Denn, and Broadbent and Mena.

Table 2: Values of λ, d and u for the Experiments in Two Viscoelastic Liquids.

Table 3: Difference in Area Bounded by Streamlines Between Upstream and Downstream Half of the Flow Field.

FIGURE CAPTIONS

Figure 1: The Experimental Configuration

Figure 2: Experimental Streamlines (Flow from Left to Right)

Figure 2a: Re = 10^{-4}, We = 10^{-2}

Figure 2b: Re = 1.5×10^{-3}, We = 0.17

Figure 2c: Re = 0.08, We = 0.62

Figure 2d: Re = 0.05, We = 1.00

Figure 2e: Re = 0.10, We = 10.0

Figure 2f: Re = 0.12, We = 22.0

Figure 3a: A Comparison of Experimental Streamlines

—— Re = 10^{-4}, We = 10^{-2}

—·— Re = 0.1, We = 10.0

Point A: 0.1 diameter away from symmetry axis.

Point B: 0.6 diameter away from symmetry axis.

Figure 3b: A Comparison of Experimental and Theoretical Streamlines

——— Re = 10^{-4}, We = 10^{-2} (Experimental, this work)

_·_·_ Re = 0.08, We = 0.62 (Experimental, this work)

– – – Re = 0.10, We = 0.50 (Theoretical, Ultman and Denn, 1971, RE Solution, N = 2)

—·— Re = 0.10, We = 0.50 (Theoretical, Ultman and Denn, 1971, MSE Solution, N = 4)

Point A: 0.16 diameter away from symmetry axis

Point B: 0.60 diameter away from symmetry axis

Table 1

Investigators	Re	We
Ultman & Denn (1971)	2×10^{-4}	3.2×10^{-3}
Broadbent & Mena (1974)	2×10^{-2}	1.0×10^{-2}

Table 2

Solution	λ(sec)	d(cm)	u(cm/sec)
1% AP30-Water by weight	3.8	1.56	0.05
		2.56	0.68 - 2.34
		0.64	1.60 - 7.40
		0.34	1.80
0.523% AP30 -	15.0	0.95	1.28 - 1.45
45.6% Water -		1.90	0.005 - 0.38
53.9% Glycerine by weight		1.75	1.04 - 1.52

Table 3

Re	We	ReWe	$\Delta A/A_{total}$ 0.1 Radius Away	$\Delta A/A_{total}$ 0.2 Radius Away	$\Delta A/A_{total}$ 0.42 Radius Away
10^{-4}	10^{-2}	10^{-6}	--†	--	--
1.5×10^{-3}	0.17	2.5×10^{-4}	--	--	--
0.08	0.62	0.05*	0.039	0.0213	--
0.08	9.25	0.74	0.1468	0.1275	0.0700
0.09	9.70	0.87	0.1798	0.1475	0.0873
0.10	10.00	1.00	0.1894	0.1539	0.0915
0.12	22.2	2.66	0.1960	0.1540	0.1033

† No measurable difference

* Same case as Ultman and Denn's theoretical streamline pictures.

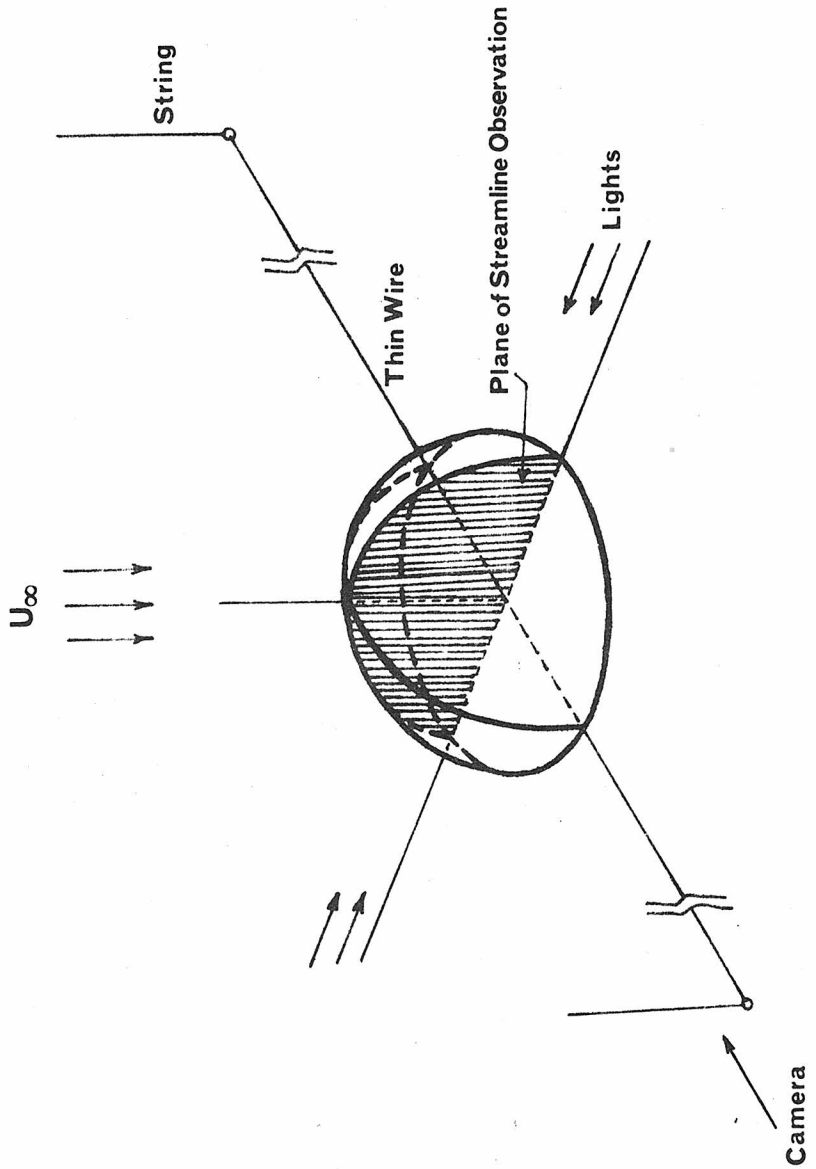
String
Thin Wire
Plane of Streamline Observation
Lights
U_∞
Camera

Figure 1

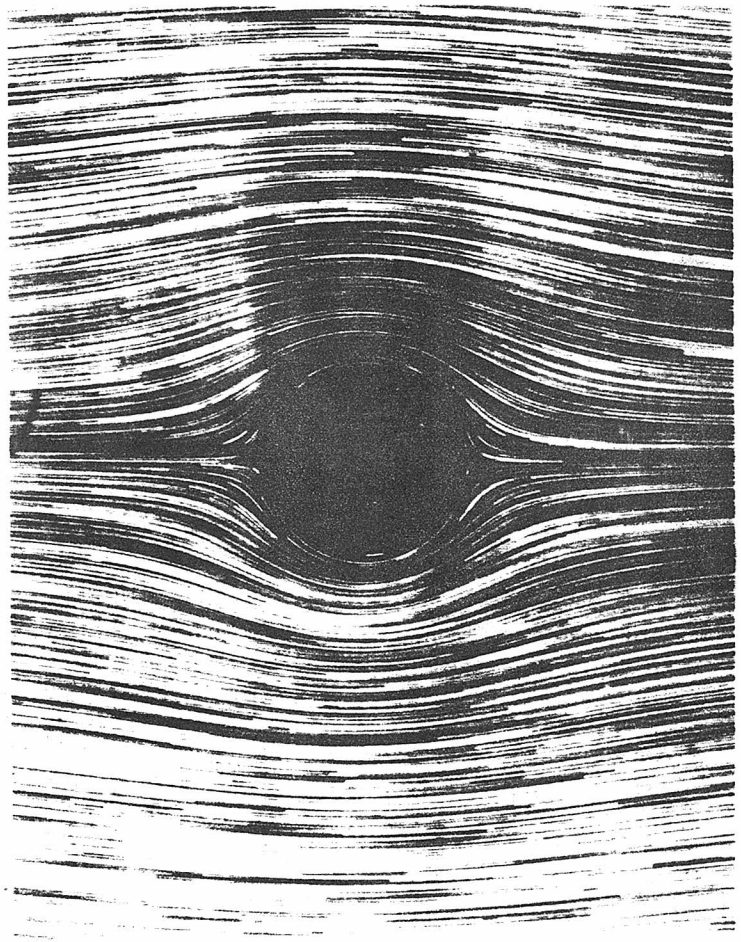

FIGURE 2a Re = 10^{-4}, We = 10^{-2}

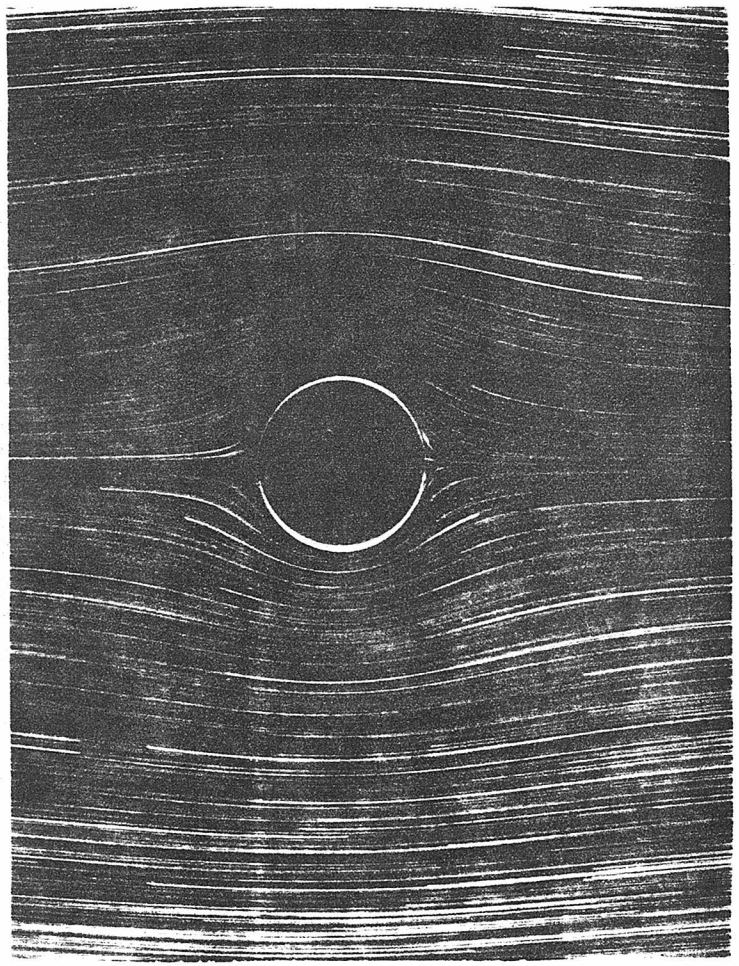

FIGURE 2b Re = $1.5X10^{-3}$, We = 0.17

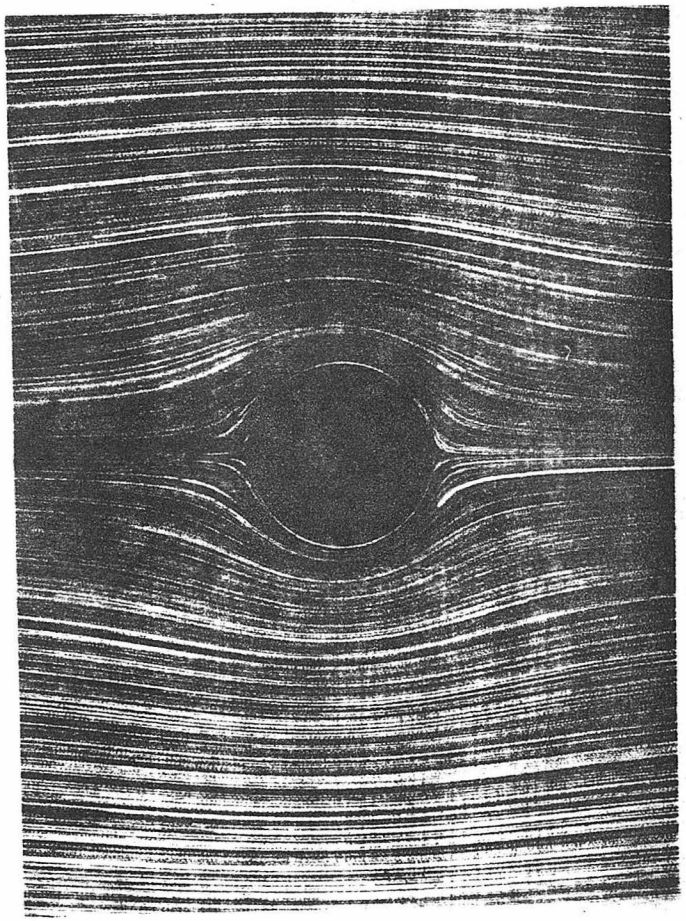

FIGURE 2c Re = 0.08, We = 0.62

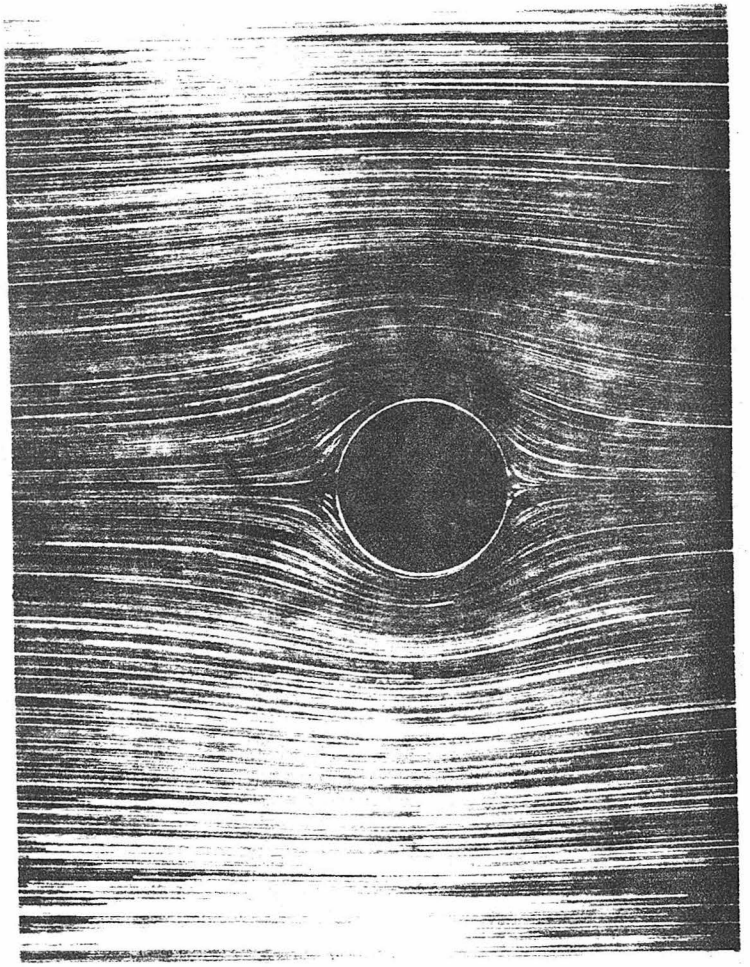

FIGURE 2d Re = 0.05, We = 1.0

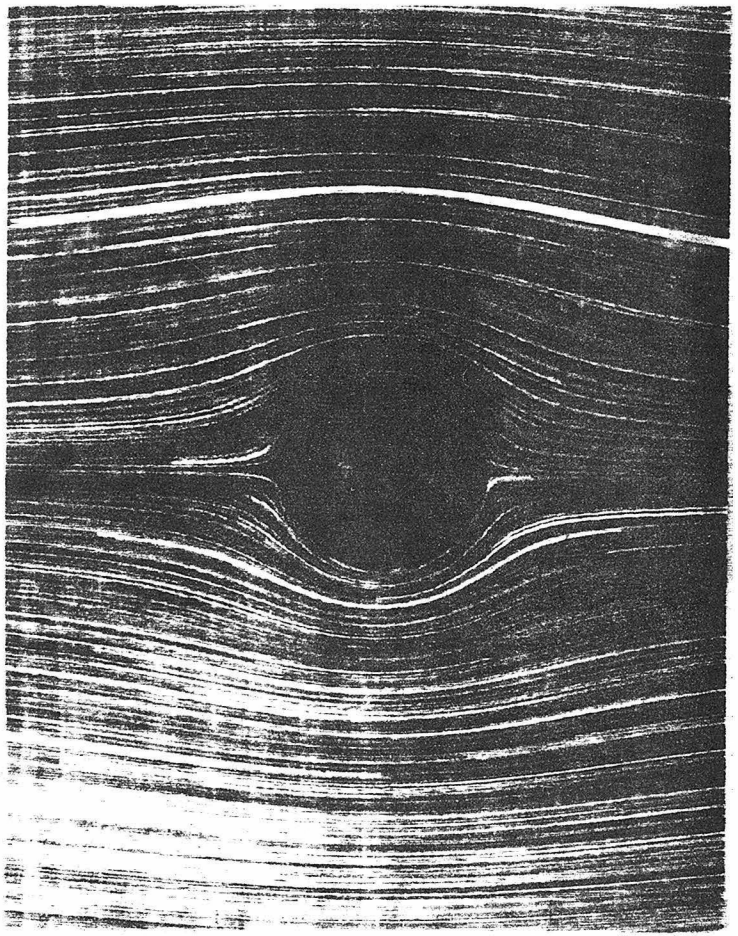

FIGURE 2e Re = 0.1, We = 10.0

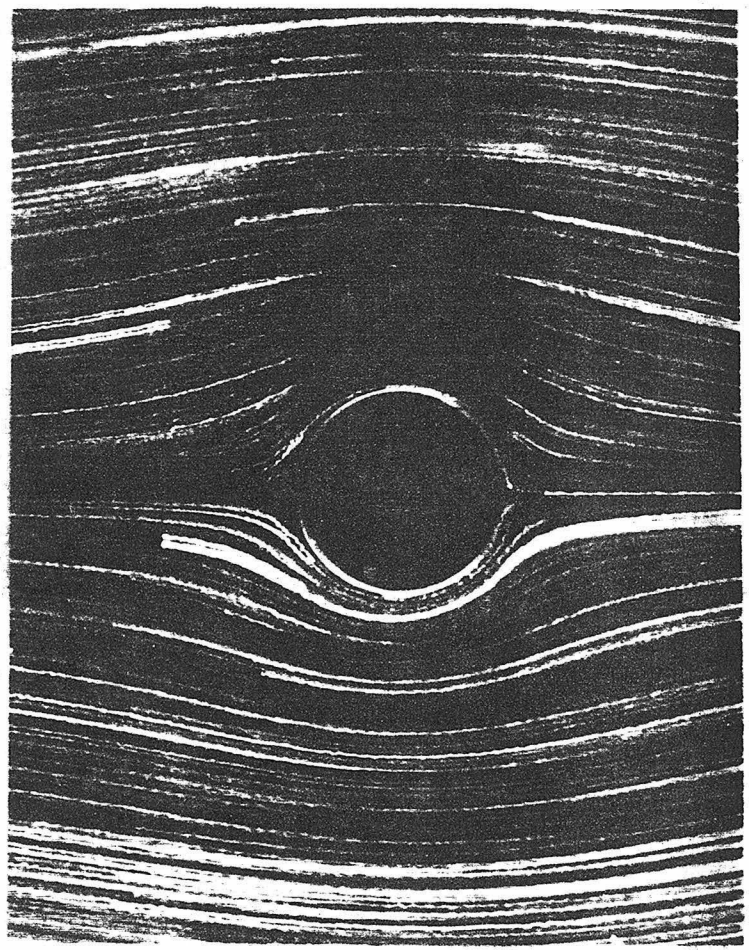

FIGURE 2f Re = 0.12, We = 22.0

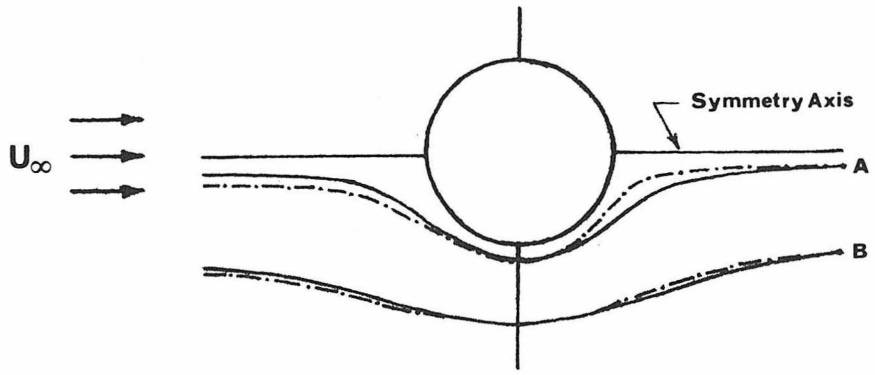

Figure 3a

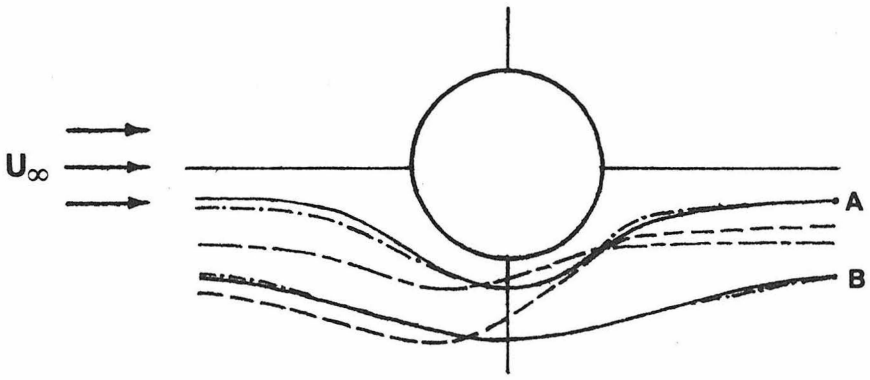

Figure 3b

CHAPTER IV

THE DYNAMICS AND DISSOLUTION OF GAS BUBBLES IN A VISCOELASTIC FLUID

The Dynamics and Dissolution of Gas Bubbles in a Viscoelastic Fluid

E. Zana and L. G. Leal

Chemical Engineering
California Institute of Technology
Pasadena, California

A. INTRODUCTION

One of the most important problems of non-Newtonian fluid dynamics is the buoyancy-induced translational motion of gas bubbles through viscoelastic materials such as polymer solutions and melts. From the technological point of view, one is particularly interested in application of the basic physical principles to the design and operation of gas-liquid contact mass transfer equipment. However, even from a more fundamental viewpoint, the problem of the motion of a single gas bubble is interesting as an example of a strongly viscometric flow which exhibits major macroscopic differences from its Newtonian counterpart. A detailed investigation of such problems is important to the gradual build-up of basic understanding of the mechanics of fully viscoelastic fluids.

Among the various changes which are observed in comparing the behavior of bubbles in Newtonian and viscoelastic fluids, none is more striking nor seemingly of greater potential technological significance than the existence, in the viscoelastic case, of an abrupt (discontinuous) transition in terminal velocity of the bubble when measured as a function of the bubble volume. The existence of such a transition was first reported by Astarita and Apuzzo (1965), who found a six-fold increase in bubble velocity at the point of transition for a 0.5% solution of the commercial J-100 polymer. Similar results have more recently been reported by Calderbank, Johnson and Loudon (1970) in 1% Polyox solutions and by Leal, Skoog and Acrivos (1971) in solutions of the commercial polymer, Separan AP30. A steep, but not abrupt, increase in velocity has also been observed in the case of liquid drops moving through viscoelastic liquids (cf. Barnett et al., 1966; Garner et al., 1957; Warshay et al., 1959; Fararouri and Kintner, 1961).

Kintner et al. (1961) proposed that the increase in velocity for drops is the result of a transition in the conditions at the drop interface from no-slip to a freely circulating regime (equivalent to the well-known transition from the Stokes to Hadamard regimes in Newtonian liquids) coupled with a change of shape corresponding to a decrease in frontal area. In the case of gas bubbles, however, Astarita and Apuzzo (1965) showed experimentally that the frontal area actually increased during the velocity transition. As a result, it was speculated that the velocity increase was solely a result of the transition in surface conditions, with viscoelasticity hypothesized as being responsible for the abruptness. Further, it was implied that the magnitude of the velocity transition could largely be accounted for by considering only the purely-viscous, shear-thinning viscosity, ignoring elastic and normal stress contributions.

A partial test of Astarita's proposal was reported several years ago by Leal, Skoog and Acrivos (1971). Their experimental measurements showed that, a) the bubble velocities for volumes less than the critical volume are precisely equal to those measured for equal volume glass spheres provided suitable density corrections are utilized; b) no terminal velocity transition occurs for the glass spheres. Hence, strong indirect evidence was found to confirm the change in interfacial conditions as the cause of the observed velocity transition. The effect of shear dependent viscosity, in the absence of viscoelastic effects, was also studied by employing an empirical (curve-fit) purely-viscous fluid model to calculate numerically the terminal velocities of non-circulating, partially circulating, and fully circulating spherical bubbles at the measured critical volume. It was found that the presence of shear-dependent viscosity alone could only

account for about 30% of the magnitude of the measured velocity transition. Hence, it was surmised that better agreement between theory and observation could only be achieved by taking account of viscoelastic effects in the fluid. Of perhaps greater significance was the subsequent conclusions, based on simple qualitative arguments, that a relatively small additional viscoelastic contribution to the force balance on the bubble would be sufficient to account for the much larger measured velocity increases. The conditions required to produce a consistent result are that the drag be reduced by the elastic effects in both the pre-transition and post-transition regimes, but with the effect being somewhat greater in the latter case.

As an initial test of the viability of this proposal, an attempt was made by the present authors (see Zana, 1975; Leal and Zana, 1975) to determine whether elastic effects in the absence of shear-dependent viscosity would contribute to the bubble drag in a manner which was consistent with this requirement. In order to investigate this question we utilized "slow flow" asymptotic solutions, based on the 6-constant Oldroyd (1958) fluid model, to compare the viscoelastic contributions to the drag on a rigid no-slip sphere and on a freely circulating spherical bubble. The rigid sphere result was taken from the solution of Leslie (1961). The solution for the case of a spherical bubble was obtained by Zana (1975). In the limit corresponding to a constant shear viscosity it was shown that the purely elastic contributions to the drag only arise at second order, $O(We^2)$, in the appropriate retarded motion expansion, and that the drag is decreased in both cases compared to the Newtonian value. Significantly, however, the decrease is much more pronounced for the bubble than for the rigid, no-slip

sphere. Thus, the "slow flow" viscoelastic approximation offers strong preliminary evidence to support the original hypothesis of Leal, Skoog and Acrivos (1971).

In spite of all of these efforts, a great deal remains to be done in order to attain a complete understanding of the terminal velocity transition, and its possible technological significance. In particular, to complete the discussion of the magnitude of the transition, further theoretical effort is necessary to obtain (numerical) solutions for the flow past spherical bodies which are not restricted to "slow" (nearly Newtonian) flows. No physical explanation has ever been proposed for the abruptness of the transition at the critical volume. Furthermore, with the exception of a single data set for CO_2 in a 1.0% of Polyox in water by Calderbank et al. (1970), no attention has yet been paid to the mass transfer characteristics in the transition regime. Indeed, little previous work has been reported in any regime for mass transfer in viscoelastic liquids.

The present investigation is primarily concerned with experimental determination of the rate of mass transfer for single gas bubbles in a viscoelastic liquid. In order to assist in data interpretation, we have also repeated some of the earlier measurements of shape and terminal velocity, with particular emphasis on the differences between dissolving and non-dissolving bubbles. The terminal velocity behavior does provide some further insight into the abruptness of the velocity transition which was reported in earlier studies. In addition to providing a more extensive correlation of mass transfer rates and rheological properties of the suspending fluid, the present study also differs fundamentally from the earlier work of Calderbank (1970) in the method of measurement. In Calderbank's work the bubble volume is held constant and the internal gas

concentration goes down, while in the present work the bubble volume changes freely as the mass transfer process proceeds.

B. DIMENSIONAL ANALYSIS AND THEORETICAL BACKGROUND

An important initial step in the design and interpretation of the mass transfer experiments is to determine the physical and rheological parameters which will play a fundamental role in the bubble dynamics and mass transfer processes. This is most easily accomplished by dimensional analysis based on the governing differential equations and boundary conditions. Let us first consider the purely dynamical problem of a bubble translating with a constant velocity through a viscoelastic fluid which, for convenience, we shall represent by the 8-constant Oldroyd constitutive equation of state. Although somewhat arbitrary, the Oldroyd model does correctly represent all of the commonly observed rheological characteristics of viscoelastic liquids in at least a qualitative sense. At any rate, for the dimensional analysis which we shall consider here, the precise form of the constitutive model is not critical. Thus, introducing the dimensionless variables (denoting by the overbar)

$$\bar{U}_i = U_i/U_\infty, \quad \bar{x}_i = x_i/R_{eq}, \quad \bar{p} = p/\left(\frac{\mu U_\infty}{R_{eq}}\right) \quad \bar{\tau}_{ik} = \tau_{ik}/\left(\frac{\mu U_\infty}{R_{eq}}\right) \tag{1}$$

and assuming the fluid to be incompressible, we obtain

$$U_k \frac{\partial U_i}{\partial x_k} = \frac{1}{Re}\left\{-\frac{\partial \bar{p}}{\partial \bar{x}_i} + \frac{\partial}{\partial \bar{x}_k}\bar{\tau}_{ik}\right\}; \quad \frac{\partial \bar{u}_i}{\partial \bar{x}_i} = 0 \tag{2}$$

where

$$\bar{\tau}_{ik} + We\left[\frac{D\bar{\tau}_{ik}}{D\bar{t}} + \frac{\mu_o}{\lambda_1}\bar{\tau}_{jj}\bar{e}_{ik} - \frac{\mu_1}{\lambda_1}(\bar{\tau}_{ij}\bar{e}_{jk} + \bar{\tau}_{jk}\bar{e}_{ij}) + \frac{\nu_1}{\lambda_1}(\bar{\tau}_{j\ell}\bar{e}_{j\ell}\delta_{ik})\right]$$

$$= 2\bar{e}_{ik} + 2We\left\{\frac{\lambda_2}{\lambda_1}\frac{D\bar{e}_{ik}}{Dt} - 2\frac{\mu_2}{\lambda_1}\bar{e}_{ij}\bar{e}_{jk} + \frac{\nu_2}{\lambda_1}\bar{e}_{j\ell}\bar{e}_{j\ell}\delta_{jk}\right\} \tag{3}$$

In the equations (1), R_{eq} is the radius of a sphere with the same volume as the bubble (which may be deformed), U_∞ is the steady, terminal velocity of translation, and D/Dt represents the generalized spin or Jaumann time derivative. The dimensionless parameters which appear in the equations (2) and (3) are the Reynolds number, $Re \equiv 2R_{eq}U_\infty|\nu$; the Weissenberg number, $U_\infty\lambda_1/R_{eq}$, and a series of quantities (μ_0/λ_1), (μ_1/λ_1), (ν_1/λ_1), (ν_2/λ_1), (λ_2/λ_1) and (μ_2/λ_1) which represent ratios of intrinsic time constants μ_i, ν_i and λ_i of the constitutive model. The time constant, λ_1, which appears in the Weissenberg number, is the so-called principal relaxation time of the fluid. The important point to note is that whereas Re and We can vary widely ($0 < Re < \infty$, $0 < We < \infty$), the ratios of dimensionless time constants are generally of order unity and vary relatively little from fluid to fluid. This means that any qualitative discussion of the dynamics based on (2) and (3) can focus on the magnitudes of the Reynolds number and Weissenberg numbers alone. In addition, of course, consideration must also be given to any parameters which may appear in the boundary conditions. However, for present purposes, we shall suppress explicit discussion of these parameters by noting that, in the simplest circumstances, it is only the surface tension which is important, and that the bubble will be more or less deformed in shape depending upon the relative magnitudes of inertia or elastic forces and the tensile surface forces.

Examination of the governing equations (2) and (3) shows that the ratio of inertia to viscous forces is measured by the Reynolds number, the ratio of elastic to viscous forces by the Weissenberg number, and the ratio of elastic to inertia forces by We/Re. Several distinct regimes are possible, depending upon the relative magnitudes of Re and We. For low Reynolds

numbers the bubble shape and other flow characteristics are determined by the balance between elastic and viscous/pressure forces. In this regime the rheological properties of the suspending fluid generally play a significant role. However, as the bubble volume is decreased, U decreases (in every case known to us) at a rate proportional to R_{eq}^{m} with $m > 1$. Thus, in such cases the Weissenberg number, $We \to 0$, and the purely viscous effects eventually dominate the dynamics for sufficiently small bubbles. The fluid motion in this regime is then identical with that in a Newtonian fluid with equivalent viscosity. As the bubble volume is increased elastic contributions become more important; however, so do inertia effects, and eventually the latter dominate the fluid dynamics <u>everywhere</u> in the flow domain. This is quite different from the case of high Reynolds number flow past a solid body where the viscous and elastic effects always remain important in a thin layer near the body, and is a consequence of the surface boundary conditions which require zero tangential stress rather than zero tangential velocity. In this inertia dominated regime the bubble shapes and other flow characteristics are completely independent of the fluid rheology.

We have suggested in the preceding paragraph that the fluid dynamical effects of viscoelasticity can be mainly accounted for by consideration of the magnitude of the Re and We numbers. It should be noted, therefore, that a fluid which has $We > 0$, but μ_0, μ_1, ν_1, ν_2 and λ_2 equal to zero, does <u>not</u> exhibit the important property of a shear-thinning viscosity. A model which retains μ_0 and λ_2, on the other hand, does exhibit this effect. Thus, in spite of the relative invariance of μ_0/λ_1 and λ_2/λ_1, it is <u>not</u> sufficient, in characterizing the non-Newtonian nature of the suspending fluid, to consider only We and Re. On the other hand, it is inconvenient and not fully adequate to keep all (or even any) of the time constant

ratios of the nondimensionalized Oldroyd constants. The primary reason is that purely-viscous fluids (such as CMC solutions) which exhibit strong shear thinning, but no other significant manifestation of viscoelasticity, cannot be included in any scheme of parameter ordering which derives from the Oldroyd model (or, indeed, from any of the presently accepted models of viscoelastic liquids).† As a convenient (if ad hoc) alternative, we shall use a simple law model

$$\underline{\underline{\tau}} = -\left\{ m\left|\frac{1}{2}\,\underline{\underline{e}}:\underline{\underline{e}}\right|^{\frac{n-1}{2}}\right\}\underline{\underline{e}}$$

to provide a second rheological parameter (n), which is capable of reflecting the degree of shear-thinning independently from the degree of elasticity as measured by We.

In the presence of mass transfer, the equations (2) and (3) must be supplemented by a third, namely the convective-diffusion equation for the dissolving material. Coupling between the fluid dynamics and the mass transfer process occurs in at least three ways. First, the velocity field enters directly into the convection terms in the convective-diffusion equation. Second, since material is being transferred either from or to the bubble, its volume will change, thus inducing a time dependent normal velocity in the vicinity of the bubble surface. Third, as the bubble volume changes, both the buoyancy force and the bubble velocity will vary continuously with time. All of these effects must be taken into account in any general analysis of the bubble mass transfer process.

If a characteristic time, a^2/D, is used to define a dimensionless time scale $\bar{t} = t/(a^2/D)$, and the governing equations are again nondimensionalized,

† In such models, small normal stresses, weak stress relaxation or recoil, or any other manifestation of weak elasticity, is invariably accompanied by weak or insignificant shear thinning.

one new parameter enters the system, namely, the Peclet number, $Pe \equiv U_\infty R_{eq}/D$. The Peclet number is measure of the relative magnitude of the convection terms compared with diffusion and time-dependent terms in the convective-diffusion equation. The characteristic time a^2/D, is chosen since the time-dependence of the bubble motion is completely due to the diffusion-induced change in the bubble volume. Peclet number may thus be seen to also provide a measure of the instantaneous velocity of rise of the bubble compared to the normal velocity induced at the bubble surface by its change in volume. Depending on the magnitude of the Peclet number, two distinct limiting cases can be identified.

When Peclet number is large, $Pe >> 1$, the velocity field is dominated by the free streaming motion which is due to the buoyancy-driven bubble rise. The induced velocity due to bubble collapse is, in this limit, asymptotically small. Thus to a first approximation, the equations (2) and (3) may be solved without consideration of the mass transfer process. The only effect of the fluid rheology on mass transfer is as an indirect result of its effect on the velocity field which must be used to evaluate the convection terms in the convective-diffusion equation.

For small values of the Peclet number the velocity field is dominated by the motion induced by the bubble collapse, and the mass transfer problem reduces at first order to the dissolution of a stationary gas bubble in a quiescent, viscoelastic fluid. In this case, the viscoelastic properties of the fluid are of direct significance. Indeed, the high stresses, which occur in a viscoelastic fluid as a result of the mainly extensional motions which are induced by the bubble collapse, can inhibit the collapse rates to such an extent that the whole mass transfer process is controlled by the fluid rheology.

In an earlier paper, Zana and Leal (1975), we analyzed the dependence of mass transfer rate on the rheological properties of the suspending fluid in some detail for the latter case Pe << 1. The present experimental work is mainly concerned with the opposite limit, Pe >> 1, for bubble volumes which are initially near to the critical size for the velocity transition phenomenon.

C. EXPERIMENTAL METHODS

1. Description of the Apparatus

A schematic diagram of the apparatus used in the experiments is shown in Figure 1. The main features are a pair of humidifying columns and an airtight test (absorption) column, a motor-driven camera platform with associated controls and lighting, a specially designed bubble release mechanism, and a pressure measuring system with associated electronics and controls. Of these features, all were used extensively in the present study except for the pressure system which is primarily intended for mass transfer measurements in less viscous fluids where the bubble shape is not steady (see section C3). The purpose of the humidifying columns is to saturate the gas bubble with water vapor before it is introduced into the absorption column. The actual test (absorption) column is constructed of 1/2 to 3/4 inch plexiglass sheet and is seven feet in height with a six-inch square cross-section.

Measurements of bubble velocity, bubble shape and instantaneous mass-transfer rates, as well as streakline flow visualization, are all carried out near the mid-line of the column where flow transients and other effects are minimized.

The velocity of bubble rise was initially measured by simple

multiple-image photography following Leal, Skoog and Acrivos (1971), and this approach was adequate for the dynamics experiments. However, in correlating mass-transfer data it was found that a more reproducible and reliable method was needed in order to minimize scatter. Hence, a simple system was designed in which bubble velocities could be measured automatically and accurately using a combination of two phototransistors with associated pencil-line light sources and an electronic counter. When the bubble passes the lower phototransistor, a pulse is generated which activates the electronic counter. A second pulse, generated by the second phototransistor, stops the counter which thus provides an accurate measure of the elapsed time between pulses. From this time, and the known distance between the phototransistors, the velocity of bubble rise may be calculated. The system is extremely reproducible provided that the bubble shape and motion does not exhibit any oscillating character, and the system is carefully aligned.

2. Bubble Formation and Release Mechanism

Poor design of the bubble release mechanism has been one of the major factors in the lack of consistency between mass-transfer data obtained by different investigators. An example of the potential difficulties are wild oscillations of shape, or local turbulence, created during the release process which have contributed to an apparent age dependence of mass-transfer rates, cf. Deindorfer and Humphrey (1961).

There are two distinct types of bubble formation and release mechanisms which have been used extensively. For small bubbles almost all of the previous investigators used glass (metal) nozzles, orifices or hypodermic needles (cf. Haberman and Morton, 1953). Larger ones were exclusively

created by a turning cup (Peebles and Garber, 1953; Leonard and Houghton, 1963; Calderbank and Lochiel, 1964; Leal, Skoog and Acrivos, 1971). Despite criticism, the turning cup technique still remains the most reliable way of producing single large bubbles. Zieminski and Raymond (1968, 1971) used a capillary tube technique which was credited with yielding more reproducible results. With this method however, it was not possible to produce bubbles larger than 0.25 cc.

In the present work both the capillary tube and the turning cup are used for different ranges of bubble sizes. Figure 2 shows the capillary tube release mechanism in more detail. The capillary tube has a nominal diameter of 2 mm, but is enlarged to 4 mm at its upper end. CO_2 gas is introduced into the tube by a hypodermic needle and is pushed out by a micro syringe filled with the same liquid that is in the absorption column. The enlargement of the tube at its upper end cause the bubble to expand gradually and assume a form close to its final shape before it leaves the tube, thus minimizing initial oscillations in shape. With a smooth, slow release we have also found that the bubble path upward through the column is extremely reproducible, a critical prerequisite to accurate flow visualization. The turning cup mechanism used for large bubbles is not as reliable, but because of the relative high viscosities of the test fluids, the initial disturbances do damp out relatively quickly.

3. Mass-Transfer Measurements

In order to determine the instantaneous rate of mass transfer from a bubble rising through a quiescent liquid, it is necessary to measure its instantaneous volume, surface area and pressure. All of the current methods use photographs to determine the surface area. However, they do differ in the method of measuring bubble volume. Two basic techniques have been

employed. The simplest is to estimate the rate of change of bubble volume from the same photographs as are used to determine surface area. With care, this method can yield quite reasonable results provided the ambient liquid is quite viscous so that the bubble shape is simple and exhibits no oscillations. The alternative approach, which is particularly useful when the bubble shape is neither simple nor steady, is to determine the change in bubble volume from an indirect measure of the space it occupies. A number of variations on this basic theme have been proposed. With the capillary method, the column is filled completely with liquid and the system is open to the atmosphere only through a small capillary tube. The change in bubble volume is correlated with the motion of the meniscus of the liquid in the capillary. The chief difficulty with this method is the delay in response of the capillary fluid due to viscous (viscoelastic) effects. A similar method, in spirit, is the constant-volume system used by Calderbank and co-workers (1970). Here the column is completely filled with liquid, closed to the atmosphere and the mass-transfer rate determined by measuring the (uniform) pressure inside the column. The bubble volume is, of course, constant assuming that the surrounding fluid is incompressible and the column rigid. Although one can clearly obtain an accurate measure of volume (and surface area) with this method, the mass-transfer rate will be relevant, in general, only if the system for which the data are to be applied is also a completely closed and filled system. Otherwise, and especially for viscoelastic liquids (see the discussion of the preceding section) the flow induced by the change in bubble volume can produce significant differences in mass-transfer rates. Indeed, for small Pe numbers we have shown in a previous paper (Zana and Leal, 1975) that the whole mass transfer process can be controlled by the rheologically imposed restrictions on the maximum

rate of bubble collapse. Even for large Pe the present experiments will show that the collapse process can play a fundamental (and in this limit, unexpected) role in the mass-transfer process, giving different rates of mass transfer depending upon whether or not the bubble volume is changing.

A second pressure related method which does not suffer from the disadvantages of Calderbank's method is the so-called airspace-pressure method in which changes in bubble volume are detected by measuring pressure (volume) changes in a small airspace which is left at the top of the column. Recently Garbarini and Chi Tien (1969) presented a comparative study of the airspace-pressure and photographic methods. The basic conclusion was that the photographic method provided more reliable results when the bubbles travel in straight paths with no oscillations and have simple, regular shapes.

The column which we used can be operated in either the airspace-pressure or photographic models. However, the ambient fluids used in the present study were all extremely viscous and/or elastic, and the bubble motions and shape were very smooth and regular. Hence, all of the mass-transfer data which we will describe in later sections were obtained using the simple photographic method.

The photographs required to determine bubble surface area and volume were obtained using a Bolex H-16 motion picture camera mounted on a well-balanced moveable platform which is driven by a motor with an electronic variable speed controller and which can be controlled manually to track the bubble. The recorder and the camera were turned on just before the bubble was released. The camera platform was activated by the bubble itself. To achieve this, a light guide which sends a thin flat beam of light through the column onto a phototransistor was mounted on the column right above the bubble release mechanism. When the beam of light was partially blocked by

the passing bubble, a pulse was generated by the phototransistor, which was amplified by a logic circuit and fed to a relay to activate the motor controller.

In order to achieve constant and reproducible framing rates, the camera motor was run using a D.C. power supply. During each run the voltage input to the camera motor was accurately set to a value determined using a previously obtained calibration between framing rate and voltage. In addition, the framing rate was checked periodically by an electronic counter, as described below.

Illumination for the pictures was provided by two General Radio electronic stroboscopes which were mounted on the camera platform. The shutter of the camera was synchronized to the strobes by rotating a small magnet which is mounted on a shaft of the camera in front of a magnetic pick-up, amplifying the signal and using it to trigger the strobe once per frame. These signals are also counted by a digital counter for a short period of time in order to accurately determine the framing rate.

In reducing the mass-transfer data, the vertical position of the bubble relative to some reference level must be known. In addition, to obtain an accurate scale factor for use in determining bubble surface area (or volume), it is necessary to know the precise lateral position of the bubble relative to the camera. In experiments of other investigators, the vertical position has usually been determined by simply putting a meter stick on the column wall opposite the camera. However, this has the disadvantage of requiring a large depth of field in order to focus simultaneously on both the bubble and the meter stick. This necessitates placing the camera further from the column, thus reducing the image size of the bubble. In the present system we have employed a set of mirrors to produce a virtual image of the meter

stick which is essentially coincident with the bubble path of rise, thus minimizing the required depth of field. The lateral position of the bubble was obtained from a second Polaroid picture taken at right angles to the movie. The Polaroid camera and necessary flood lights were automatically triggered by a microswitch and relay attached to the moving platform for the motion picture camera.

4. Data Reduction

Depending on the velocity of rise, 500 to 1000 frames of film were used for each run. The location and the dimensions of the bubble were obtained from every fifth or sixth frame, and its age during ascent determined from the frame number and framing rate. The bubble volume and surface area were determined by direct measurement of the circumference and projected cross-sectional areas using the observed fact that the bubbles were axisymmetric in all cases. The latter measurement was carried out as follows. The frame to be analyzed was projected onto the 2 foot by 2 foot screen of a microfilm editor. The screen of the editor was furnished with a hairline whose position from some preset position was proportional to a measurable voltage obtained from a potentiometer. The potentiometer signal was fed into a digital voltmeter which digitizes the signal and relays the information to an automated IBM card punch where it was reproduced for later numerical analysis of the bubble area and volume. The measured projected distances are converted to actual length in the experiment by calibration using a photograph of a grid which was suspended in the test column at a distance from the camera which was equal to that of the bubble. The same grid was also used to determine the amount of length-scale distortion from the center of the film to the edges. No measurable distortion could be detected. For a typical data point, approximately 60-80 equally spaced points were

measured around the bubble surface. Final values for surface area and volume were determined by a numerical integration.

D. MATERIALS

As we have noted earlier, the present study was intended to investigate the role of viscoelasticity on the dynamics and dissolution of single gas bubbles. Therefore, in designing the experiments an attempt was made to encompass a series of ambient fluids which range from Newtonian to strongly viscoelastic in their rheological behavior.

The Newtonian fluid which we used was an 89% (wt/wt) aqueous solution of glycerine. This specific concentration had previously been used by Calderbank et al. (1970) in their study of bubble dynamics and mass-transfer, and so was an extremely convenient choice for the present study.

The viscoelastic fluids which we used were water and water/glycerine solutions of the commercial coagulation polymer, Separan AP30. An increase in viscoelasticity can be most easily attained by either increasing the polymer concentration in solution, or by increasing the solvent viscosity (cf. Bruce and Schwarz, 1969). In the present study the solutions in increasing order of viscoelasticity were 0.1%, 0.5% and 1% wt/wt solutions of Separan AP30 in water, and a solution of 0.523% (wt/wt) Separan AP30, 45.6% water and 53.9% glycerine.

The zero-shear viscosity, the density and the power-law index, n, for these materials is listed in Table 1. As discussed in section B, we shall use the power-law parameter as a measure of the degree of thinning of the shear viscosity. In general, the density and the zero-shear viscosity for each solution was checked for two samples, one from the top of the absorption column and one from the bottom, before and after each set of experimental

runs in order to check the uniformity and degree of constancy of the solutions in the column.

The properties listed in Table 1 are all intrinsic parameters of the materials used. As we have noted in section B, it is necessary to consider the Weissenberg number and the Reynolds number in order to fully characterize the relative contributions of fluid elasticity. The latter parameters do not depend only on the intrinsic fluid properties, but also on the velocity and length scales relevant to the flow itself. The needed rheological data, namely λ_1 as a function of shear rate, can be deduced from measurements of the primary normal stress difference, N_1, and the shear viscosity of the solutions as a function of the shear (deformation) rate, γ. For the aqueous Separan solutions, the required data can be obtained from Leal et al. (1971). The data for Separan AP30/water/glycerine is available in Hill (1969).

E. BUBBLE SHAPES

As we have noted previously, the main purpose of the present study was to assess the importance of the velocity transition on mass transfer characteristics for single, soluble gas bubbles. With this objective in mind, a rather short range of bubble size was used, $0.18 \text{ cm} \lesssim R_{eq} \lesssim 0.42$, centered around the nominal critical radius for the transition, $R_{eq} \sim 0.3$ cm, which was obtained by Leal et al. (1971). On the other hand, the present experiments do cover a reasonably broad spectrum of ambient rheological properties and include both bubbles of constant volume (air) and bubbles (CO_2) whose volume is decreasing as a result of mass-transfer. Thus, we believe that it is worthwhile to present some of the data which we have obtained for bubble shape and terminal velocity in the present study.

We have noted in section B that the bubble shape should depend on the

relative magnitudes of the Reynolds number and Weissenberg number for fully viscoelastic liquids. Two distinct domains may be identified. For low values of the Reynolds number, Re << 1, the relative importance of the fluid's elasticity is measured by the We. For Re >> 1, however, one must compare the elastic effects, not with the purely-viscous forces, but instead with the inertial forces. The relative importance of the elastic contributions is then expected to correlate with the magnitude of We/Re rather than We alone. For the range of bubble sizes which we have considered, the four viscoelastic solutions actually span a range of Reynolds number from approximately 10^{-3} to 10^{2}. The dependence of Reynolds number on bubble size (R_{eq}), for each solution, is shown in Figure 3 and listed in Table 2. The 1% Separan/water and the Separan/water/glycerine solutions have Re < 1, while the 0.1% and .5% Separan/water solutions produce Re > 1 (with the exception of the three smallest bubble sizes in the latter case). Also shown in Table 2 is the Weissenberg number as a function of bubble size in the four viscoelastic solutions.

Bubble shapes were determined from photographs in all four Separan solutions both for air bubbles of constant volume and for dissolving CO_2 bubbles. In the latter case the images used were instantaneous visualizations taken directly from a motion picture of the bubble motion. Significantly, in the low Re cases where inertia effects were not important, no differences could be detected in the bubble shape for a given volume between the dissolving and non-dissolving cases. This observation is consistent with the qualitative expectations from section B where it was suggested that the flow induced by the collapse process plays a secondary role in the instantaneous bubble dynamics, provided only that Pe >> 1. In the present experiments, Pe = $O(10^{3} - 10^{6})$ in every case.

A pictorial representation of bubble shape as a function of bubble size for the four viscoelastic solutions is presented in Figure 4. The effect of fluid elasticity on shape is most clearly seen for the 1% Separan/water and the Separan/glycerine/water solutions where the Reynolds number is small. It is well-known that the equilibrium shape for a Newtonian fluid in the low Reynolds number range is spherical for any value of the surface tension. Thus the deviations from sphericity in these two cases are due entirely to the non-Newtonian characteristics of the ambient fluid. It may be seen that the main qualitative effect is an elongation in the direction of motion into a prolate teardrop shape. A convenient measure of the degree of deformation is the bubble eccentricity, which we define as its maximum width divided by its maximum dimension in the direction of motion (i.e. $E < 1$ for a prolate shape). The measured eccentricities are plotted as a function of We in Figure 5a, again for all four solutions. For the two solutions which give low Re, it may be seen that the data all correlate very well when plotted in this fashion. One implication of this may be that the main influence of the fluid rheology on shape is manifest in the purely elastic properties rather than the purely-viscous characteristic of a shear-thinning viscosity. Since We increases with bubble size, as shown in Table 2, the eccentricity or degree of deformation increases with bubble size for $Re < 1$. For the 0.1% and 0.5% solutions, where $Re > 1$, the eccentricities do not correlate well when plotted against We. As we have noted in section B, We alone cannot be used as a measure of the relative importance of elasticity for $Re \gg 1$. Instead, one must consider the parameter, We/Re, which is proportional to the rate of elastic to inertial forces. The measured eccentricities are plotted as a function of We/Re in Figure 5b. As expected, it is now the higher Re data which correlate

reasonably well. Since We/Re decreases with increasing bubble size, the relative importance of the prolate deformation induced by elasticity obviously decreases as the bubble gets larger (when Re >> 1) in favor of inertia-induced flattening in the streamwise direction.

A qualitative rationale for the prolate shapes induced by fluid elasticity was attempted recently in Zana and Leal (1975). In brief, it was suggested that a prolate shape was consistent with the general tendency of viscoelastic fluid flows to adopt configurations which reduce the likelihood of very large induced stress levels. In the motion of rigid bodies, the flow is streamlined with reduction in the local rates of deformation, by increasing the length of the region fore and aft in which the flow is significantly influenced by the body (cf. Zana, Tieffenbruck and Leal, 1975). For bubbles and drops, a similar effect can also be achieved by deformation of the bubble shape to an elongated form. This may provide at least a partial explanation for the prolate teardrop shapes which are actually observed. No detailed theory of bubble shape in viscoelastic systems is available.

F. BUBBLE RISE VELOCITIES

Instantaneous values were obtained for the velocity of rise for the CO_2 bubbles as a function of volume by careful frame-by-frame analysis of 16 mm motion pictures which were taken in conjunction with the mass transfer experiments. The framing rate for the velocity measurements was 16 frames/sec. The results for the aqueous glycerine solution and for the four viscoelastic Separan solutions are plotted in Figures 6-10. Also shown in these figures are measured values for the terminal velocity of air bubbles in the same materials. Finally, as a partial check on the accuracy of the present measurements, we have also included the data of Leal, Skoog and Acrivos (1971) for

0.1%, 0.5% and 1% Separan/water solutions. A discussion of the general characteristics of the velocity/volume relationship for bubbles in a viscoelastic fluid was presented by us in an earlier publication, Leal and Zana (1975). Included in that discussion are such features as the approach to the Davies-Taylor relationship for large bubbles, and the decreasing influence of elasticity in the small volume regime. Here we concentrate our attentions on the so-called velocity transition.

Examination of the data for air bubbles shows the existence of a large and discontinuous change in the terminal velocities in the 0.5% and 1% solutions, as well as the Separan/glycerine/water solution. The magnitude of the transition increases from a factor of about 4 for the 0.5% solution to a factor of 7 for the Separan/glycerine/water case, which is also the most viscoelastic. The bubble volume at transition is very nearly the same in all three cases. All of these features, plus the existence of a discontinuous transition, have been noted earlier, as indicated in the introduction to the present communication.

The new and significant feature in the data of Figures 8-10 is the fact that no discontinuity could be detected in the case of the dissolving CO_2 bubbles. For bubble volumes somewhat above and below the critical value, the measured instantaneous velocities for CO_2 bubbles are indistinguishable from the terminal velocities obtained for air bubbles of the same value. It is only in the immediate vicinity of the transition point that the data differ significantly. In each case, for volumes below the critical value, the velocities for the CO_2 bubbles are significantly larger than for the air bubbles. Since the air bubbles are known to behave as solid spheres before transition (cf. the comparison of bubble and solid sphere data in Leal et al., 1971), it may be surmised that, whereas a transition in surface

conditions apparently occurs abruptly for bubbles of essentially constant volume (air), the continuous decrease in volume of the CO_2 bubbles leads to a change in the ability of the surface to sustain tangential stress, thus leading to an intermediate regime of partial internal circulation. The difference in the air and CO_2 cases can only be ascribed to some transient phenomena associated with conditions at the bubble surface. In particular, neither transient phenomena in the bulk hydrodynamics, nor the induced radial flow due to bubble collapse, could possibly account for the observations. Dimensional analysis, including mass transfer and associated transient hydrodynamic effects as described briefly in section B (and in detail in Zana and Leal, 1975a) shows that both the induced radial velocity and the local fluid acceleration due to transients (i.e. $d\vec{u}/dt$) are of $O(Pe^{-1})$. As we have already noted, Pe numbers in the present experiments ranged from $O(10^3)$ to $O(10^6)$. Experimentally, it may also be noted that the deviations between the two cases initially increase with bubble volume, while Pe^{-1} decreases. Furthermore, if either of these bulk hydrodynamic phenomena were significant, the deviations between the CO_2 and air bubbles would not be confined to the transition region, but would cause significant changes for larger and smaller bubbles where the data show no difference between the two cases. It is generally conceded (see the introduction), and the present experiments provide some further indirect evidence, that the "transition" in terminal velocities for $R_{eq} \sim 0.3$ cm occurs due to a change in effective surface conditions from no-slip for small bubbles to zero tangential stress for larger bubbles. As we have indicated in the introduction, previous studies have strongly suggested that the increase in magnitude of the velocity change from 1.5 in the Newtonian case, to O(5 - 10) in viscoelastic fluids, can be largely attributed to the changes in bulk rheological

properties of the ambient fluid. The present experiments produce no information to contradict this hypothesis. Indeed, in Table 3 we have tabulated the magnitude of the velocity transition from all of the available studies as a function of the power-law parameter n and the We. Reasonable correlation can be seen for both parameters. This not only provides some further evidence that the bulk rheology is important, but also shows that both (purely-viscous) shear-thinning and elastic effects play a significant role in establishing the magnitude of the transition, as suggested by Leal et al. (1971).

No physical explanation has ever been offered for the abruptness of the velocity transition compared to the Newtonian case. Clearly, however, any model which is proposed to account for the abruptness with bubbles of constant volume, must also be able to accommodate a continuous change in the velocity when the bubble is undergoing a continuous decrease in volume. Two possibilities suggest themselves, which we shall first consider in light of the experimentally observed abrupt transition for constant volume air bubbles. We shall call the first the film model. The film model may be most easily explained as the formation on small bubbles of a membrane-like third (polymer) phase in which the polymer molecules are highly entangled, or otherwise interact in such a way as to affort the film some tensile strength. The abrupt transition is then envisioned as resulting from a rupture of the film, deriving from an instability for small disturbances (i.e. infinitesimal local variations in film properties) acted upon by the applied tangential shear stress from the fluid. One experimental observation which appears consistent with this suggestion is the fact that the quantity ($\mu U/a$) at transition, representing the magnitude of the shear stress, is essentially a constant. The only other work in the bubble dynamics literature which

appears to be related to this concept of a bursting film was due to Griffith (1962) who reported that the paths of bubbles rising through glycerine containing oleic acid were sometimes made up of vertical rises separated by sudden lateral jumps. Griffith speculated that this jump stemmed from a non-symmetrical rupture of a film at the bubble surface. It is interesting to note that the existence of these lateral jumps was only reported for the oleic acid/glycerine system, and that oleic acid is a moderately long chain molecule, not unlike a polymer.

The second possible model for explaining the abruptness of the velocity transition is most conveniently called the surfactant model. In this case the polymer molecules are viewed as acting in the familiar manner of more common surfactant materials (cf. the recent review by Harper, 1975), with the no-slip condition for small bubbles arising due to the existence of flow-induced gradients of surfactant (and hence of surface tension) on the bubble surface. With this model the abruptness of the transition can only be explained as being an indirect result of its large magnitude. In the Newtonian case where the difference between the no-slip and zero-shear stress conditions is only a factor of 1.5 in the terminal velocity, it is relatively easy to establish intermediate regimes of partial circulation as represented, for example, by the familiar Savic cap model (cf. Davis and Acrivos, 1964). In the viscoelastic fluid, however, the magnitude of the velocity change associated with even a partially circulating condition is so large that the "cap" may simply not be able to exist in an intermediate state of partial coverage.

Although neither the film nor surfactant model has been subjected to any meaningful theoretical (or experimental) study in the present context, it is nevertheless appropriate to see whether either is capable of conceptual

extension to the case of dissolving bubbles of constantly decreasing radius. Turning first to the film model, we can only say that it is difficult to see why a film which must be collapsing or folding onto itself (in view of the constant decrease in surface area) should be capable of allowing the appearance of partial internal circulation. The film model appears to us to be an "all or nothing model" in the sense that it can only allow complete circulation or complete no-slip conditions. Thus, from the point of view of generalization to the continuous velocity spectra of a collapsing bubble, the film model seems particularly deficient. In passing, it may also be noted that the mass transfer for data to be presented in the next section shows no sign of inhibition prior to transition, relative to the rates for a "clean" surface, as might be expected if one took the third-phase film concept seriously. In contrast to the film model, the surfactant model does appear to offer a possible mechanistic explanation for the observations with both constant volume and collapsing bubbles. With large concentrations of surfactant (polymer) in the bulk fluid (as we have in the present experiments) it is generally believed that at steady state the surfactant material takes on a surface concentration distribution with a minimum value at the front stagnation point and maximum (saturation) values at and near the balk. The dynamics of establishing this equilibrium configuration are complex, involving bulk diffusion and convection of the polymer molecules to and from the bubble surface, absorption (and desorption) onto or off of the surface, and advection/diffusion of the polymer molecules on the surface itself. For large surfactant molecules it is generally believed that a time scale of O (1 minute) is required to attain a steady state surface concentration distribution (cf. Griffith, 1962). When the bubble is collapsing, the available surface area is constantly decreasing,

and so the distribution of surfactant (polymer) on the surface must be continuously readjusting itself. In particular, as the local surface area is decreased, surface concentrations of surfactant (polymer) near the rear of the bubble will exceed the equilibrium saturation value and desorption of surfactant (polymer) molecules must occur. At the same time a redistribution on the surface must occur toward a new equilibrium configuration. A little thought will show that this redistribution will correspond to a net advection of the molecules (and thus of the surface itself) from front to back, i.e. to a crude approximation of the partial slip condition at the interface. Since the characteristic collapse time for the bubbles in the present experiments (equal to $a/(\vec{U} \cdot \vec{n})$) is considerably shorter (i.e. $\sim$ 10 seconds) than the time scales of O (1 minute) for complete establishment of a new steady state, it may be suggested that the surface concentration distribution will always be in a transient state, thus leading to a surface which is continually "flowing" from front to back in pursuit of a new equilibrium configuration. In this latter "model" the collapse process and especially its rate of occurrence plays a critical role as it should.

Presently we are pursuing several lines of experimental and theoretical analysis which will be capable of allowing a much more careful study of the influence of surface conditions on bubble dynamics in non-Newtonian, viscoelastic fluids. Hopefully these studies will provide more insight into the most appropriate physical model for the effects of polymer molecules at a bubble surface.

G. MASS TRANSFER

We now turn to the main objective of the present work, the experimental measurement of mass transfer rates from single gas bubbles in viscoelastic

ambient fluids. Of particular interest is the correspondence between rates of mass transfer and the sharp (but continuous) change in bubble velocity near the critical transition volume.

The common practice among experimentalists has been to correlate mass transfer data in terms of the liquid phase mass transfer coefficient, k_L, defined as

$$k_L = - \frac{dn/dt}{A(c^* - c_L)} \tag{16}$$

Here A is the surface area of the bubble available for mass transfer, dn/dt the rate of change of bubble mass, and c* and c_L the CO_2 concentrations at the gas-liquid interface and in the bulk of the solution, respectively. More convenient for theoretical work are the dimensionless Sherwood and Peclet numbers

$$Pe \equiv \frac{2R_{eq}U}{D_L} \; ; \quad Sh \equiv \frac{2R_{eq}k_L}{D_L} \tag{17}$$

where R_{eq} is the equivalent radius, U the instantaneous velocity of rise, and D_L the liquid phase diffusion coefficient. Whether k_L or Sh is used, however, experimental determination of the rate of mass transfer requires measurement of

i. the instantaneous bubble surface area

ii. the instantaneous bubble volume

iii. the rate of change of bubble volume

iv. the instantaneous vertical position of the bubble relative to the surface of the liquid

In addition, calculation of the Peclet number requires

v. the instantaneous rise velocity

The quantities ii and iii are used to determine the rate of change of the

moles of gas, dn/dt, through the perfect gas law, PV = nRT, and the instantaneous internal pressure, which is calculated using iv. It is assumed in this calculation that the mass transfer process occurs sufficiently slowly that the internal pressure is always in equilibrium with the local hydrostatic pressure. The quantity c* is calculated from the internal pressure using Henry's law. The Henry's law constant is assumed to be the same as for pure water or water/glycerine. Measurements by Calderbank (1970) and others indicate that this is quite a good approximation at the relatively low polymer concentrations considered here.

Among the experimentally measured quantities, the most difficult to determine accurately are the bubble surface area and volume. As we have noted earlier, these quantities were determined by numerical integration using a cross-sectional photograph of the bubble, and the assumption of axisymmetry (a good assumption in our system). Most previous studies have used a more crude method in which volume and area are calculated from the measured "major" axes of the bubble assuming its shape to be spheroidal. In the Newtonian case such a procedure may yield quite accurate results, especially for small deviations from sphericity. However, in the viscoelastic fluids considered here the bubble shape is clearly not spheroidal so that an approximation of this type could lead to considerable errors in the calculated mass transfer rates. Calderbank et al. (1970) used a modified version of the spheroidal geometry approximation. To estimate the magnitude of error introduced by the spheroid assumption we calculated the ratio of the directly measured (exact) to approximated surface areas. The calculated approximate values were consistently larger than the exact measured ones; however, the errors are smaller than might be expected, approximately 8 to 10%. In addition, as shown in Figure 11, the "exact" values are within 5 to 20%

of the area of a sphere with the same volume. In spite of these surprisingly reasonable approximate results we shall use the "exact" measured values of surface area in the present work.

Before discussing the experimental data on bubble mass transfer rates, it is useful to recall the various theoretical results which are available. We consider here only those expressions which are relevant to Pe >> 1. For Re << 1, and a Newtonian ambient fluid, Levich (1962) showed that

$$Sh = 0.991\ Pe^{1/2} \qquad (Pe >> 1,\ Re << 1) \tag{18}$$

for a rigid sphere, and

$$Sh = 0.65\ Pe^{1/2} \qquad (Pe >> 1,\ Re << 1) \tag{19}$$

for a spherical bubble with free circulation. For a circulating sphere at large Reynolds number, Boussinesq (1905) used the potential flow solution for the velocity field to obtain

$$Sh = 1.13\ Pe^{1/2} \qquad (Pe >> 1,\ Re >> 1)\ . \tag{20}$$

The latter result is, of course, not restricted to a Newtonian fluid. As we have noted earlier, if Re is sufficiently large that the inertia terms in the equation of motion are dominant over viscous or elastic contributions, the velocity field will be the potential flow solution <u>independent</u> of the bulk rheological properties. Thus, for sufficiently large bubbles in either the Newtonian or viscoelastic fluids, one would expect to find data correlation according to (20), provided the bubble shape remained spherical. Even for nonspherical shapes, however, the general result

$$Sh = cPe^{1/2}$$

will hold, with the constant c depending on bubble shape. No comprehensive theory of bubble mass transfer in viscoelastic fluids is available at low Reynolds numbers. The reason is simply that no comprehensive theory has yet been developed for the velocity field and bubble dynamics. The only

results available are (like the velocity field modifications) limited to small deviations from a Newtonian fluid. For a power-law fluid with $|n - 1| << 1$, Hirose and Moo-Young (1969) have shown that the Sherwood number for a circulating bubble in the creeping flow regime is given by

$$Sh = 0.65 \left[1 - \frac{4n(n-1)}{2n + 1}\right]^{1/2} Pe^{1/2} . \qquad (Re << 1, Pe >> 1) \quad (21)$$

More recently, the same authors considered the small We limit for a Maxwell fluid in the creeping flow regime to show

$$Sh = 0.65 \left\{1 + 0.16\ We^2\right\} Pe^{1/2} \qquad (Re << 1, Pe >> 1) \qquad (22)$$

for $We << 1$. Neither (21) nor (22) is directly applicable to the strongly non-Newtonian solutions used in the present study in view of the restrictions on $|n - 1|$ and We. However, they can at least be examined for qualitative trends which may be useful outside their strict range of validity. In this sense, equation (21) predicts an enhancement in the mass transfer rate over its Newtonian value as a result of shear dependence of viscosity. Furthermore, the enhancement increases monotonically with decrease of the flow index, n. The predictions of (22) are similar to that of equation (21). It shows an increase in the mass transfer rate with increasing viscoelasticity, i.e. with We number.

Measured mass transfer rates for CO_2 bubbles in 88% glycerine-12% water solution are shown in Figure 12. Also shown in Figure 12 is the experimental data of Calderbank et al. for the same system. The agreement between the two is excellent. This is significant, because the Calderbank et al. mass transfer data were obtained in a "closed" system where the bubble volume remains constant during its rise through the column. We have noted previously, in section C, that this could lead to significant differences in mass transfer rate when compared to an "open" system where the bubble volume is allowed to

vary. The difference between an "open" and a "closed" system could be important if modifications of the bulk hydrodynamics for cases in which the flow induced by the interface motion is significant compared to the translational motion of the bubble. In glycerine/water solution the mass transfer rates are very small due to extremely small liquid phase diffusivity, D_L, and hence the interface motion is negligibly small. As a result, in the absence of significant transient effects associated with the interface itself (as seem to occur in the viscoelastic case--see previous section), the "closed" and "open" systems are expected to yield comparable results in the glycerine/water solution. For completeness the bubble rise velocities of Calderbank et al. are shown against our data in Figure 6. The agreement between the rise velocities of air bubbles, CO_2 bubbles measured in this work, and CO_2 bubbles obtained by Calderbank et al., is excellent. We have also plotted the theoretical expressions (18)-(20) in Figure 12. Agreement between the data and (20) is good for the larger bubbles where Re is moderate.

The mass transfer data for the 0.1, 0.5, 1.0% Separan AP30/water solutions and the Separan/water/glycerine solution are shown in Figures 13-16, plotted as Sh against Pe. Also shown in each figure are the most appropriate of the theoretical expressions, equations (18)-(21).

Initially, a point of surprise regarding these data is the fact that they appear smooth over the whole range of Pe, with no apparent region of sharp increase as found in the velocity data of the preceding section. It is thus important to point out that a corresponding transition actually does occur, which would be evident if Sh were plotted as a function of R_{eq} instead of Pe. Pe involves U and so itself increases sharply in the transition region. This causes the corresponding sharp increase in Sh to be spread out horizontally, thus producing the smooth curves of Figures 13-16.

For all of the systems studied here Pe $\geq 10^3$, so that one of the restrictions of equations (18)-(21) is automatically satisfied. As we have noted in section D, the four viscoelastic solutions fall into two groups with respect to Re. In the higher Re group, glycerine/water and 0.5% Separan/water have Reynolds numbers ranging from $\sim$ 3 to 20, while 0.1% Separan/water ranges from $\sim$ 15 to 70. Our comparison of the experimental data for the Newtonian glycerine/water system with the equation (20) showed good agreement for the larger bubble sizes where the Re is largest. It should be noted, however, that the bubble shapes differed substantially from spherical so that this agreement may be fortuitous. Indeed, for the two comparable viscoelastic systems (.1 and .5%), the data cross over the high Reynolds number theoretical expression to values which are 10-13% larger in the 0.1% solution, and 22-25% greater for 0.5% Separan/water. We shall discuss this apparent enhancement in mass transfer rates in more detail later in this section. However, we may note that we believe the enhancement to be a genuine product of the viscoelasticity and shear-thinning properties of the fluid.

For the 1% AP30/water and AP30/glycerine/water solutions, Re varies from 10^{-3} to 0.5, and the experimental data must be compared with the low Reynolds number theories, as indicated in Figures 15 and 16. For the 1% AP30/water solution, the data start between the theoretical curves for solid and freely circulating spheres, and increase to values, for the largest bubbles, which are substantially greater than either the Newtonian or power-law expressions (20) and (21). The intermediate values obtained for the smallest bubbles are actually consistent with the velocity data of the preceding section. It was noted there that the velocities for the CO_2 bubbles in viscoelastic solutions are always greater than the corresponding

velocities of air bubbles for $R_{eq} < R_{critical}$, and it was argued that this increase could be due to a partial internal circulation for the CO_2 bubbles. The mass transfer data are consistent with this hypothesized existence of partial circulation, since they lie halfway between the no-slip and freely circulating theoretical predictions. It is also significant, as we pointed out in the previous section, that the polymer molecules at the bubble surface do not appear to directly inhibit CO_2 transfer to the surrounding fluid. Turning to Figure 16, it may be noted that the mass transfer data for A30/water/glycerine lie strictly above the predictions of equations (20) and (21). This is again consistent with the velocity data for CO_2 bubbles in the same solution (Figure 10), which show that the smallest bubbles represented in the mass transfer data (R_{eq} = 0.20 cm) have a velocity very close to the velocity of the fully circulating, post-transition air bubbles.

Table 4 shows the percentage increase in experimental mass transfer rates over the predicted Newtonian values both for the four viscoelastic solutions used in the present study and also for all other available mass transfer data in non-Newtonian fluids. Also listed are Re, n, and either We or We/Re, depending upon where Re < 1 or Re > 1, respectively. Finally, we have also listed the percentage increase above the predictions of $|n - 1| << 1$ power-law theory for those cases where Re < 1. It will be noted that the various cases are listed in order of decreasing power-law index, n.

Turning first to the four cases studied in the present work, it may be seen that the 10 to 13% and 22 to 25% increases for 0.1 and 0.5% AP30/water correlate well with an increasing level both of shear-thinning (n) and of effective fluid elasticity (We/Re). Likewise for 1% AP30/water and

AP30/water/glycerine where n is further decreased, the increase in mass transfer rate above the Newtonian value is also further increased to 56 to 60 and 60 to 65%, respectively, and ordered with respect both to n and to the appropriate measure of elasticity, We, for the low Re cases.

Considering all of the cases which are listed, we may note

(i) The degree of increase in mass transfer rates correlates perfectly with the power-law index, n, for all cases except the 0.14% Carbopol solution studied by Hirose and Moo-Young. We believe that the lack of correlation in this one case is extremely significant since all of the solutions listed are fully viscoelastic except for Carbopol which is a shear-thinning, purely-viscous liquid. The implication is that the fully viscoelastic values of mass transfer rate represent the additive contribution of shear-thinning and of separate elastic effects. In other words, one cannot, in general, expect correlation of the enhancement of mass transfer rates and n, without also taking into account the appropriate measure of importance of elastic effects. For all solutions except 0.1 and 0.5% AP30/water, this is We. For these two cases, one must use (We/Re) as the measure of elasticity since the Reynolds numbers of the bubble motion are moderate to large.

(ii) The increase in mass transfer rates is greater than predicted by the power-law model of Hirose and Moo-Young. Although this theory is strictly valid only for $|n - 1| \ll 1$, it was suggested by Calderbank et al. (1970) that the experimental data even in strongly viscoelastic liquids could be predicted by using the power-law theory with measured values

of n. Since the power-law model represents only the effect of a shear-thinning viscosity, it was thus suggested that the influence of elasticity was of negligible importance. This result is, of course, surprising in view of the potential influence of elasticity on the flow patterns, and is also at odds with the prediction for small We given by equation (22). The present experimental results show that increases of as much as 25% can be obtained above the power-law theory when the ambient fluid is fully viscoelastic. Furthermore, these increases correlate strongly with the relevant measure of the fluid's elasticity, i.e. We or We/Re in every case.

CONCLUSIONS

i. It is shown through a dimensional analysis of the Oldroyd 8-constant rheological equation of state that the effect of fluid elasticity on the bubble shapes, rise velocities, and mass transfer rates can be correlated in terms of We number when $Re \ll 1$, and (We/Re) number when $Re \gg 1$.

ii. It is found experimentally that the effect of elasticity on the bubble shape is to stretch it along the streamlines to a prolate teardrop shape. This shape of bubble is consistent with the streamline pictures of a viscoelastic liquid past a solid sphere.

iii. It is observed that the rise velocities of bubbles are enhanced as a result of fluid elasticity and shear dependence of viscosity in both rigid and circulating boundary regimes. The effect of fluid elasticity is more prominent in circulating boundary regime than rigid sphere regime. It is observed for the first time that

a discontinuous increase in velocity of rise in transition from a rigid to a circulating bubble only occurs for non-dissolving (constant volume) air bubbles, and that the transition is gradual for dissolving (varying volume) CO_2 bubbles. Two models called the film model and the surfactant model are presented as possible explanations to the abruptness of the velocity transition.

iv. The mass transfer data for one Newtonian and four viscoelastic liquids are measured. The data show that in the region of bubble sizes studied, the CO_2 bubbles are already in partial circulation, and quickly reach to a full circulation. The mass transfer rates are found to be greatly enhanced as a result of viscoelasticity. The increase in mass transfer rates over the corresponding Newtonian values are found to increase with increasing shear dependence of viscosity and/or viscoelasticity. It is shown that the shear dependence of viscosity cannot alone be accounted for the large increase in mass transfer rates, and hence the elasticity has to be included in any successful analysis of the mass transfer data for viscoelastic fluids.

APPENDIX A

Calculation of Drag on a Spherical Bubble Moving in an Oldroyd Type Fluid

A. INTRODUCTION

Astarita and Apuzzo (1965) observed a large and discontinuous transition in terminal velocy of an air bubble rising in a viscoelastic dilute polymer solution. Similar results have more recently been reported by Calderbank et al. (1970) and Leal et al. (1971) in different polymer solutions. Kintner et al. (1961) proposed that the increase in velocity for drops is the result of a transition from a no-slip to a freely-circulating regime. Astarita and Apuzzo (1965) claimed that the magnitude of the velocity transition could be largely accounted for by considering only the purely-viscous, shear-thinning viscosity, ignoring viscoelastic contributions. To check the validity of Astarita's claim, Leal et al. (1971) studied the effect of shear-dependent viscosity, in the absence of viscoelastic effects, by employing an empirical purely-viscous fluid model to calculate numerically the terminal velocities of non-circulating, partially circulating, and fully circulating spherical bubbles. It was found that the presence of shear dependent viscosity could only account for about 30% of the magnitude of the measured velocity transition. Hence, it was surmised that better agreement between theory and observation could only be achieved by taking account of viscoelastic effects in the fluid. Leal et al. (1971) showed, based on simple qualitative arguments, that a relatively small additional viscoelastic contribution to the force balance on the bubble would be sufficient to account for the much larger measured velocity increases. The conditions required to produce a consistent result are that the drag be reduced in both pre-transition and post-transition regimes, but with the effect being somewhat greater in the

latter case.

As an initial test of the viability of this proposal, it was desired to determine whether elastic effects, in the absence of shear-dependent viscosity, would contribute to the particle drag in a qualitatively consistent manner. In order to investigate this question, a "slow-flow" asymptotic solution, based on the 6-constant Oldroyd (1952) fluid model, is used to compare the viscoelastic contributions to the drag on a rigid no-slip sphere and on a freely circulating spherical bubble. The rigid sphere result has already been given by Leslie (1961). A brief description of the solution for the case of a spherical bubble will now be presented.

B. THE GOVERNING EQUATIONS

Spherical polar coordinates (r, θ, ϕ) are chosen with origin at the center of the sphere. The upstream direction corresponds to $\theta = 0$. Due to axial symmetry the solution is independent of ϕ. All tensor quantities are expressed in terms of their physical components referred to spherical polar coordinates.

Equations of motion and continuity for steady, incompressible flow of a fluid of density ρ are

$$\nabla \cdot \underline{\underline{\tau}} = \rho \vec{u} \cdot \nabla \vec{u} - \nabla p \qquad \text{(A.1)}$$

$$\nabla \cdot \vec{u} = 0 \qquad \text{(A.2)}$$

In order to define the system completely a relation between the dynamic variable $\vec{U}$, and the kinematic variable $\underline{\underline{\tau}}$ is needed. For a Newtonian fluid $\underline{\underline{\tau}}$ is directly proportional to the gradient of U, the proportionality constant being viscosity. The equations of state describing viscoelastic liquids are, in general, very complex and highly non-linear. There are numerous models for viscoelasticity but none has been shown to represent all the known

characteristics of viscoelastic fluids. Oldroyd's 6-constant model has been shown to predict most of these characteristics of viscoelastic liquids, at least qualitatively (cf. Bird et al., 1967).

$$\underline{\underline{\tau}} + \lambda_1 \frac{\delta}{\delta t}\underline{\underline{\tau}} + \mu_0 \underline{\underline{e}}(\underline{\underline{\tau}} : \underline{\underline{\delta}}) + \nu_1(\underline{\underline{e}} : \underline{\underline{\tau}})\underline{\underline{\delta}}$$
$$= -2\eta_0 \left\{ \underline{\underline{e}} + \lambda_2 \frac{\delta}{\delta t}\underline{\underline{e}} + \nu_2(\underline{\underline{e}} : \underline{\underline{e}})\underline{\underline{\delta}} \right\} \qquad (A.3)$$

where $\underline{\underline{e}}$ is the rate of strain tensor, λ_1, λ_2, μ_0, ν_1, ν_2 the characteristic times and η_0 the zero shear viscosity. The derivative denoted by $\delta/\delta t$ is called "convective derivative" and defined as

$$\frac{\delta}{\delta t}\underline{\underline{\tau}} = \frac{\partial}{\partial t}\underline{\underline{\tau}} + \vec{u}\cdot\nabla\underline{\underline{\tau}} + (\underline{\underline{\Omega}}\cdot\underline{\underline{\tau}} - \underline{\underline{\tau}}\cdot\underline{\underline{\Omega}}) - (\underline{\underline{e}}\cdot\underline{\underline{\tau}} + \underline{\underline{\tau}}\cdot\underline{\underline{e}}) \qquad (A.4)$$

where $\underline{\underline{\Omega}} = (\nabla\vec{U} - \nabla\vec{U}^T)/2$ is vorticity.

Equations (A.1)-(A.3) are non-dimensionalized using

$$\bar{r} = r/a \qquad \bar{u}_i = u_i/u_\infty \qquad \bar{e}_{ij} = e_{ij}/(u_\infty/a)$$
$$\bar{\tau}_{ij} = \tau_{ij}/(\eta_0 u_\infty/a) \qquad \bar{p} = p/(\eta_0 u_\infty/a) \qquad \bar{\Omega}_{ij} = \Omega_{ij}/(u_\infty/a)$$

Dropping the bars over the variables for convenience, the components of equations (A.1)-(A.3) are

$$\frac{\partial \tau_{rr}}{\partial r} + \frac{1}{r}\frac{\partial \tau_{r\theta}}{\partial \theta} + \frac{1}{r}(2\tau_{rr} - \tau_{\theta\theta} - \tau_{\phi\phi} + \tau_{r\theta}\cot\theta) = \frac{\partial p}{\partial r} + O(Re) \qquad (A.5)$$

$$\frac{\partial \tau_{r\theta}}{\partial r} + \frac{1}{r}\frac{\partial \tau_{\theta\theta}}{\partial \theta} + \frac{1}{r}\{(\tau_{\theta\theta} - \tau_{\phi\phi})\cot\theta + 3\tau_{r\theta}\} = \frac{1}{r}\frac{\partial p}{\partial \theta} + O(Re) \qquad (A.6)$$

$$\frac{1}{r^2}\frac{\partial}{\partial r}(r^2 u_r) + \frac{1}{r\sin\theta}\frac{\partial}{\partial \theta}(u_\theta \sin\theta) = 0 \qquad (A.7)$$

$$\tau_{rr} + We\left\{u_r\frac{\partial \tau_{rr}}{\partial r} + \frac{u_\theta}{r}\left(\frac{\partial \tau_{rr}}{\partial \theta} - 2\tau_{r\theta}\right) + 2\tau_{r\theta}(\Omega_{r\theta} - e_{r\theta}) - 2e_{rr}\tau_{rr} + \zeta e_{rr}\sum_i \tau_{ii}\right.$$
$$\left. + \xi\left(\sum_i e_{ii}\tau_{ii} + 2e_{r\theta}\tau_{r\theta}\right)\right\}$$
$$= 2\left\{e_{rr} + We\left[\epsilon\left(u_r\frac{\partial e_{rr}}{\partial r} + \frac{u_\theta}{r}\left(\frac{\partial e_{rr}}{\partial \theta} - 2e_{r\theta}\right) + 2e_{r\theta}(\Omega_{r\theta} - e_{r\theta}) - 2e_{rr}^2\right) + \eta\left(\sum_i e_{ii}^2 + 2e_{r\theta}^2\right)\right]\right\} \qquad (A.8)$$

$$\tau_{\theta\theta} + We\left\{u_r\frac{\partial\tau_{\theta\theta}}{\partial r} + \frac{u_\theta}{r}\left(\frac{\partial\tau_{\theta\theta}}{\partial\theta} + 2\tau_{r\theta}\right) - 2\tau_{r\theta}(\Omega_{r\theta}+e_{r\theta}) - 2e_{\theta\theta}\tau_{\theta\theta} + \zeta\sum_i \tau_{ii} + \xi\left(\sum_i e_{ii}\tau_{ii} + 2e_{r\theta}\tau_{r\theta}\right)\right\}$$
$$= 2\left\{e_{\theta\theta} + We\left[\epsilon\left(u_r\frac{\partial e_{\theta\theta}}{\partial r} + \frac{u_\theta}{r}\left(\frac{\partial e_{\theta\theta}}{\partial\theta} + 2e_{r\theta}\right) - 2e_{r\theta}(\Omega_{r\theta}+e_{r\theta}) - 2e_{\theta\theta}^2\right) + \eta\left(\sum_i e_{ii}^2 + 2e_{r\theta}^2\right)\right]\right\} \quad (A.9)$$

$$\tau_{\phi\phi} + We\left\{u_r\frac{\partial\tau_{\phi\phi}}{\partial r} + \frac{u_\theta}{r}\frac{\partial\tau_{\phi\phi}}{\partial\theta} - 2e_{\phi\phi}\tau_{\phi\phi} + \zeta e_{\phi\phi}\sum_i \tau_{ii} + \xi\left(\sum_i e_{ii}\tau_{ii} + 2e_{r\theta}\tau_{r\theta}\right)\right\}$$
$$= 2\left\{e_{\phi\phi} + We\left[\epsilon\left(u_r\frac{\partial e_{\phi\phi}}{\partial r} + \frac{u_\theta}{r}\frac{\partial e_{\phi\phi}}{\partial\theta} - 2e_{\phi\phi}^2\right) + \eta\left(\sum_i e_{ii}^2 + 2e_{r\theta}^2\right)\right]\right\} \quad (A.10)$$

$$\tau_{r\theta} + We\left\{u_r\frac{\partial\tau_{r\theta}}{\partial r} + \frac{u_\theta}{r}\left(\frac{\partial\tau_{r\theta}}{\partial\theta} + \tau_{rr} - \tau_{\theta\theta}\right) + \tau_{\theta\theta}(\Omega_{r\theta} - e_{r\theta}) - \tau_{rr}(\Omega_{r\theta} + e_{r\theta}) - \tau_{r\theta}(e_{rr} + e_{\theta\theta}) + \zeta e_{r\theta}\sum_i \tau_{ii}\right\}$$
$$= 2\left\{e_{r\theta} + We\,\epsilon\left[u_r\frac{\partial e_{r\theta}}{\partial r} + \frac{u_\theta}{r}\left(\frac{\partial e_{r\theta}}{\partial\theta} + e_{rr} - e_{\theta\theta}\right) + e_{\theta\theta}(\Omega_{r\theta} - e_{r\theta}) - e_{rr}(\Omega_{r\theta} + e_{r\theta}) - e_{r\theta}(e_{rr} + e_{\theta\theta})\right]\right\} \quad (A.11)$$

where $Re = U_\infty a\rho/\eta_0$, $We = U_\infty\lambda_1/a$, $\epsilon = \lambda_2/\lambda_1$, $\zeta = \mu_0/\lambda_1$, $\xi = \nu_1/\lambda_1$, $\eta = \nu_2/\lambda_1$ and a is the bubble radius. The boundary conditions are

$$\begin{aligned} &u_r = 0 \quad ; \quad \tau_{r\theta} = 0 \quad @\ r = 1 \\ &u_r = -\cos\theta \ ; \quad u_\theta = \sin\theta \quad @\ r = \infty \end{aligned} \quad (A.12)$$

C. SOLUTION

A perturbation solution is obtained by expressing all the variables in the form of a power series in We number,

$$A = A^{(0)} + We\,A^{(1)} + We^2\,A^{(2)} + \ldots \quad (A.13)$$

where A stands for U_r, U_θ, τ_{rr}, $\tau_{\theta\theta}$, $\tau_{\phi\phi}$, $\tau_{r\theta}$, p, e_{rr}, $e_{\theta\theta}$, $e_{\phi\phi}$, $e_{r\theta}$, $\Omega_{r\theta}$ in turn. Substituting (A.13) and the stream function ψ

$$u_r = -\frac{1}{r^2\sin\theta}\frac{\partial\psi}{\partial\theta} \quad ; \quad u_\theta = \frac{1}{r\sin\theta}\frac{\partial\psi}{\partial r} \quad (A.14)$$

into equations (A.5)-(A.12) and equating the terms of the same order in We, a general form of streamfunction equation is obtained after a lengthy algebraic exercise

$$D^4\psi^{(i)} = f_i\,(\psi^{i-1}) \tag{A.15}$$

where $i \equiv 0, 1, 2$, etc. and functions f_i are given in the Appendix. Note that f_0 corresponds to the Newtonian case and hence identically equal to zero. The solutions of (A.15) involve an enormous amount of algebra. Therefore, only the final expressions will be given here.

$$\psi^{(0)} = \frac{1}{2}(r^2 - r)\sin^2\theta \qquad \text{(Newtonian solution)} \tag{A.16}$$

$$\psi^{(1)} = \frac{1}{10}(1-\epsilon)\left\{3 - \frac{5}{r} + \frac{2}{r^2}\right\}\sin^2\theta\cos\theta \qquad \text{(First order correction to Newtonian solution)} \tag{A.17}$$

$$\begin{aligned}\psi^{(2)} = {} & \frac{(1-\epsilon)^2}{10}\left(-\frac{359}{98r} + \frac{9}{8r^2} - \frac{15}{392r^3} + \frac{25}{21r^3}\ln r + \frac{5}{2r^4}\right)\sin^4\theta \\ & + \frac{4(1-\epsilon)^2}{50}\left(\frac{r}{6} + \frac{4075}{1176r} - \frac{5}{4r^2} + \frac{13}{392r^3} - \frac{25}{21r^3}\ln r - \frac{5}{2r^4}\right)\sin^2\theta \\ & - (1-\epsilon)\left(\frac{60}{49r} - \frac{21}{8r^2} + \frac{549}{392r^3} + \frac{3}{7r^3}\ln r\right)\sin^4\theta \\ & - \frac{4}{5}(1-\epsilon)\left(-\frac{3r}{40} - \frac{205}{196r} + \frac{5}{2r^2} - \frac{2073}{1960r^3} - \frac{3}{7r^3}\ln r\right)\sin^2\theta\end{aligned} \tag{A.18}$$

Using (A.16)-(A.18), (A.5) and (A.8)-(A.11), $p^{(i)}$, $\underline{\underline{\tau}}^{(i)}$ ($i = 0, 1, 2$) are obtained. Again, procedure is straightforward but involves lengthy algebra and hence it will not be given here.

D. THE DRAG ON THE BUBBLE

The drag on a spherical bubble is given by

$$D = 2\pi\eta_o U_b a\left\{\int_0^{\pi}(\tau_{r\theta})_{r=1}\sin^2\theta\,d\theta + \int_0^{\pi}(p - \tau_{rr})_{r=1}\sin\theta\cos\theta\,d\theta\right\} \tag{A.19}$$

Evaluating the integrals in (A.19), it is found that

$$D_{BUBBLE} = 2\pi\eta_o U_b a \{ 2 - 0.066(1-\epsilon)(30+\epsilon) We^2 + \cdots \} \qquad (A.20)$$

Hence, to first order in We number the drag is unchanged from its value for a purely viscous liquid but to the second order the drag is decreased since $\epsilon < 1$ (i.e. $\lambda_1 < \lambda_2$). A similar result for the drag on a solid sphere is reported by Leslie (1961).

E. CONCLUSIONS

The drag expression for a rigid sphere is given by Leslie (1961)

$$D_{SPHERE} = 2\pi\eta_o U_s a \{ 3 - 0.016(1-\epsilon)(3+\epsilon) We^2 + \cdots \} \qquad (A.21)$$

Comparing expressions (A.20) and (A.21), it may be seen that the purely elastic contribution to the drag causes a decrease in both cases at $O(We^2)$, but that the effect is much more pronounced for the bubble than for the rigid sphere. Thus the "slow flow" viscoelastic approximation offers strong preliminary evidence to support the original hypothesis of Leal, Skoog and Acrivos (1971).

APPENDIX : Function f_i's

$$f_0 = 0$$

$$f_1 = 12(\epsilon-1)\frac{\sin^2\theta\cos\theta}{r^4}$$

$$f_2 = \frac{(1-\epsilon)^2}{10r^6}\left(36 + \frac{736}{r} - \frac{480}{r^2}\right)\sin^2\theta$$
$$+ \frac{(1-\epsilon)^2}{5r^6}\left(27 + \frac{450}{r} - \frac{300}{r^2}\right)\sin^4\theta$$
$$+ \frac{(1-\epsilon)}{r^6}\left(108 - \frac{48}{r}\right)\sin^2\theta$$
$$- \frac{(1-\epsilon)}{r^6}\left(18 - \frac{6}{r}\right)\sin^4\theta$$

APPENDIX B

Details of Experimental Apparatus and Procedure

A. PREPARATION OF SOLUTIONS

The polymer used in this study is a polyacrylamide produced by Dow Chemical Company and known as Separan AP30, which is in powder form. The solutions used are prepared in a large container (about 15 gallon capacity). The amount of polymer needed to make a desired weight percentage solution is carefully weighed. Upon the recommendation of the manufacturer, the solvent (distilled water or a mixture of water-glycerine) is violently agitated with a blunt object such as a round wooden rod. Bluntness of the object is important since sharp edges may cause break-up of polymer chains during agitation. After the initial agitation, a motor-driven propeller with blunt blades is used to mix the solution for about half a day. The uniformity of the solution after half a day's mixing is found to be excellent. Usually the most concentrated solution is made first, then the less concentrated solutions are obtained by diluting the original solution. The solutions were stored in glass bottles (5 gallons each) in a completely dark room when not being used (manufacturer warns that long exposure to light may cause degradation). The solutions are stable for six months to a year under above mentioned conditions (it may be stable for a longer period, but it was never necessary to check that during this work). Basically four different polymer solutions are used in this study, 0.1, 0.5 and 1.0% solutions of Separan AP30 in distilled water and 0.523% AP30 - 45.6% distilled water - 53.9% glycerine solution.

B. OPERATION PROCEDURE FOR MASS-TRANSFER MEASUREMENTS

A schematic diagram of the apparatus used in the experiments is shown in Figure 1 of chapter 4.

I. Preparation of the Adsorption Column: The column is filled with the dilute polymer solution. The uniformity of the solution is checked by taking samples of solution from the top and the bottom of the column and measuring density and viscosity. The room and column temperatures and the barometric pressure are measured before each experiment.

II. Transportation of CO_2 from Tank to the Column: Several minutes prior to each experiment the gas regulator is opened and CO_2 gas is allowed to flow through the humidifying columns. The purpose of humidifying columns is to saturate CO_2 gas with water vapor and hence prevent any mass-transfer into the bubble during its ascent in the absorption column. By closing valve V3 and opening V2 and V4, the gas line is purged to clean the system of any air. The gas syringe is then filled with CO_2 by closing V4. The rest of the procedure goes as follows:

(1.)* The solenoid valve (11)† is closed.

2. Valve (V5) is opened and liquid is sucked into the liquid syringe either from the column or a reservoir.

3. Valve (V3) is opened and the gas is injected into the capillary tubing. The valve (V3) is closed when the desired amount of gas is injected.

4. Using the liquid syringe (5) the bubble is pushed out of the

* A parenthesis around the step number indicates that that step is only necessary when the pressure method is used to obtain bubble volume.

† The number in parenthesis refers to identification number in Figure 1 of chapter 4.

capillary tubing.

(5.) The solenoid valve (11) is opened and closed instantaneously. This brings the air pressure back to the atmospheric pressure. This step takes less than 1/20 of a second.

(6.) Bubble is released by inverting the turning cup.‡

III. Follow-up of Bubble in the Column: As soon as the bubble is released it needs to be followed up by a movie camera to register its size, shape, etc. as it rises in the column. As it is seen from steps (1)-(7) above, one has to perform several operations within a few seconds and sometimes two operations simultaneously. This is an impossible task for one person and therefore many electronic devices are used to automate certain parts of the operations. Below we itemized the operations and briefly describe how they are achieved.

1. An intense light source (7), which generates a narrow light beam, and, on the other side of the column, a phototransistor (B), which receives the light beam, are located a few inches above the bubble release mechanism. When the bubble goes through the light beam a signal is generated by the photo-transistor as a result of blockage of the light beam by the bubble.

2. The signal generated in step 1 is fed into platform control circuitry (32). The signal is amplified here and sent to activate the motor controller (16) and to the DC power supply for the camera motor (31).

‡ This step is also used in photographic method for large bubbles.

3. Motor controller (16) activates the motor (15) and drives it at a preset RPM. The shaft of the motor is tied to a steel cable which pulls the platform (13) on which the movie camera (17) and the strobe lights (18) are located. The platform is balanced by a weight (14) so that the power to pull the platform up is minimized.
4. Signal that was generated and sent to power supply (28) turns the power supply on which drives the camera motor. The input to power supply (28) is adjusted by a variac (30) and hence the power input to the camera motor can be adjusted to any level. The camera film speed is calibrated with the voltage input. Consequently, the camera can be run at any frame speed by adjusting the variac.
5. A small magnet is attached to a shaft on the camera that makes one full revolution per frame. A magnet pick-up is mounted across the magnet. Each time the magnet passes by the magnetic pick-up it generates a signal. This signal is sent to the strobe lights. This causes strobes to flash. This step takes place so fast that the strobe flash is at peak intensity when the camera shutter is full open, i.e. strobe flash is synchronized with camera shutter.

Steps 1-5 take place in a fraction of a second and, as a result, as soon as the bubble is released, camera starts taking pictures, strobes start flashing, and camera platform starts following the bubble, all being accomplished automatically.

6. Camera platform is fitted with two circular viewers. When the bubble is on the imaginary line connecting the centers of the

two viewers, it is also in the frame of the camera. During bubble's rise in the column, platform speed is adjusted by motor controller so that bubble is always within the camera frame.

(7.) During bubble's rise in the column, pressure of the air space is measured by a transducer (12) and transducer indicator (26). The signal from the indicator is fed into one channel of a multichannel recorder (35). Also recorded in the recorder are the signals from the magnetic sensor amplifier which gives an independent measure of filming speed.

The film used in the movie camera is a high-speed Kodak 4-X Reversal. The strobe lights are manufactured by General Radio and set at medium intensity range.

C. STREAKLINE FLOW VISUALIZATION

The photographic set-up for the mass transfer measurements is also used in slightly modified form for flow visualization. H-16 movie camera is replaced by a standard Graflex Reflex camera, fitted with a Polaroid film holder, and an area about six inches long at the lateral (front to back) centerline is illuminated using two very narrow slits and quartzline lamps. The solid sphere or cylinder is suspended in the middle of the column as shown in Figure 1 of chapter 3. The sphere is connected to the steel cable that pulls the camera platform by a thin thread. Consequently the sphere is raised at a speed precisely the same as that of camera platform and the rise speed of sphere can be adjusted to any terminal value by adjusting the motor controller. Until the sphere comes into the area of flow visualization, the slit lights are off and the column is illumiated by a flood light. As

soon as the sphere enters the area mentioned above the following series of operations take place automatically.

1. The flood light is turned off.
2. The slit lights are turned on.
3. The Polaroid camera is triggered to take a time-exposure picture of the sphere.

As noted above, two narrow slits are used to form a very thin plane of light. Thus, it is critical for the lateral position of the sphere or the slit lights be adjusted such that the sphere is precisely bisected by the lighted plane region.

REFERENCES

Astarita, G. and Apuzzo, G., AIChE J., 11, 815 (1965)

Calderbank, P. H., Johnson, D. S. L. and Loudon, J., Chem. Eng. Sci., 25, 235 (1970)

Leal, L. G., Skoog, J. and Acrivos, A., Can. J. Chem. Eng., 49, 569 (1971)

Barnett, S. M., Humphrey, A. E. and Litt, M., AIChE J., 12, 253 (1966)

Garner, F. H., Mathus, K. B. and Jensen, V. G., Nature, 180, 331 (1957)

Warshay, F. H., Bogusz, E., Johnson, M. and Kintner, R. C., Can. J. Chem. Eng., 37, 29 (1959)

Fararouri, A. and Kintner, R. C., Trans. Soc. Rheol., 5, 369 (1961)

Zana, E., Ph.D. Dissertation, California Institute of Technology (1975)

Zana, E. and Leal, L. G., First International Conference on Bubbles and Drops, Jet Propulsion Lab., Calif. Inst. of Tech., Pasadena, Calif. (1974)

Oldroyd, J. G., Proc. Roy. Soc., A245, 278 (1958)

Leslie, F. M., Quart. J. Mech. and Appl. Math., 14, 36 (1961)

Zana, E. and Leal, L. G., Accepted for publication at I & EC Fund. (1975)

Deindorfer, F. H. and Humphrey, A. E., I & EC Fund., 53, 755 (1961)

Habermann, W. L., and Morton, R. K., Trans. Am. Inst. Civil Engr., 121, 227 (1956)

Peebles, F. N. and Garber, H. Y., Chem. Eng. Prog., 49, 88 (1953)

Leonard, T. H. and Houghton, G., Trans. Instn. Chem. Engs., 32, 18 (1954)

Zieminski, S. A. and Raymond, D. R., Chem. Eng. Sci., 23, 17 (1968)

Raymond, D. R. and Zieminski, S. A., AIChE J., 17, 57 (1971)

Garbarini, G. R. and Chi Tien, Can. J. Chem. Eng., 47, 35 (1969)

Bruce and Schwarz, J. Pol. Sci., A-2, 7, 909 (1969)

Hill, C., Ph.D. Dissertation, University of Wisconsin (1969)

Zana, E., Tieffenbruck, G. and Leal, L. G., Submitted to Rheol. Acta (1975)

Harper, J. F., "Advances in Applied Mathematics", 59 (1973)

Griffith, R. M., Chem. Eng. Sci., 17, 1057 (1962)

Levich, V. G., "Physicochemical Hydrodynamics", Prentice Hall, Englewood Cliffs, N. J. (1962)

Boussinesq, J., J. Math., 6, 285 (1905)

Hirose, T. and Moo-Young, M., Can. J. Chem. Eng., 47, 265 (1969)

TABLE CAPTIONS

FIGURE CAPTIONS

Table 1: Physical Parameters of the Solutions

Liquid (@ 25°C)	η_o(p)	ρ(gm/cc)	n
89% aqueous solution of glycerine	1.80	1.234	1.0
0.1% AP30/H_2O	2.48	0.997	0.80 ± 0.10
0.5% AP30/H_2O	23.92	0.997	0.72 ± 0.05
1.0% AP30/H_2O	123.00	0.997	0.48 ± 0.02
0.523% AP30-45.6% H_2O-53.9% glycerine	280.00	1.138	0.28 ± 0.02

Table 2:

	0.1%				0.5%				1%				AP30-H_2O-Glyc			
R_{eq}	Re	We	Re/We	E	Re	We	Re/We	E	Re	We	Re/We	E	Re	We	Re/We	E
0.20	13.93	3.67	0.268	0.94	0.23	1.85	8.04	0.87	0.002	1.96	980.0	0.87	0.008	2.45	306.0	0.82
0.22	21.67	3.72	0.171	0.92	0.46	2.12	4.61	0.83	0.006	2.15	358.0	0.80	0.014	2.91	208.0	0.78
0.24	30.53	3.83	0.125	1.08	0.80	2.25	2.81	0.81	0.011	2.38	216.0	0.78	0.022	2.96	135.0	0.74
0.26	35.86	3.82	0.106	1.18	1.30	2.35	1.81	0.84	0.022	2.69	122.0	0.79	0.034	2.98	88.0	0.73
0.28	40.96	3.85	0.093	1.28	1.83	2.48	1.36	0.84	0.040	2.96	74.0	0.76	0.050	3.28	65.0	0.72
0.30	43.20	3.92	0.090	1.42	2.45	2.54	1.04	0.85	0.066	3.04	46.0	0.76	0.072	3.46	48.0	0.71
0.32	46.18	3.70	0.080	1.48	3.41	2.52	0.74	0.85	0.103	3.28	32.0	0.74	0.114	3.65	32.0	0.70
0.34	48.96	3.68	0.075	1.54	4.18	2.60	0.62	0.89	0.219	3.29	15.0	0.72	0.151	4.01	27.0	0.69
0.36	51.02	3.67	0.072	1.64	5.32	2.65	0.50	0.90	0.306	3.42	11.0	0.71	0.231	4.10	18.0	0.68
0.38	53.15	3.51	0.066	1.72	8.15	2.68	0.33	0.96	0.401	3.49	8.7	0.71	0.268	4.13	15.0	0.66
0.40	66.62	3.51	0.052	2.00	10.17	2.71	0.27	1.00	0.555	3.53	6.4	0.70	0.361	4.16	12.0	0.65

Table 3: Velocity Transition

Solution	n	We	(Velocity Increase Factor) U_b/U_s
Newtonian	1.00	0	1.50
0.3% ET497 (Astarita & Apuzzo)	0.56	NA	2.22
0.25% J-100 (Astarita & Apuzzo)	0.55	NA	2.35
0.5% AP30-H_2O (this work)	0.72	1.85-2.54	4.00
1.0% Polyox (Calderbank et al.)	0.52	NA	4.15
1.0% AP30-H_2O (this work)	0.48	2.20-3.28	5.00
0.5% J-100 (Astarita & Apuzzo)	0.46	NA	5.55
0.7% ET497 (Astarita & Apuzzo)	0.44	NA	5.86
AP30-H_2O-glycerine	0.28	2.70-3.48	6.80

NA Not available

Under the column We number, first number corresponds to bubble We number just before transition, and the second number corresponds to the bubble We number just after the transition.

Table 4: Comparison of Experimental Mass Transfer Rates with Predictions of Newtonian Theory

Solution	Re	n	We	We/Re	% Increase in Sh^* Over the Newtonian Value (Experimental)	% Increase Over Power-law Model (equation 23)
2.5% CMC-H_2O (Hirose & Moo-Young)	Re < 1	0.86	0.50	Not applicable	9-12%	1-4%
0.1% AP30-H_2O (this work)	40-70	0.85	Not applicable	0.08	10-13%	Not applicable
0.5% AP30-H_2O (this work)	5-10	0.72	Not applicable	0.27	22.25%	Not applicable
1.0% HEC (Hirose & Moo-Young)	Re < 1	0.70	0.80	Not applicable	25.30%	9-14%
1.0% Polyox (Calderbank et al.)	Not available	0.54	Not available	Not available	40-45%	15-20%
1.0% AP30-H_2O (this work)	0.1-0.4	0.48	3.40	Not applicable	56-60%	35-39%
0.14% Carbopol (Hirose & Moo-Young)	Re < 2	0.34	0.00	Not applicable	30-35%	3-5%
AP30/H_2O/Glycerine (this work)	0.07-0.4	0.28	3.80	Not applicable	60-65%	37-42%

LEGEND for Figure 1

1. CO_2 gas tank
2. Humidifying column
3. Humidifying column
4. Micro syringe (gas injection)
5. Micro syringe (liquid injection)
6. Capillary tubing
7. Thin light beam source
8. Photo transistor
9. Turning cup
10. Absorption column
11. Solenoid valve
12. Pressure transducer
13. Camera platform
14. Counter weight
15. Motor
16. Motor controller
17. Camera
18. Stroboscope
19. Mirror
20. Meter stick
21. Narrow light slit (two of them)
22. Photo transistors (two)
23. Microswitch
24. Flood lamp
25. Bleed valve
26. Pressure transducer indicator
27. Magnetic sensor amplifier
28. Digital voltmeter
29. Slit-light control relay
30. Variac
31. DC power supply for camera motor
32. Platform control circuitry
33. Velocity measuring circuitry
34. Digital counter
35. 4-channel recorder

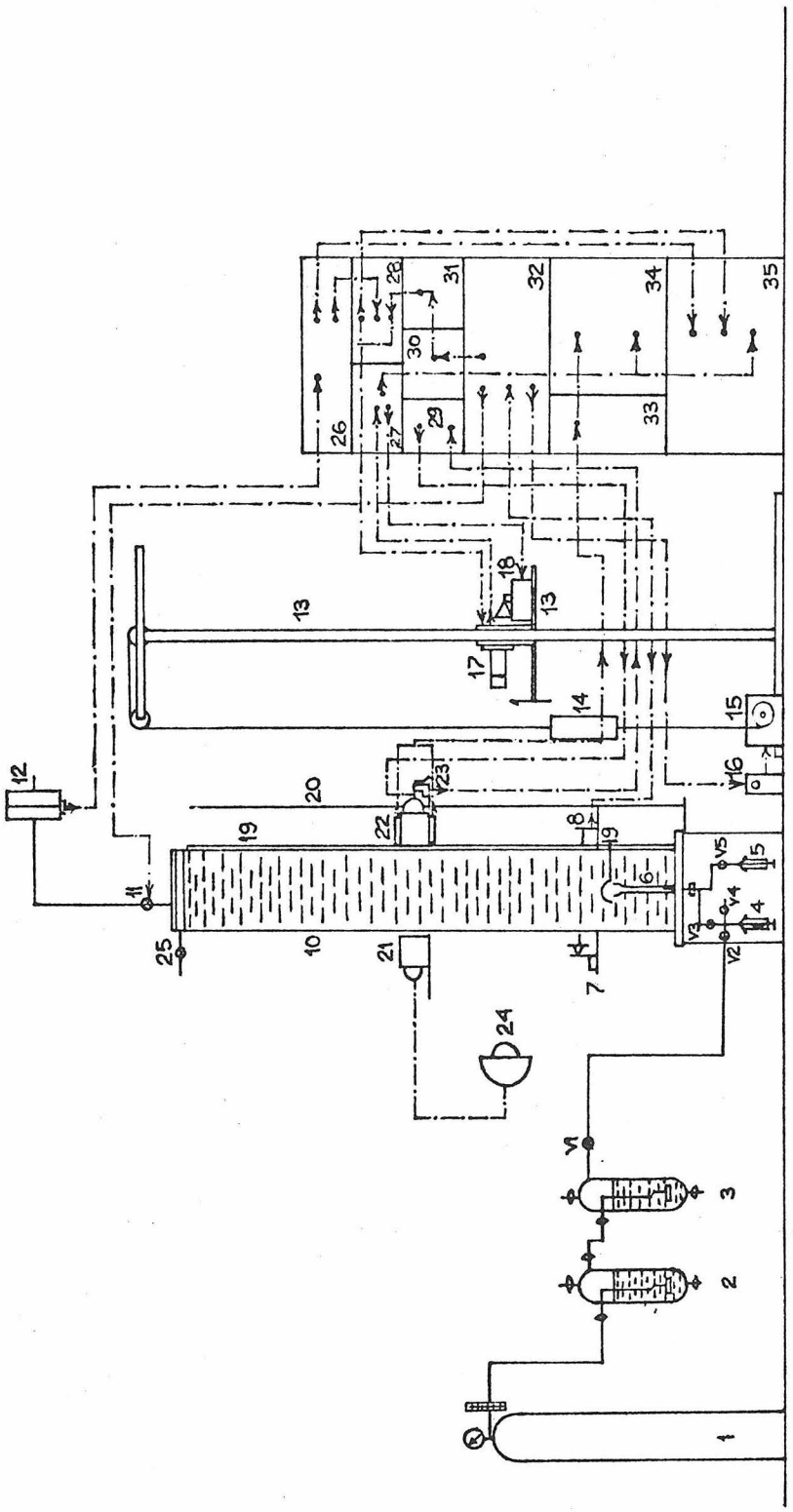

Figure 1: Experimental Apparatus

LEGEND for Figure 2

1. Graduated capillary tube
2. Bottom plate of the absorption column
3. Screws to hold the seal plate
4. Seal plate
5. Gas jet
6. Purge line
7. 3-way valve
8. Liquid reservoir line
9. Carbon dioxide line
10. Graduated gas syringe
11. Liquid syringe

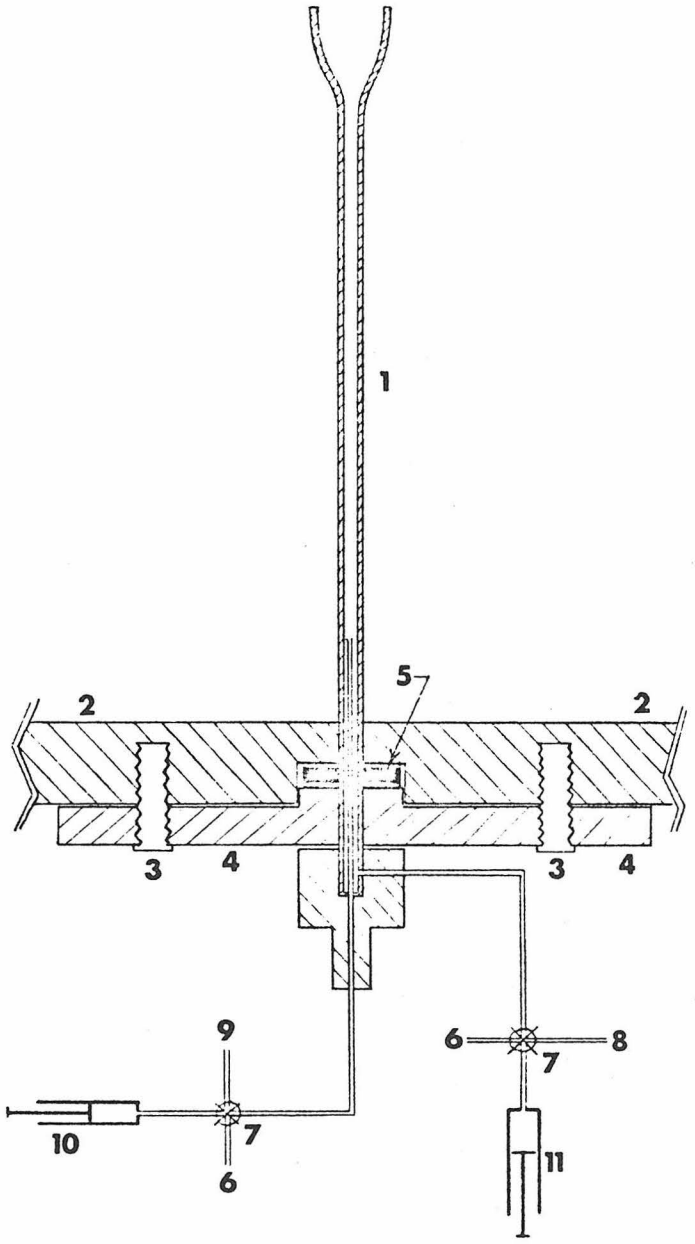

Figure 2: Bubble Release Machanism

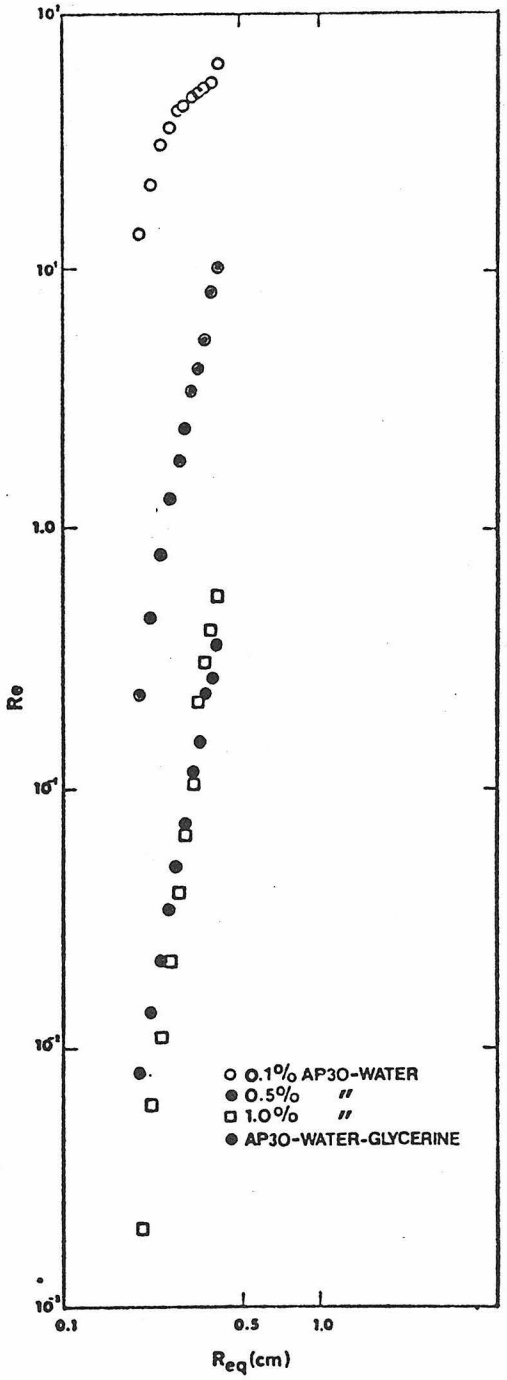

Figure 3: Re Number for the Four Viscoelastic Solutions

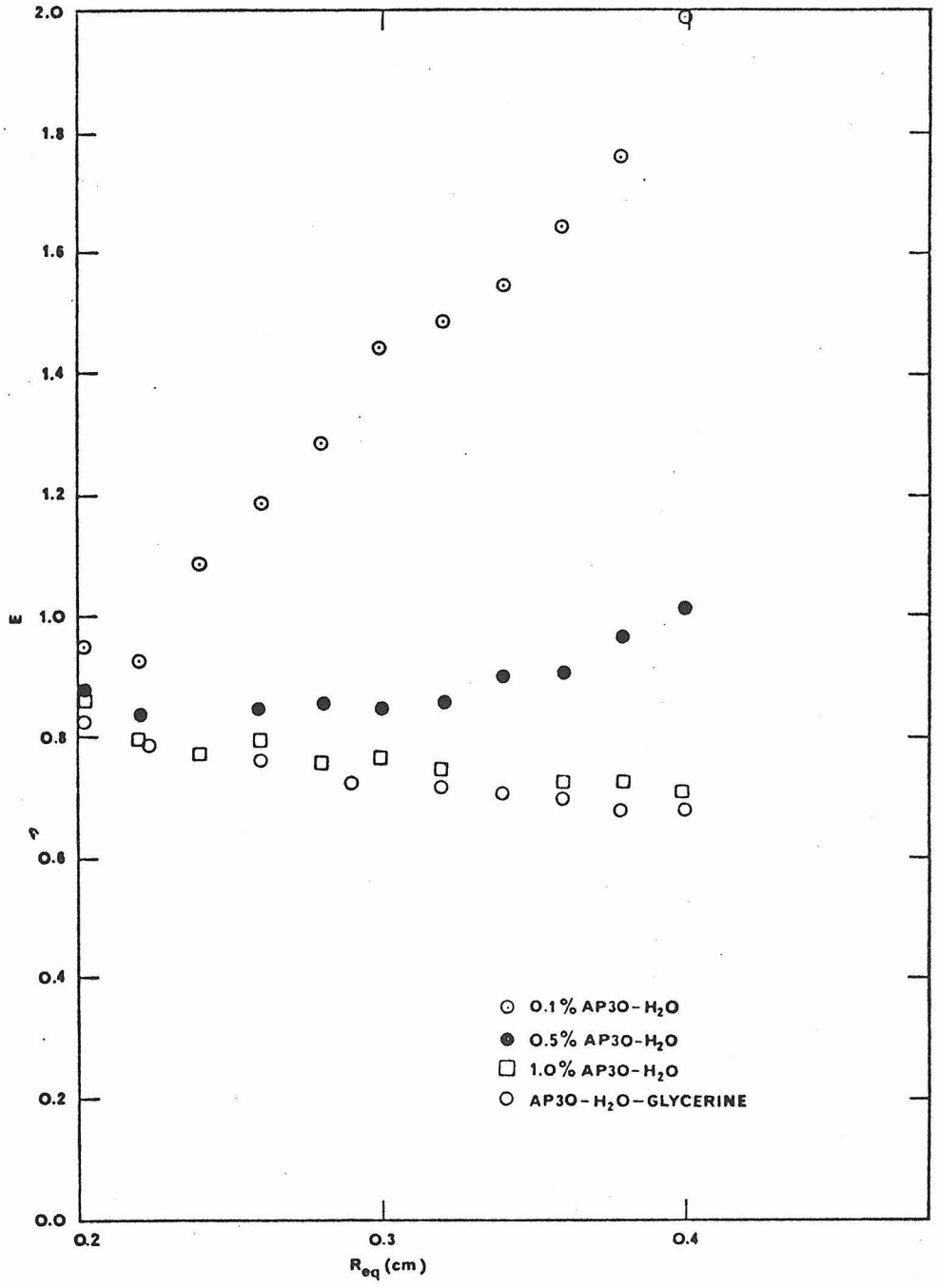

Fig. 5: Eccentricities vs. Bubble Size

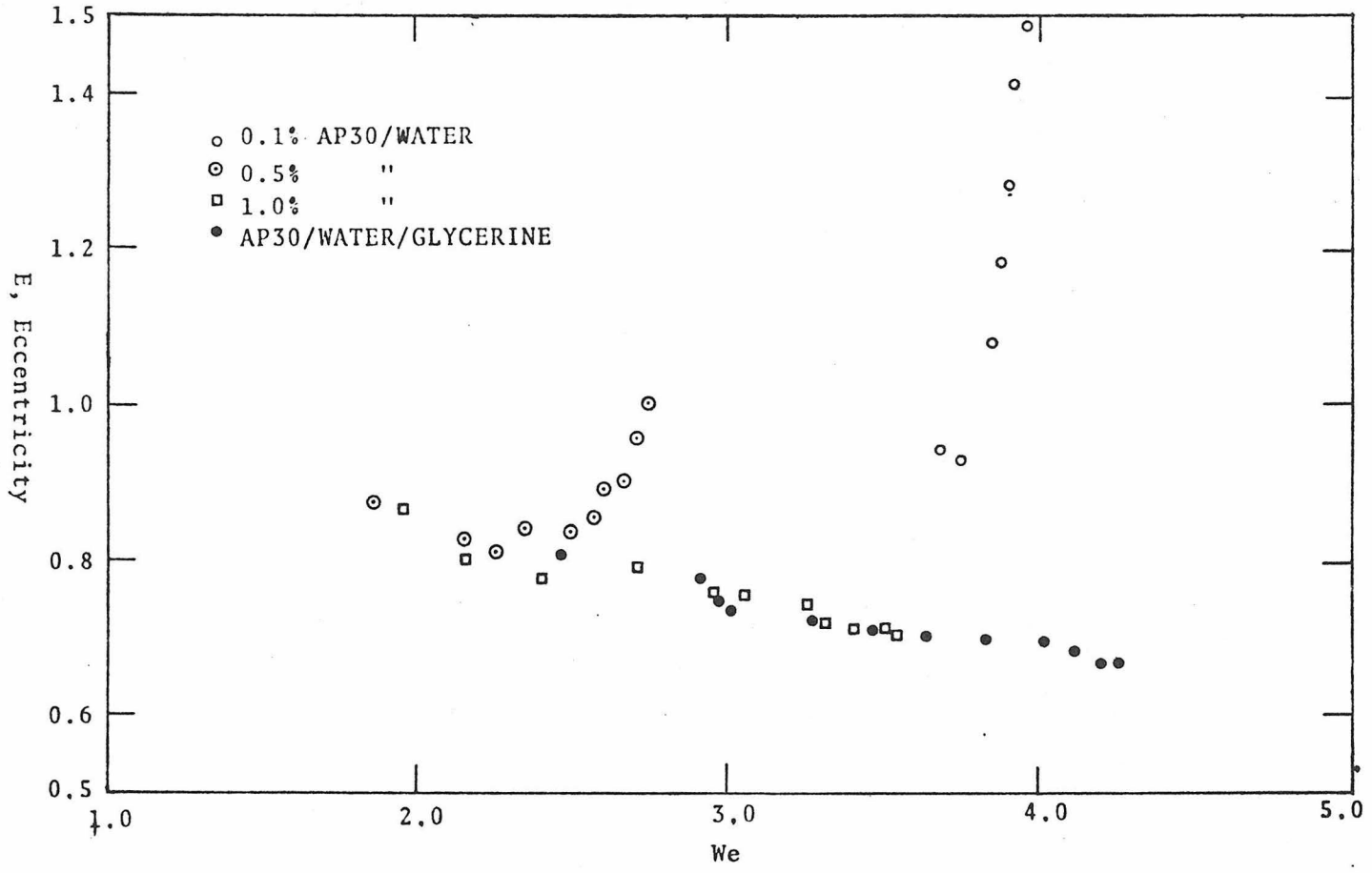

Fig.5a: Eccentricities vs. Weissenberg Number

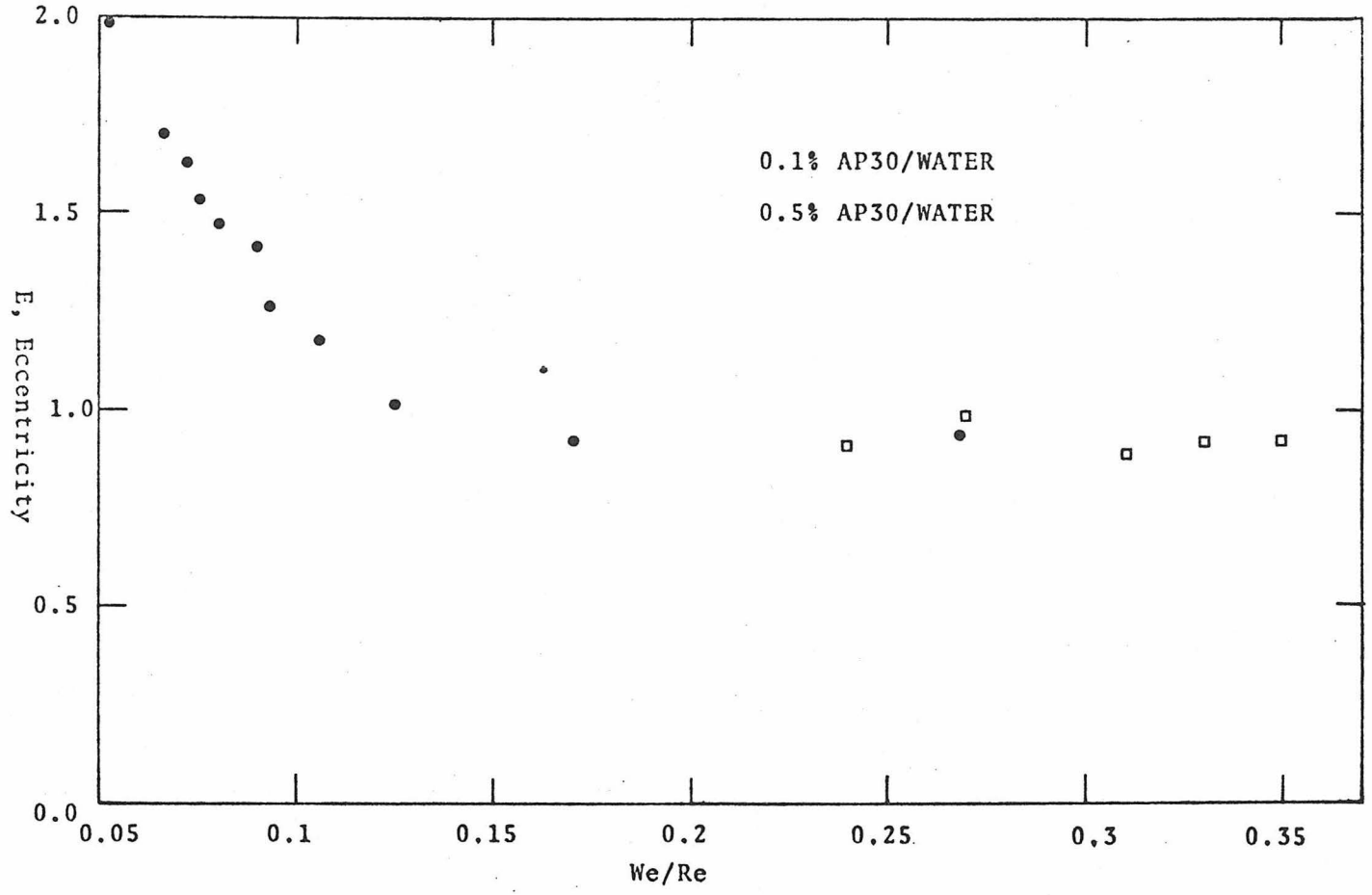

Fig. 5b: Eccentricity vs. We/Re

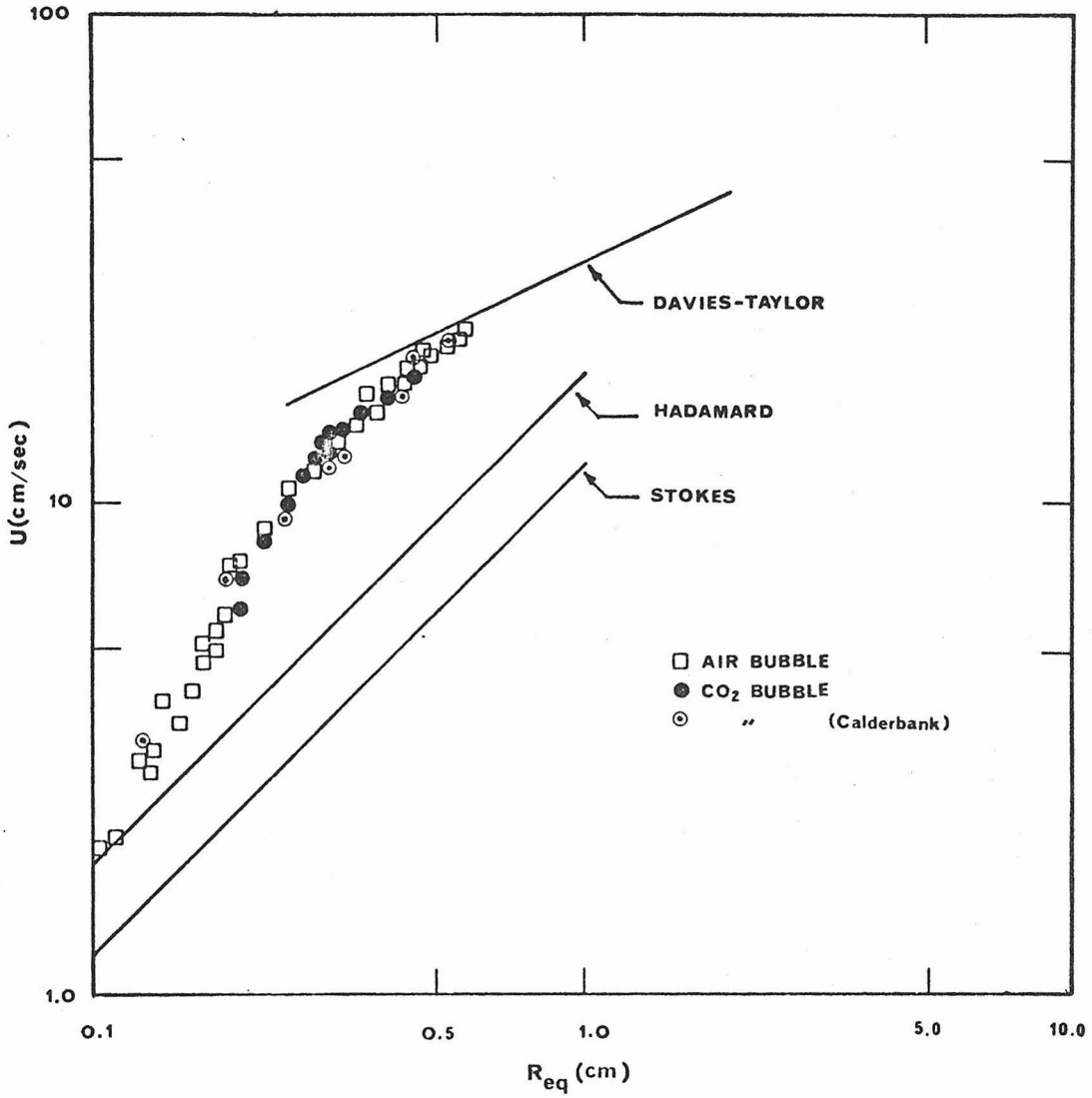

Fig. 6: Bubble Rise Velocity vs. Size for 89% Glycerine/Water Solution

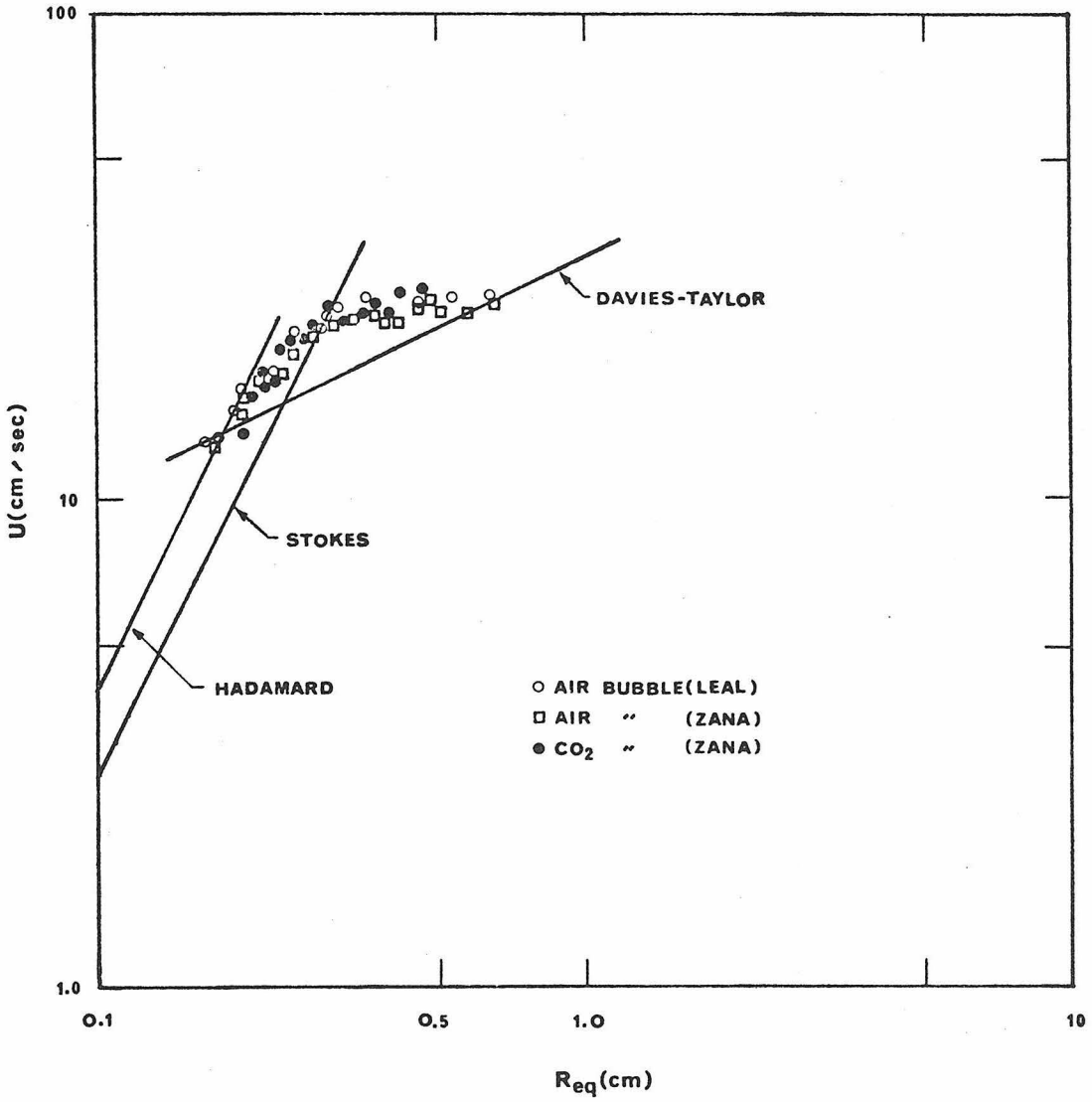

Fig. 7: Bubble Rise Velocity vs. Size for 0.1% AP30/Water Solution

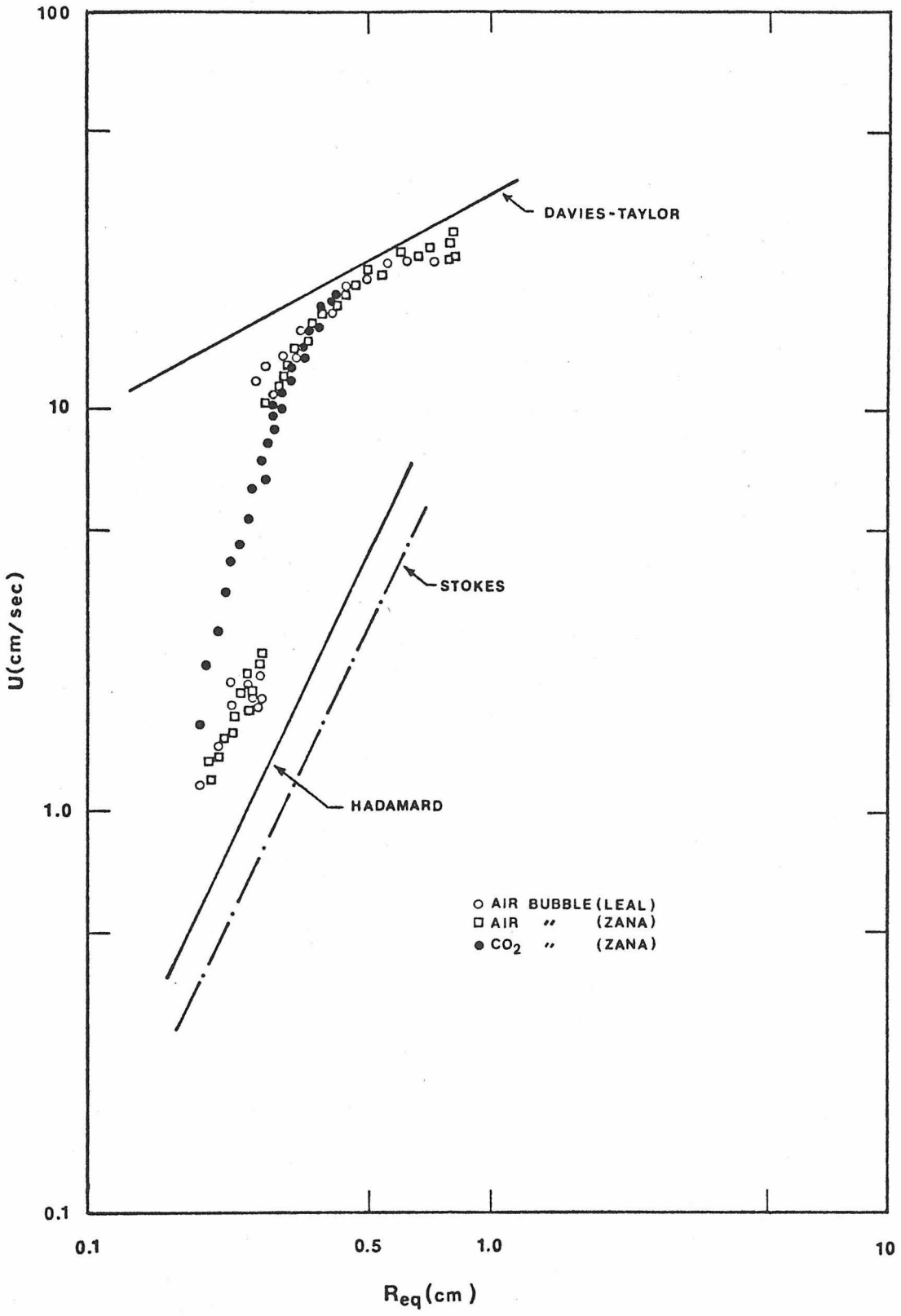

Fig. 8: Bubble Rise Velocity vs. Size for 0.5% AP30/Water Solution

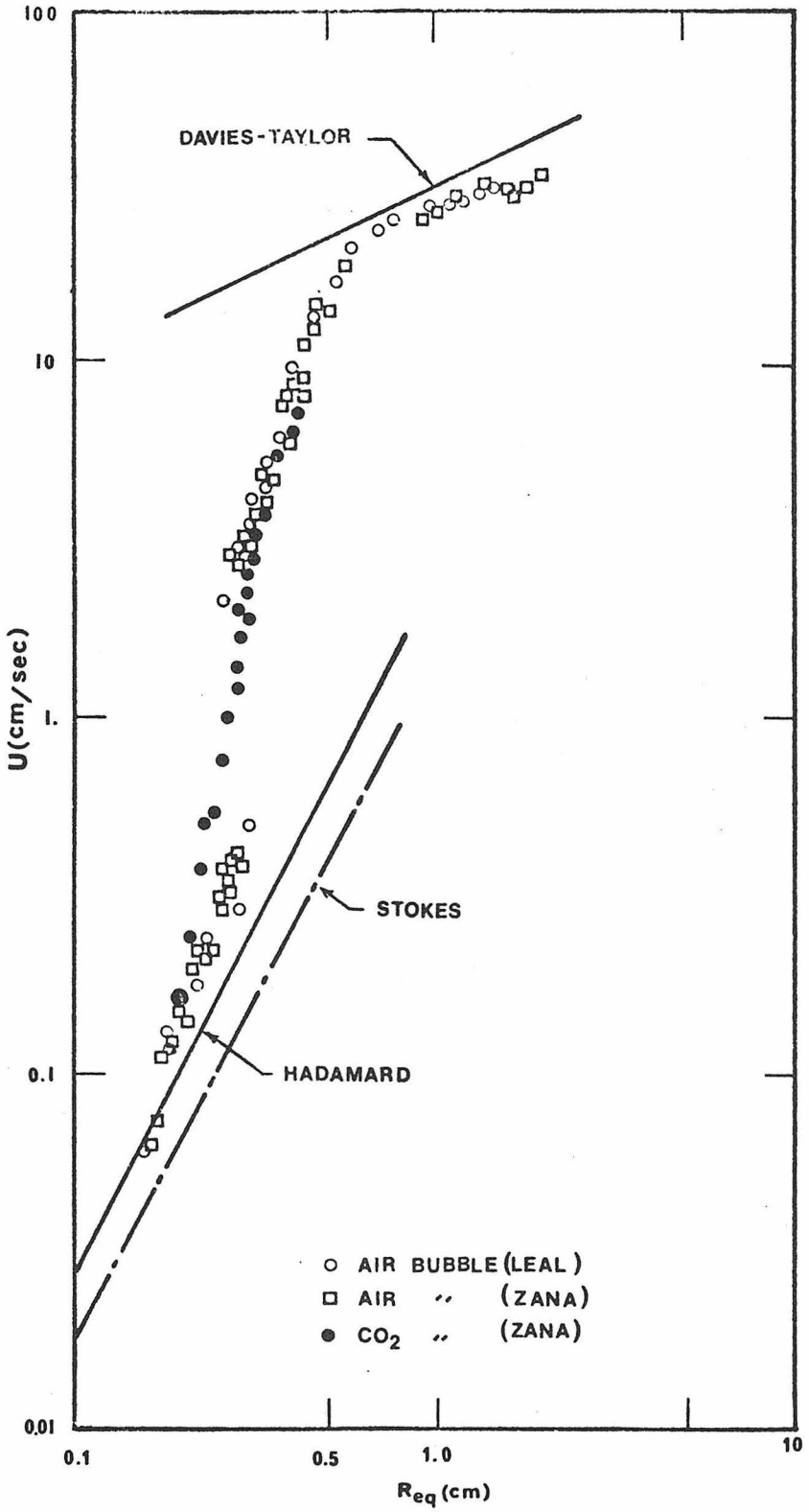

Fig. 9: Bubble Rise Velocity vs. Size for 1.0% AP30/Water Solution

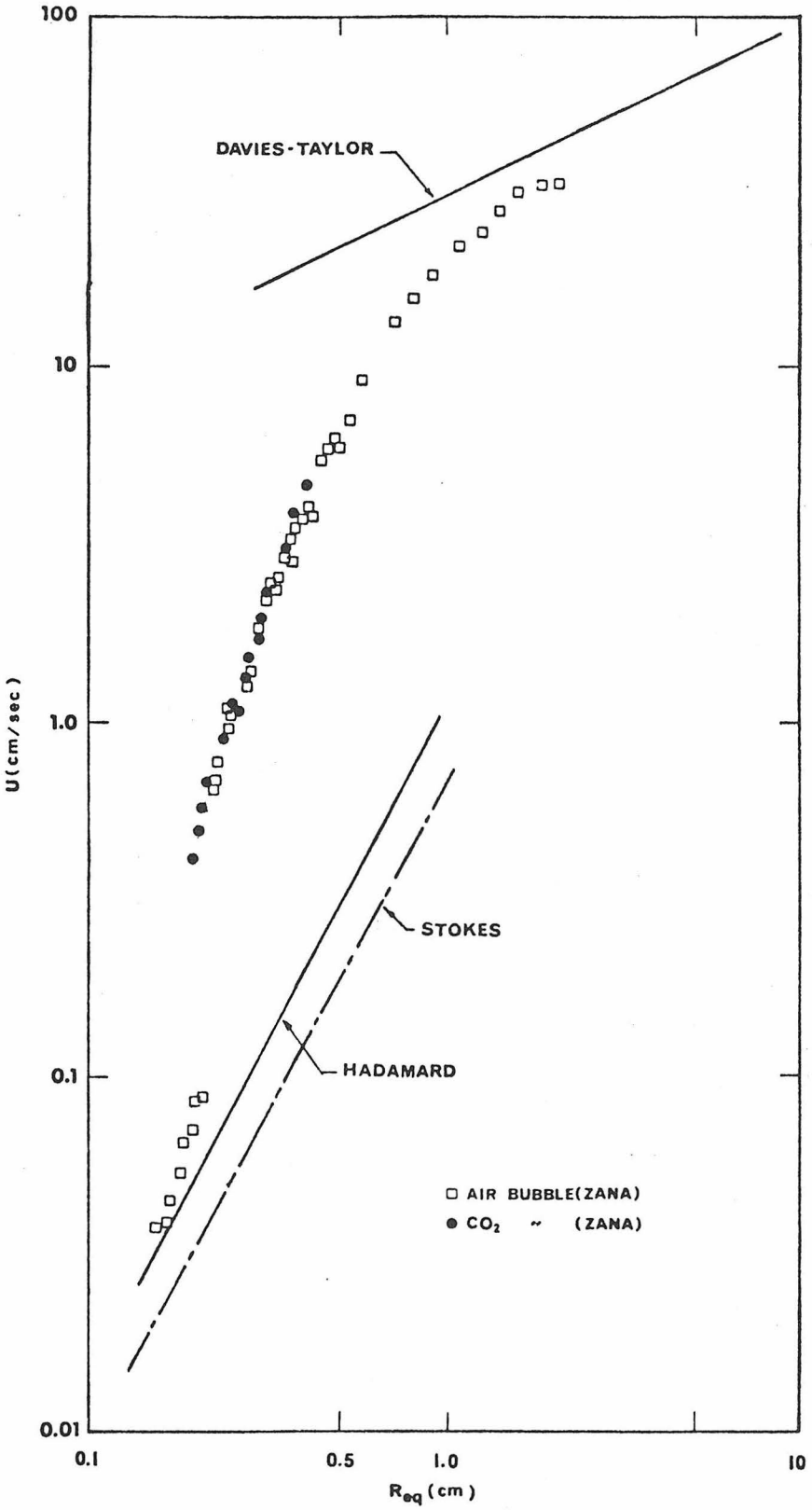

Fig. 10: Bubble Rise Velocity vs. Size for AP30/Water/Glycerine Solution

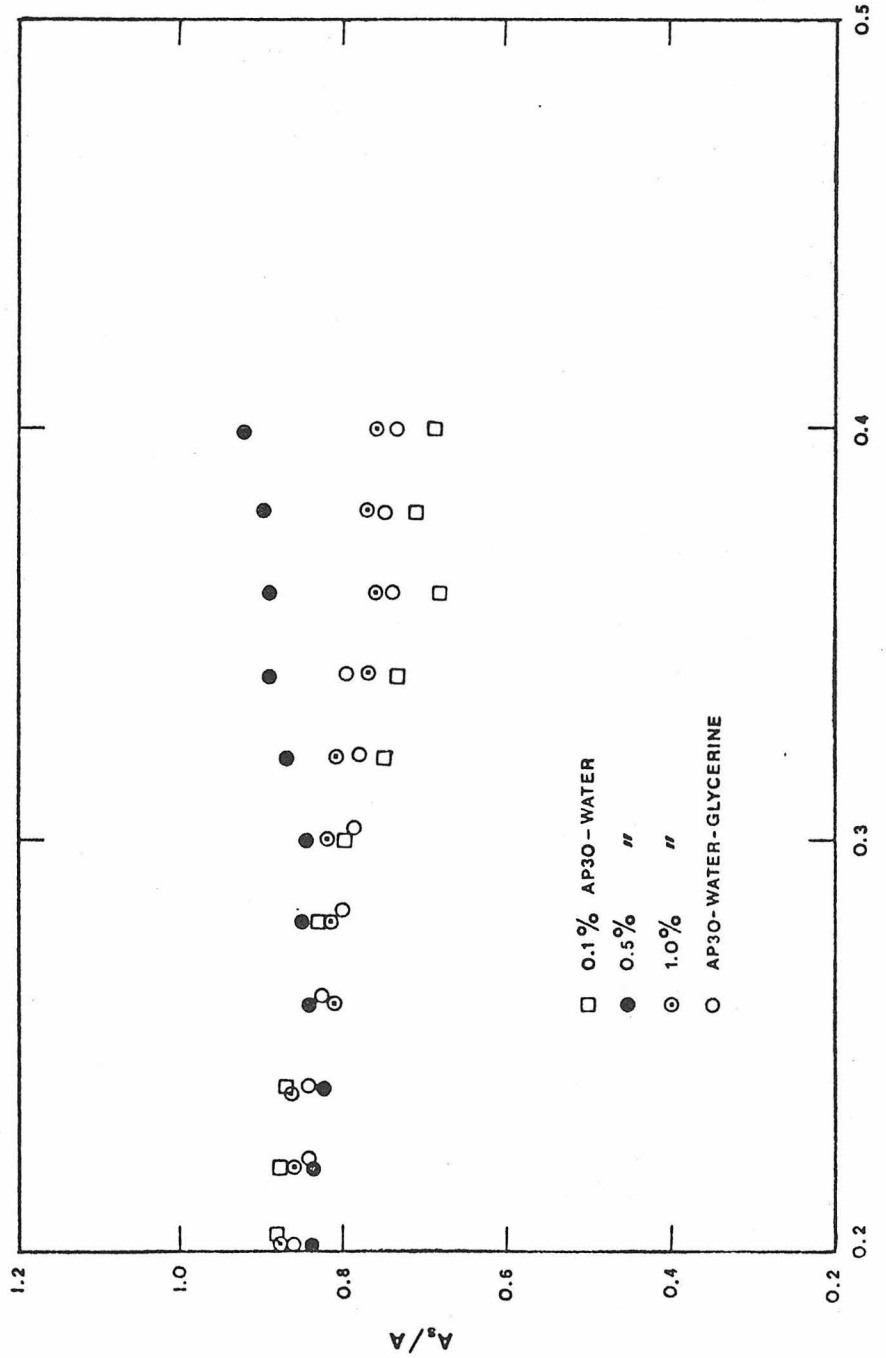

Fig. 11: Ratio of Equivalent Spherical Area to Bubble Surface Area vs. Bubble Size

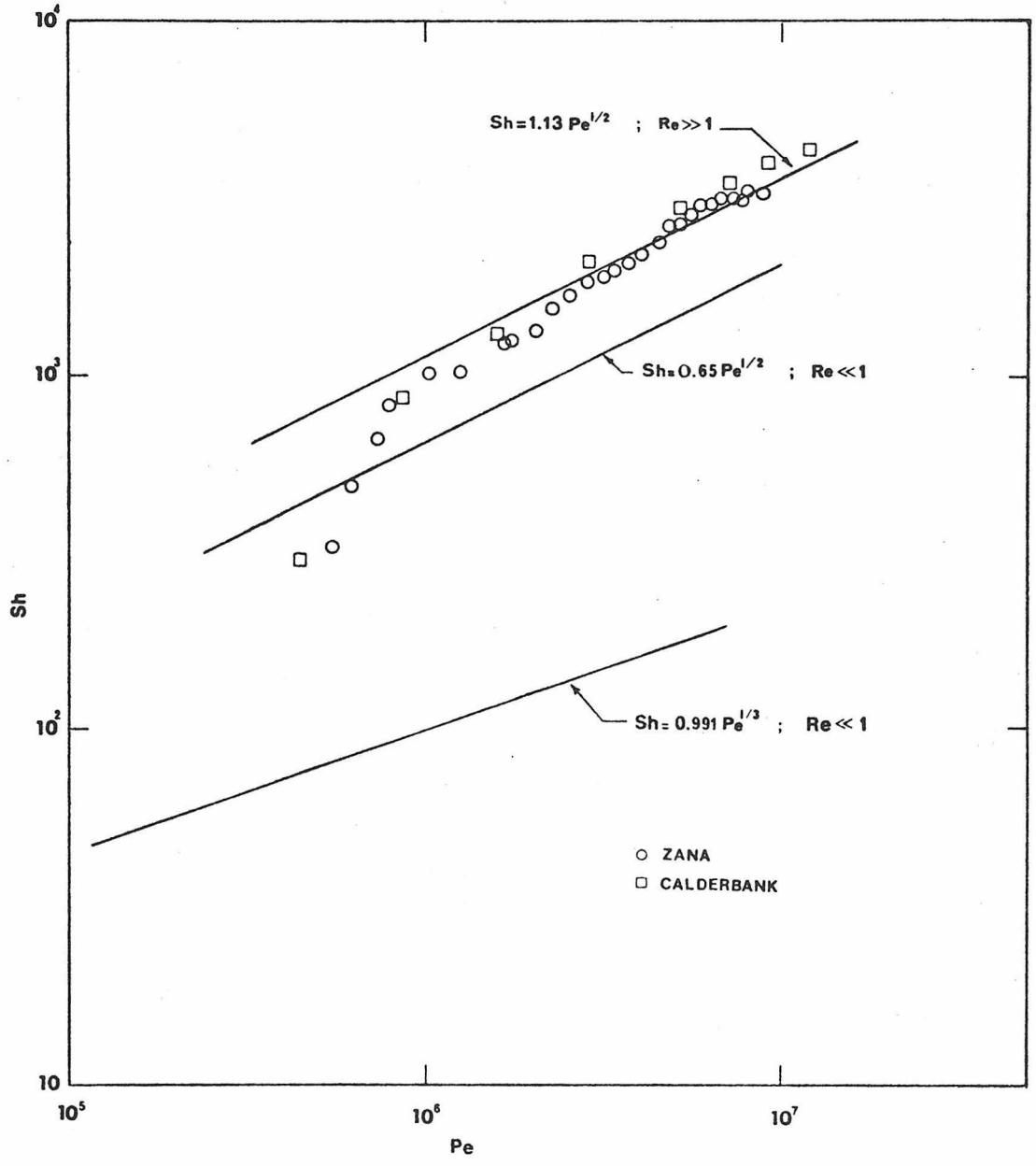

Fig. 12: Sh Number vs. Pe Number for 89% Glycerine/ Water Solution

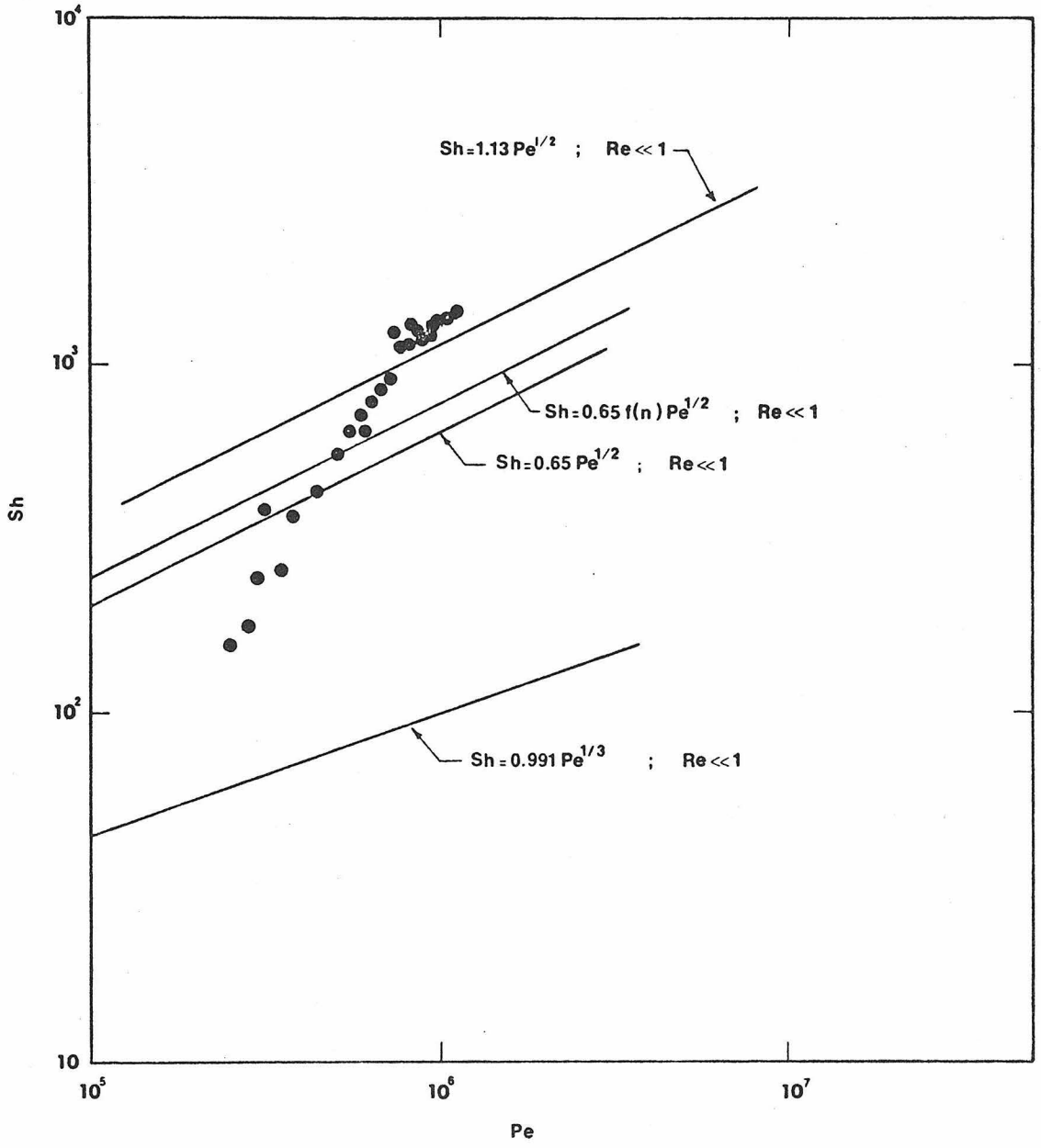

Fig. 13: Sh Number vs. Pe Number for 0.1% AP30/Water Solution

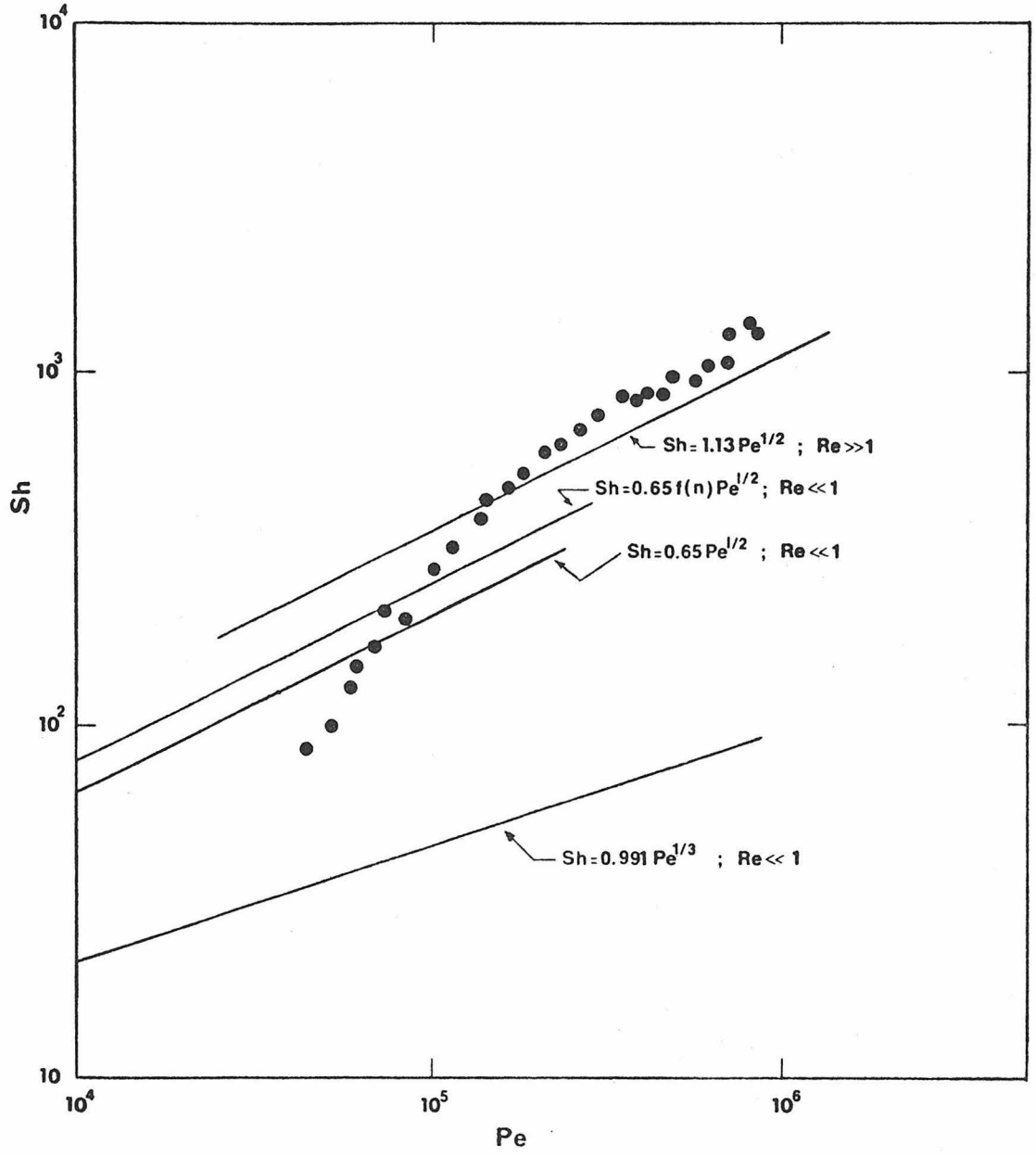

Fig. 14: Sh Number vs. Pe Number for 0.5% AP30/Water Solution

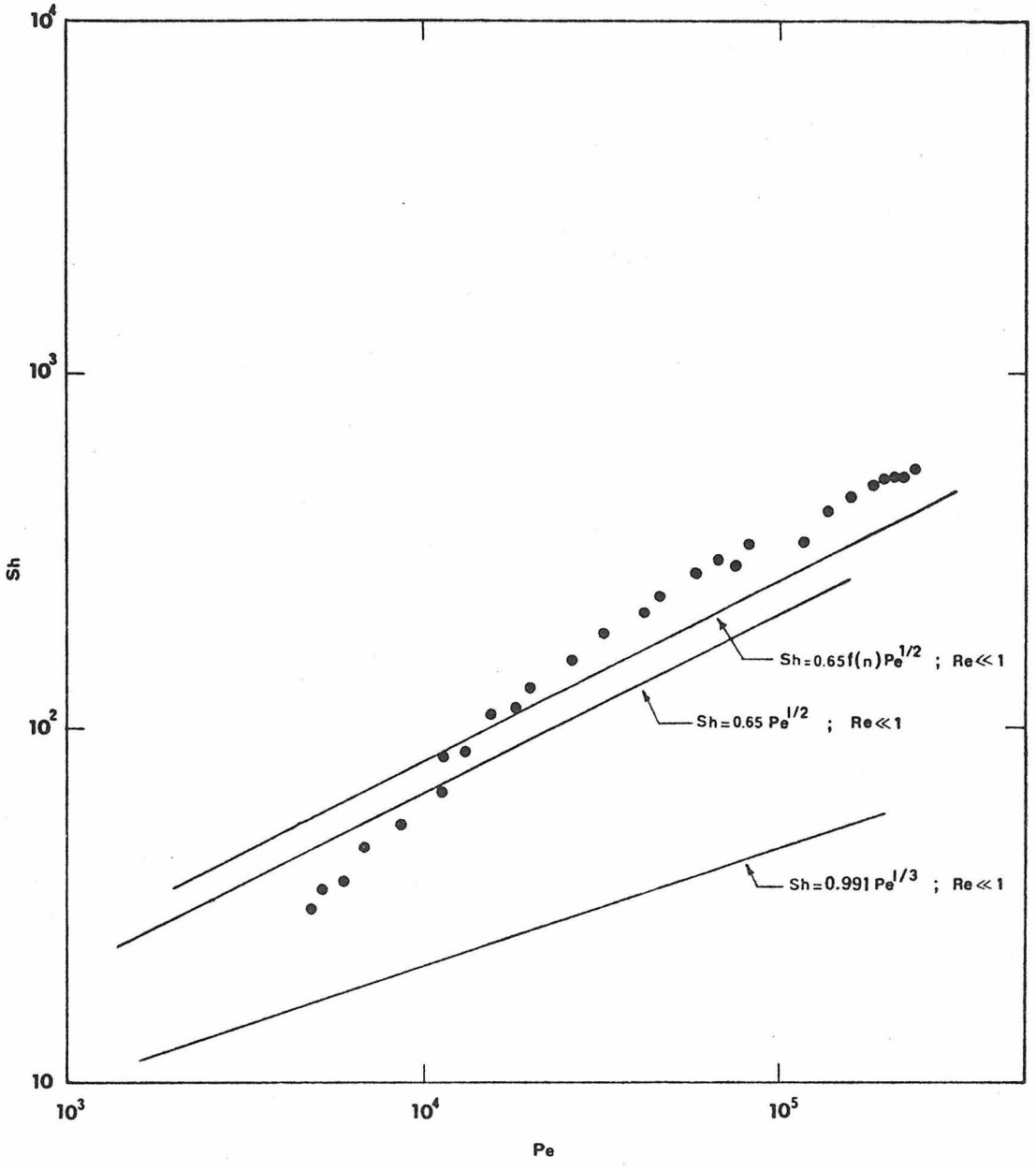

Fig. 15: Sh Number vs. Pe Number for 1.0% AP30/Water Solution

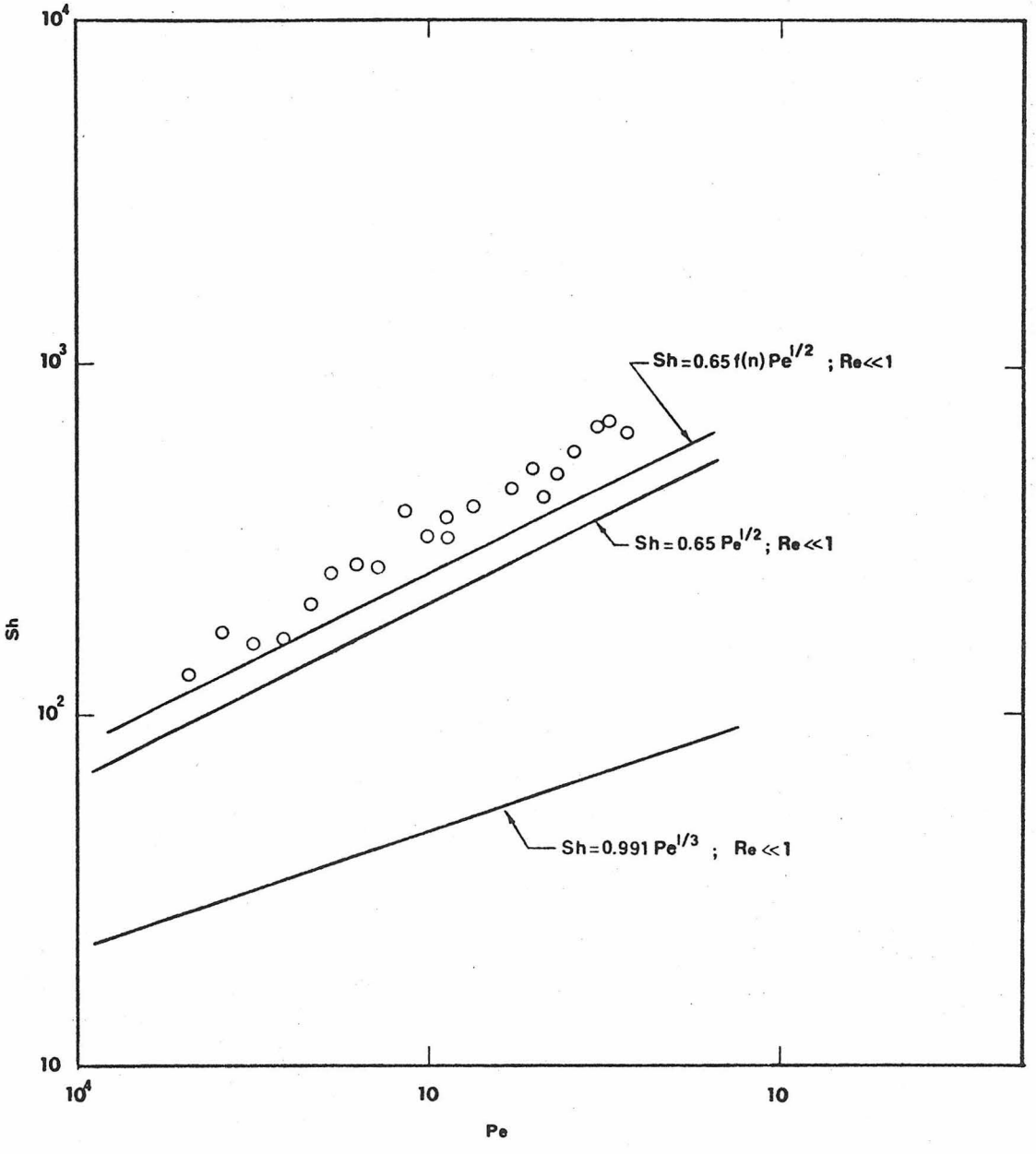

Fig. 16: Sh Number vs. Pe Number for AP30/Water/ Glycerine Solution

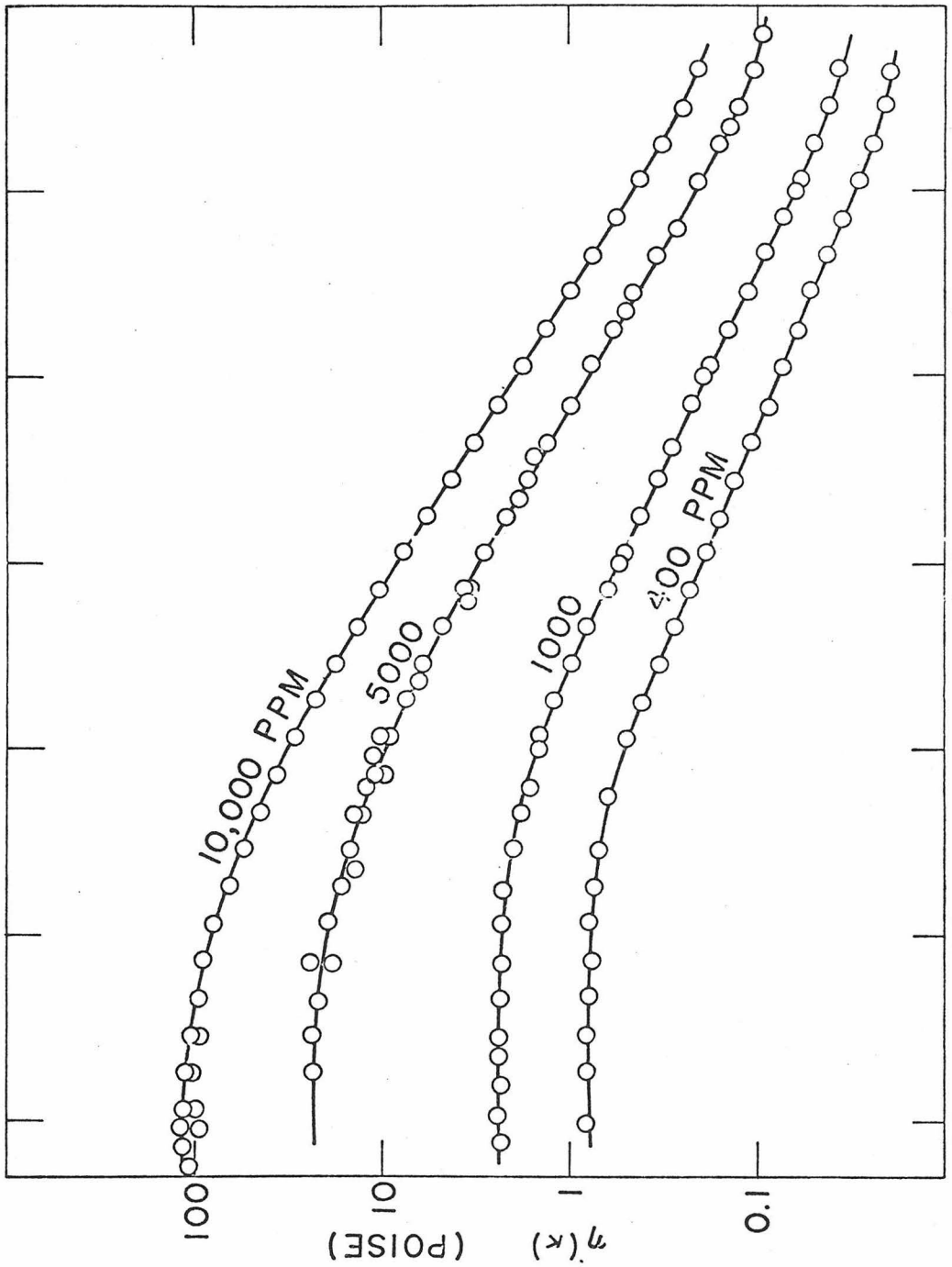

Fig. 17: Viscosity vs. Shear Rate for AP30/Water Solutions

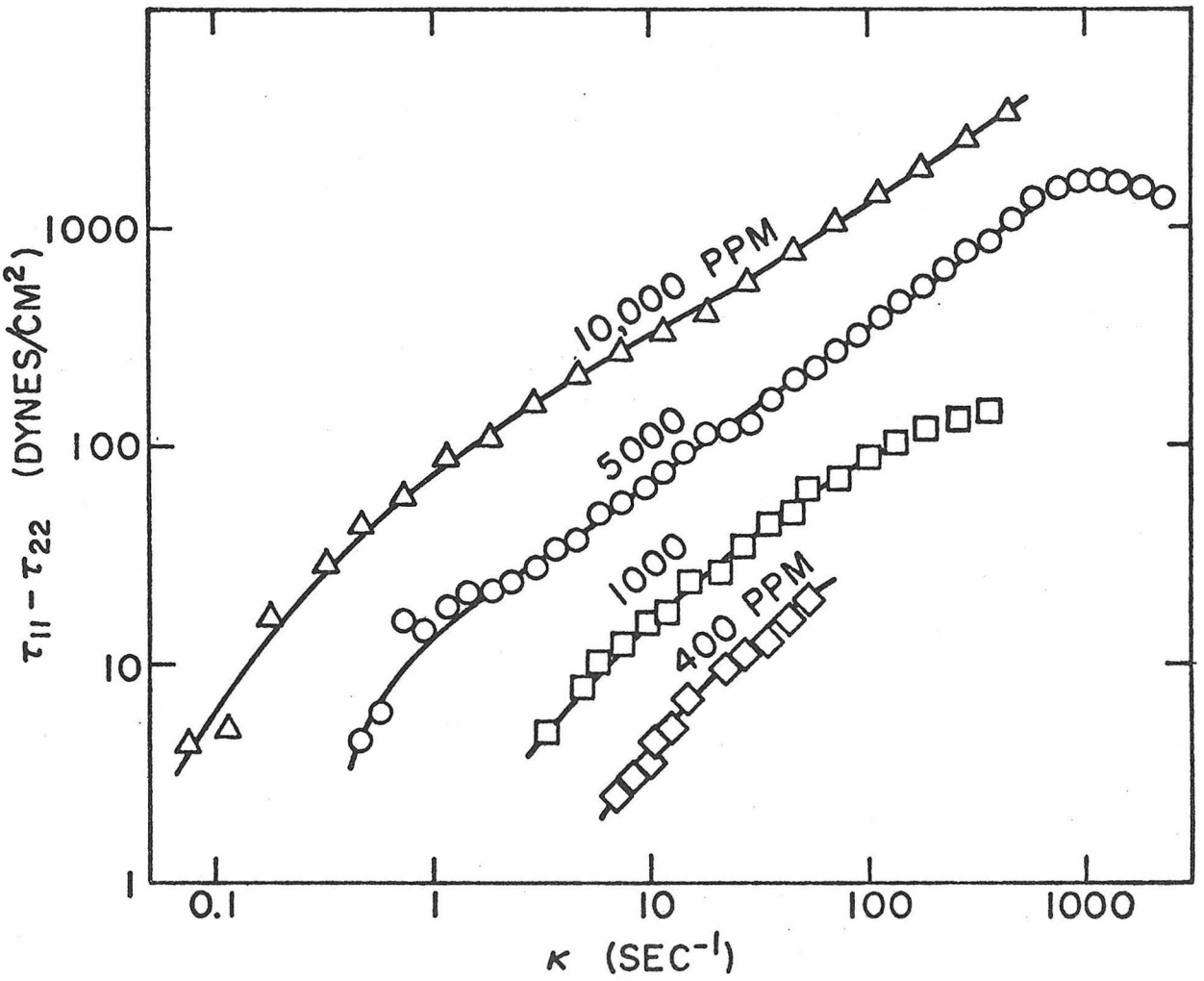

Fig. 18: Primary Normal Stress Difference vs. Shear Rate for AP30/Water Solutions

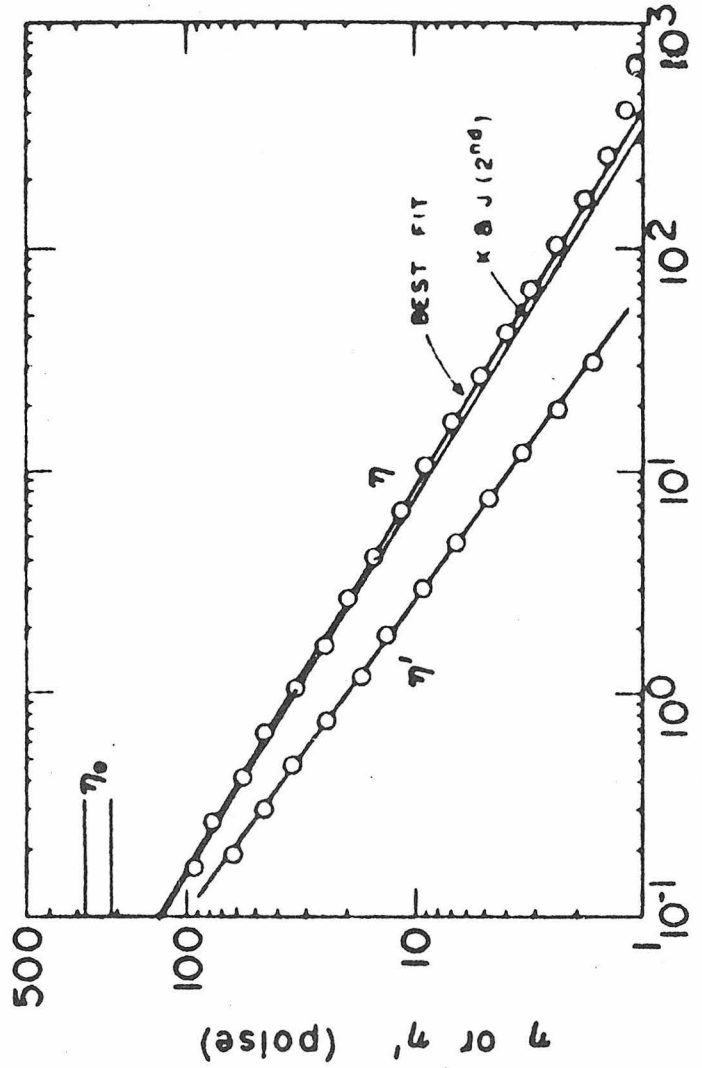

Fig. 19: Viscosity vs. Shear Rate for AP30/Water/Glycerine Solution

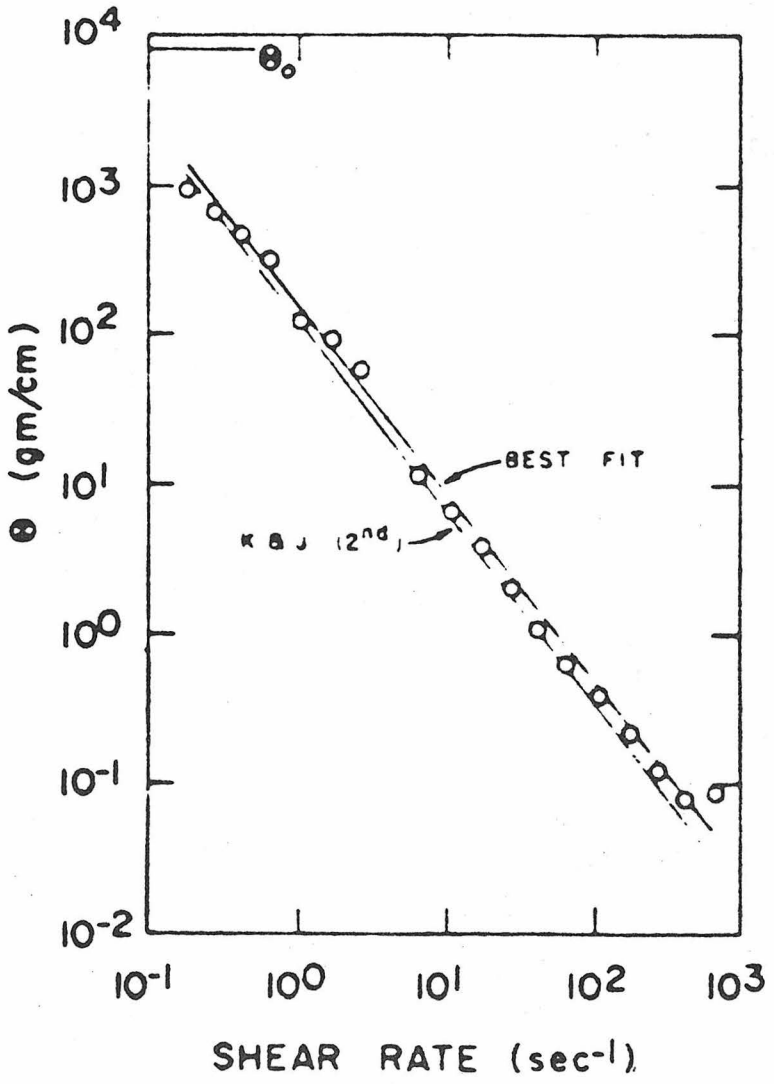

Fig. 20: Primary Normal Stress Difference vs. Shear Rate for AP30/Water/ Glycerine Solution

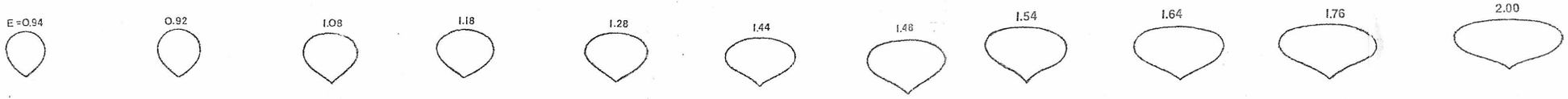

0.1 % AP30-WATER

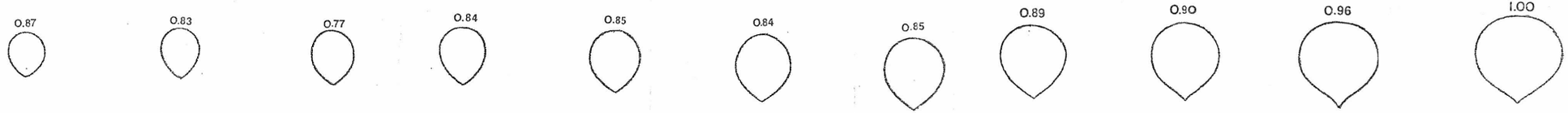

0.5 % AP30-WATER

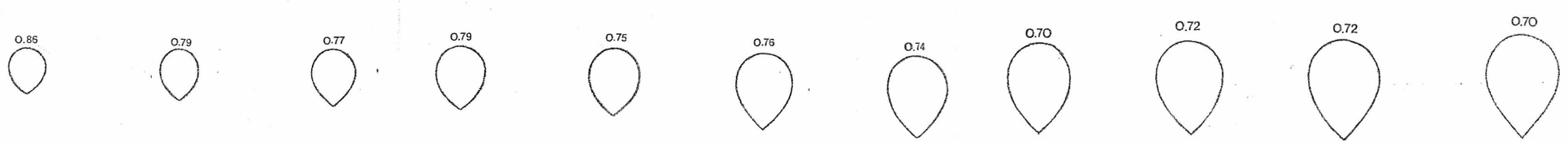

1.0 % AP30-WATER

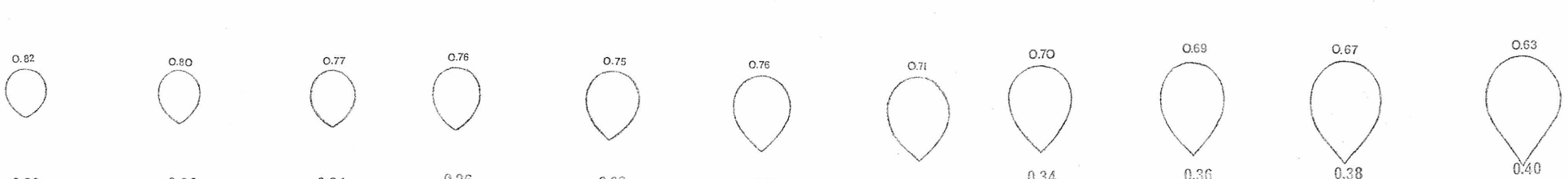

AP30-WATER-GLYCERINE